Spatial and temporal analysis of information processing in the ascending tectofugal visual system

Doctoral thesis

Dr. Antal Berényi

Department of Physiology

Faculty of Medicine, University of Szeged

2009.

List of publications related to the subject of the thesis

I. **Berényi A**, Benedek G, Nagy A. (2007) Double sliding-window technique: a new method to calculate the neuronal response onset latency. *Brain Res.* **1178**:141-8.

II. Eördegh G, Nagy A, **Berényi A**, Benedek G. (2005) Processing of spatial visual information along the pathway between the suprageniculate nucleus and the anterior ectosylvian cortex. *Brain Res. Bull.* **67**:281-9.

III. Nagy A, Paróczy Z, Márkus Z, **Berényi A**, Wypych M, Waleszczyk WJ, Benedek G. (2008) Drifting grating stimulation reveals particular activation properties of visual neurons in the caudate nucleus. *Eur. J. Neurosci.* **27**:1801-8.

1 Table of contents

2 Introduction

From a philosophical point of view, it might be said that the most important function of the brain is to serve as the physical structure underlying the mind. From a biological point of view, though, the most important function is to generate behavioural patterns that promote the welfare of an animal. Even single-cell organisms may be capable of extracting information from the environment and acting in response to it. (Gehring, 2005) However, sophisticated control of behaviour on the basis of complex sensory input requires the information-integrating capabilities of a centralized brain, which is carried out by the cooperation of billions of neurons. Despite rapid scientific progress, much about how brain works remains a mystery. The operations of individual neurons and synapses are now understood in a considerable detail, but the way they cooperate in ensembles of thousands or millions has been very difficult to decipher. Methods of observation such as EEG recording and functional brain imaging tell us that brain operations are highly organized, but these methods do not have the resolution to reveal the activity of individual neurons. From a biological perspective, the function of a brain is to generate behaviours that promote the survival of an animal. (Carew, 2000) To do this, it extracts relevant information from the environment via the sensory organs to refine actions. Sensory signals may stimulate an immediate response; they may modulate an ongoing pattern of activity as in the effect of light-dark cycles on an organism's sleep-wake behaviour; or their information content may be stored for future use. The brain manages its complex task by orchestrating functional subsystems, which can be categorized in a number of ways: anatomically, chemically, and functionally.

2.1 Theoretical relation between sensory input and motor output

Generally speaking the task of the nervous system is to convert sensory information which reflects both important and irrelevant features of the environment into appropriate motor responses considering previous experience, and the actual conditions as well. The main quest for the neural sciences is obvious: decode the algorithm with which our brain transforms the input signals into output actions. One of the most effective tools in our hands is measuring the response characteristics of single neurons and/or groups of neurons responding to a specific stimulus in different structures along the individual information processing pathways. By comparing the similarity (common information content) of responses in adjacent stages, one can build a theoretical

model which reflects the properties of the investigated subsystem. With the help of these artificial models the behaviour of the system becomes more or less predictable. However, the complexity of the neural network and its compact structure will presumably keep the secret of the mind buried for a long time (if not forever).

2.2 Introduction to the ascending tectofugal visual system

The tectal sensorimotor function is a phylogenetically old capacity of vertebrates. Its relatively simple structure and connectional system as well as the possibility that it can be studied even in cold-blooded species made it available for theoretical studies concerning stimulus-response characteristics of the brain. While the descending projections of the tectum were widely analysed much less is known about the ascending tectofugal systems. As in 1958 Freygang introduced the extracellular recording technique, the registration of single unit activity in the forebrain became easier and more effective. Neurophysiologists during the second half of the 20th century made a great effort to bind different brain regions to different stimulus modalities by investigating into their responsivity in different species. This systematic work led to the discovery of several multimodal sensory area of the feline brain (e.g.: Loe and Benevento, 1969). The visual responsivity of the anterior ectosylvian visual area (AEV) along the banks of the anterior ectosylvian sulcus (AES) was discovered at the beginning of 1980s (Muckle et al., 1982; Olson and Graybiel, 1983, 1987). After tracking neuronal connections of this structure, the concept of an ascending tectofugal visual system in the mammalian brain emerged. The existence of separate geniculate and extrageniculate visual systems has been proven by both morphological and physiological studies. The latter receives visual input through the superior colliculus (SC), which, beside the dorsal lateral geniculate nucleus (LGNd), receives direct innervation from the retina. Anatomical connections in the extrageniculate tectofugal visual system were extensively studied; numerous areas were discovered, which play a role in sensory information processing beside motor output control. However, the physiological role of the connections and the mechanism of information processing are still largely unclear.

2.2.1 Anatomical connections within the ascending tectofugal visual system

The two major destinations of the projection of retinal ganglion cells are the thalamic LGNd and the SC in the mesencephalic tectum. The importance of the latter connection is supported by the fact that in lower vertebrates the optic tectum is the major visual processing centre. However, in some mammalian lines, such as carnivores and primates, an enormous expansion of neocortical processing centres has taken place and in these species the thalamocortical system has become the major target of the retinofugal projection. (Brecht, 1996) Still, from a functional point of view, the visual system of these species can be divided into three discrete, yet partially overlapping subsystems, namely the geniculo-striate, the tectal visual, and the oculomotor systems. (Fig 1.)

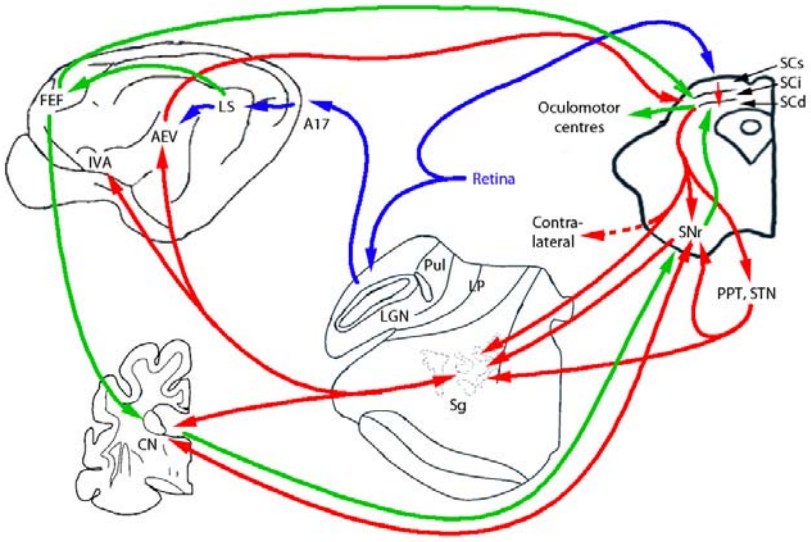

Figure 1.: Connections of the geniculo-striate, tectal, and oculomotor circuitry.
Connections within the tectal visual system are marked with red arrows, while the oculomotor circuitry is denoted with green. Retinal inputs and relevant parts of the geniculo-striate system are indicated with blue arrows.
Abbreviations: *SCs, Sci, SCd*: superior colliculus superficial, intermediate and deep layers respectively; *SNr*: substantia nigra pars reticulata; *PPT*: pedunculopontin-tegmental nucleus; *STN*: subthalamic nucleus; *Sg*: suprageniculate nucleus; *LGN*: lateral geniculate nucleus; *Pul*: pulvinar; *LP*: lateral-posterior nucleus of the thalamus; *CN*: caudate nucleus; *FEF*: frontal eye field; *IVA*: insular visual area; *AEV*: anterior ectosylvian visual area; *LS*: lateral suprasylvian area; *A17*: area 17.

The tectal visual system forms a complex circuitry involving basal ganglia formerly known as motor centres, as well as cortical structures in the parietal region. It fundamentally differs from the geniculo-striate system in the sense, that while the LGNd relays the retinal input towards the primary visual cortex without any noteworthy modification, the axons of retinorecipient neurons in the superior layer of the SC massively converge as they reach the intermediate and deep output

layers (Isa and Saito, 2001), causing a fundamental modification in the size of the receptive fields, Following this integration the information may reach the suprageniculate nucleus (Sg) of the posterior thalamus via several pathways (Katoh and Benedek, 2003; Hoshino et al., 2004). Axons originating from the intermediate layers of the SC (SCi) and the deep layers of the SC (SCd) project directly toward the thalamus, and indirectly by terminating on neurons located in the reticular part of the substantia nigra (SNr), which in turn projects toward the Sg. It should also be noted that the dorsolateral caudal part of the caudate nucleus (NC) is also strongly connected to this system. That the visual information travelling toward the AEV (through the Sg) is tectal in origin was confirmed by morphological experiments. However, the distinction between the striate and extrastriate (tectal) visual systems is not obvious. Even the AEV, a region formerly regarded as the only cortical area which receives visual information totally bypassing the LGNd, seems to receive input of geniculate origin from area 17, via the posteromedial lateral suprasylvian (PMLS) and posterolateral lateral suprasylvian (PLLS) areas (Grant and Shipp, 1991; Norita et al., 1986; Rosenquist, 1985) The main integrative and distributive centre of the tectal visual pathway may be the Sg, since it receives afferentation and sends efferent fibres from almost every visually responsive structure belonging to this system.

Another centre which receives afferent axons from diverse structures, and thus may serve as an integrator, is the substantia nigra pars reticularis (SNr). Anatomical studies indicate two sets of neural circuits that could transmit visual information from the retina to the substantia nigra (SN). First, visual information might reach this structure through a cortico-striatal route (Saint-Cyr et al., 1990; Norita et al., 1991). Second, the visually active SNr neurons might receive their visual input through direct and indirect tectonigral pathways (Tokuno et al., 1994; Comoli et al., 2003). Comoli et al. (2003) postulated that neurons in both the SN and the ventral tegmental area receive direct tectal inputs. The SC is known to send out efferent projections that terminate in the pedunculopontine nucleus (Redgrave et al., 1987) and in the subthalamic nucleus (Tokuno et al., 1994). Both make direct contacts with neurons in the SN (Lokwan et al., 1999). The basal ganglia circuits that include the subthalamic nucleus could be another source of visual information toward the SN (Jiang et al., 2003). Jiang et al. (2003) raised the idea that this input from the subthalamic nucleus might be of an excitatory nature. Further, the SC sends strong visual efferents to the Sg of the posterior thalamus (Katoh et al., 1995a,b), which in turn provides visual information to the CN (Harting et al., 2001a,b), thereby forming a tecto-thalamo-striatal route. Although the SN receives

predominantly inhibitory inputs from the striatum, an excitatory striatonigral pathway (Rodríguez et al., 2000) may also transmit visual information to the nigral neurons.

The complexity of the network that exists between the above mentioned visually responsive nuclei suggests that the structure itself does not resolve the function of the visual system, but on the contrary: it serves as an underlying universal infrastructure, where the dynamic processing along the numerous different cross talking parallel channels determine together the effect generated by a specific stimulus. This concept explains the functional dependence of the whole system on its previous dynamic state, and supports the role of physiological functional investigations.

2.2.2 Visual response properties of the tectal visual system

There are three aspects of neuronal activity which play a role in information coding and transmission. The current stage of technical development in neuroscience led to the propagation of the reductionist techniques. During neurophysiologic studies usually the frequency code is analyzed; the temporal distribution of the action potentials of a single cell can be characterized from a few different points of view. One can describe the change in the firing rate triggered by some external event, or may average the activity over repetitive trials to eliminate non-stimulus-locked distortions. The analyses of distribution of interspike intervals, or burst activities are also preferred methods. Single unit activity measurements by themselves are inadequate tools to properly describe the gross, generalized properties of a neuronal population; although it is often impossible to measure direct correlation between the consecutive stages of a processing pathway due to technical difficulties (which otherwise might be an optimal way to track the transformation of data).

Those following the holistic approach record and analyze the gross activity of a certain population of neurons. Since traditional electroencephalography is not able to explore deep brain structures in connection with the tectal visual system, usually local field potentials (LFP) recorded through microelectrodes are utilized to obtain information about the population code within a certain volume of tissue. Unfortunately, the analytical tools for LFPs are limited and it is difficult to interpret the results. Moreover, even the estimates of the size of the registered region are disparate, ranging from hundreds of microns to a few millimetres. Despite its weaknesses, the LFP is increasingly used in neuroscience (for an overview see Katzner et al., 2009). In our opinion holism and reductionism has to be regarded as complementary viewpoints. Both are needed to give a proper account of a given system.

2.2.2.1 Physiological issues of information flow between structures – latency introduction

The third aspect of neuronal information transmission in addition to the frequency and population codes is the timing of the activity, which is known as the latency (temporal) code. Estimation of the neuronal response onset latency may provide important data concerning the direction of information flow within the central nervous system (Berson, 1987; Dreher and Sefton, 1979). Despite the fact that the response onset latency comprises a source of information other than the well-discussed properties of neuronal responses, i.e. the neuronal firing frequency, response duration and stimulus threshold, only a small proportion of neuronal recordings are generally analyzed from this aspect, presumably because of the weakness of automated latency estimation methods. In the automation of the estimation of latency a basic problem is to extract a signal from the spontaneous activity, which is determined by environmental and physiological noise. Poisson spike-train analysis is currently the most frequently applied method of latency estimation (Legéndy and Salcman, 1985). The neuronal response onset is calculated by averaging the time positions of a number of arbitrarily chosen bursts in the given trials. The cumulative sum technique (CUSUM) was the first method in which the latency of neuronal responses was calculated via the analysis of peristimulus time-histograms (PSTH) (Ellaway, 1978). The value of this method lies in the detection of change in the mean level of the activity. Since the change in the mean may happen to be small relative to the variation in the individual values, an arbitrary threshold level (usually 1, 2 or 3 standard deviations (SD) above the mean of the spontaneous activity condition) is often chosen to quantify the start-point of the increment in the cumulative sum curve (Ouellette and Casanova, 2006). The CUSUM technique has the weakness that it is not possible to determine precisely which temporal component of the response should be analyzed. Accordingly, Falzett et al. (1985) introduced a combination of the CUSUM technique with a second-order difference (SOD) function.

It is important to note that averaging methods are effective in reducing noise; however, they may lead to false conclusions, especially in the case of recordings with high intertrial variability. First, this method ignores the existing noise in neuronal signal transmission, thus reducing the limit of detectability of stimuli. According to Lennie's concept (1981) averaging of responses on multiple repeated presentations of a chosen stimulus is an artificial technique since brain has no equivalent method. Perception of single occurrence may significantly vary during later perceptions in a continuously repeated stimulus train, and even more from an artificial averaged response. This

concept appears in practice in the case of neurons where the latency variability is high from trial to trial. In these cases averaging may cause the loss of important information (e.g.: the latency variability) or, just on the contrary, produces a well defined latency that never exists in vivo.

Despite the numerous methods proposed, none of them can be applied reassuringly as a universal latency estimation method. Indeed, the estimation of the neuronal response onset latency of structures with high spontaneous activity and weak responsiveness (like the SNr and the CN) is not possible using the above mentioned methods.

2.2.2.2 A general overview of the physiological properties of single-cell activity in the ascending tectofugal visual system

The physiological experiments on the tectal visual system were carried out mainly on anesthetized cats by extracellular single-cell recordings. This visual system differs characteristically from the geniculo-striate one in the following properties: Fibres between structures show heavy convergence, which results in the rapid stage-by-stage enlargement of receptive fields, and loss of their retinotopic organization (Mucke et al., 1982; Benedek et al., 1988; Hicks et al., 1988a,b). The receptive field properties of neurons and responsiveness for visual stimuli are roughly identical in all parts of this system (except the SC), thus it is possible to give a general description about the whole system irrespectively of the region in question (Benedek et al., 1996, 1986; Hicks et al., 1988; Stein & Meredith, 1993). A striking feature of these structures is that they show an overwhelming sensitivity to object motion, while they are less responsive to stationary contrast differences and shapes. Despite of the large receptive fields of these neurons (they cover nearly the whole visual field of the contralateral eye) they prefer small stimuli moving with high velocities in a particular direction (Benedek et al., 1996; Hicks et al. 1988a,b.). Frequency decomposition of preferred stimuli shows that the spatial and temporal frequency preferences of the tectal system are clearly different from those in the geniculo-striate one. The neurons in the ascending tectofugal system responded optimally to gratings of low spatial frequencies and exhibited low spatial resolution and fine spatial frequency tuning. On the other hand, these neurons preferred high temporal frequencies, and exhibited high temporal resolution and fine temporal frequency tuning. The spatial and temporal visual properties of these structures enable them to serve as spatiotemporal filters in the low spatial and high temporal frequency domain. Another interesting aspect of the tecto-thalamo-cortical system is its sensitivity for multiple sensory modalities, which gives

additional support to the theory that it is involved in the control of sensory guided eye movements (Hikosaka and Wurtz, 1983). Increasing amount of evidence suggests that its exact role might be the adjustment of the motor behaviour to the changes of the environment (Mucke et al., 1982; Wang et al., 1998).

2.2.3 Sensory-motor integration along the visual system: visual perception and related saccadic responses

The conscious brain is continuously bombarded by an enormous amount of information reflecting the whole environment. To selectively handle the relevant events, an effective filtering is required to reduce the mass of incoming data. In visual perception, a first-step filtering happens due to the anatomical heterogeneity of the retina. Since the photoreceptor density (and thus the resolution) is higher with orders of magnitude in the fovea than on the periphery, those objects which are projected onto the fovea are extremely overrepresented in the received information mass. The adjustment of this filter is carried out by orienting the eyes in order to track the most salient objects in space. This process is called foveation, which is maintained by six independent control systems. Although the fovea develops only at the primate stage of mammalian development, the orientation of attention is similar in carnivores too. In the future we'll refer to this process as foveation. Saccadic eye movements shift the fovea rapidly to a visual target in the periphery. Smooth pursuit movements keep the image of a moving target on the fovea. Vergence movements, vestibulo-ocular movements, and optokinetic movements help holding images in focus during dislocations. The sixth system, the fixation system helps holding the eyes in a constant position by an active suppression of the aforementioned systems. The main structures involved in controlling saccades and pursuit eye movements are the frontal eye field (Br. 8), the CN, SC, SNr, and the oculomotor centres. This means that many components of the oculomotor system, as a member of the tectal visual system, contribute in visual sensory information processing.

The role of the SN in visually-guided saccades was extensively studied by Hikosaka and Wurtz (1983), who described the activity of GABAergic neurons in the SNr in the saccades of behaving monkeys, reporting that these units responded with an inhibitory response to stationary visual stimuli. Their work established the saccade-initiation theory (Wurtz and Hikosaka, 1986), which assumes that suspension of the tonic inhibitory GABAergic activity of the SNr over the SC might be an initiative permissive step toward a consequent saccadic eye movement. These findings

were later extended by the observation of the increased activity of the GABAergic SNr cells in response to visual stimulation (Magariños-Ascone et al., 1994; Handel and Glimcher, 1999) and of the responsiveness of the SNr to moving visual stimuli (Schwarz et al., 1984; Nagy et al., 2005a,b, 2006). The more vigorous responses to moving stimuli are not surprising, since the drifting of an object in space is a more natural stimulus than the appearance or disappearance of a static spot. To drive the gaze and hence the attention toward the unexpected movement, and keep it focused, a motion-dependent forecasting of the trajectory of the object is needed, with resultant elimination of the deficit caused by the latency in eye positioning.

3 Aims of the study

The aim of our experiments was to investigate the information flow in the ascending tectofugal visual system, in order to achieve a better understanding of its functional role in motion analysis, and in visuomotor processes. Our specific aims were as follows:

1. To record activity from visually active neurons in the structures of the ascending tectofugal system (SC, Sg, AES cortex and CN). .
2. To describe the visual responsiveness of neurons in the SNr to moving visual stimuli
3. To develop a reliable automated latency estimation technique, and to validate it on a large dataset
4. To analyze the way of information flow in specific bidirectional pathways, with the help of latency estimation, temporal modulation analysis and receptive field study
5. To develop a hypothesis on the role of the ascending tectofugal system in oculomotor control.

4 Materials and Methods

4.1 Animal preparation and surgery

The experiments were carried out on 10 adult cats of either sex weighing from 2.5 to 4.0 kgs. All procedures were carried out in a way that allowed us to minimize the number of the animals, and strictly followed the European Communities Council Directive of 24 November 1986 (86/609 ECC) and the National Institutes of Health Guidelines for the Care and Use of Animals for Experimental Procedures. The experimental protocol had been accepted by the Ethics Committee for Animal Research at the Albert Szent-Györgyi Medical and Pharmaceutical Center of the University of Szeged.

The anaesthesia was initiated with ketamine hydrochloride (30 mg kg^{-1}, i.m.). After cannulation of the femoral vein and the trachea, the animals were placed in a stereotaxic headholder. The wound edges and pressure points were treated regularly with procaine hydrochloride (1%). The anaesthesia was continued with halothane (1.6% during surgery and 1.0% during recordings, the MAC level of halothane being held between 1 and 0.5). The depth of anaesthesia was monitored by regular inspection of the pupil size, and by the examination of electrocorticogram and electrocardiogram recordings. The animals were immobilized with gallamine triethiodide (Flaxedyl, 20 mg kg^{-1}, i.v.). During the experiment, a solution containing gallamine (8 mg $(kg\ h)^{-1}$), glucose (10 mg $(kg\ h)^{-1}$) and dextran (50 mg $(kg\ h)^{-1}$) in Ringer's solution was infused continuously at a rate of 3 ml $(kg\ h)^{-1}$. Atropine (0.1%, 0.2 ml, s.c.) and ceftriaxone (Rocephin, 40 mg $(kg\ day)^{-1}$, i.m.) were administered regularly. The end-tidal CO_2 level and the rectal temperature were monitored continuously and kept constant at 3.8–4.2% and 37–38 °C, respectively.

4.2 Recording and stimulation

Electrophysiological single-cell recordings were performed extracellularly with parylene-insulated tungsten microelectrodes (AM System Inc., 2 MΩ). Vertical penetrations were performed in the SN between Horsley-Clark coordinates anterior 4-7, lateral 4-6 at a stereotaxic depth between 4 and 7. The GABAergic SNr neurons were selected on the basis of the duration of their action potentials and their spontaneous firing rate (Ungless et al., 2004). Further recordings were carried out from the NC (Horsley-Clark coordinates: A:12-16, L:4-6.5, D:12-19), from the AEV (Horsley-

Clark coordinates: A:11-14, L:12-14, D:13-19) and from the Sg of the posterior thalamus Horsley-Clark coordinates: A:4.5-6.5, L:4-7, D:10-13. Individual action potentials were selected either with the help of a data acquisition system (SciWorks Datawave system) or with a spike-separator system (SPS-8701; Australia). The number and temporal distribution of the action potentials recorded during visual stimulations were stored for off-line analysis (sampling rate: 20 kHz) and were visualized as PSTHs.

In order to estimate the response characteristics of GABAergic SNr neurons we chose a very simple stimulus for visual stimulation, which provides a high contrast ratio, and whose parameters are easy to quantify: moving contrast spots were projected onto a tangent screen (LCD projector, refresh rate 100 Hz; resolution 1.280x720 pixel; contrast ratio: 1.300:1; response time: 8 ms) centred on the area centralis and positioned at a distance of 57.3 cm from the eye of the animal. The extents of the visual receptive fields of the neurons were estimated subjectively by listening to the neuronal responses to the movements of a light spot generated by a hand-held lamp. The stimulated area covered almost the whole visual field of the contralateral eye. The diameter of the contrast spot was 1° or 5°. A standard stimulus set of 80 stimulus parameter combinations was used to test the visual responsiveness of the single neurons; we moved each contrast spot to eight different directions of the projected space (0-315° in 45° increments), with 5 different velocities (5, 20, 40, 80 and 160°/s). For each recorded neuron, each stimulus combination was presented at least 10 times. In each trial the prestimulus time of recording (without visual stimulation) was 1000 ms, as was the peristimulus time (a moving visual stimulus was shown).

For response modulation analysis, an 18-inch computer monitor (refresh rate, 85 Hz) was placed 42.9 cm in front of the animal. The diameter of the stimulation screen was 22.5 cm, and the cat therefore saw it under 30° (if the stimulus diameter on a tangent screen is 22.5 cm and the distance between the eye and the centre point of the screen is 42.9 cm the viewing angle of the stimulus is 30 degrees). The mean luminance of the screen was 23 cd/m^2. In order to investigate the spatiotemporal characteristics of the neurons, high-contrast (96%) drifting sinusoidal gratings were used. The sinewave gratings were moved along four different axes in eight different directions (0–315° at 45° increments) to find the preferred (optimal) direction of movement for each unit. This optimal direction of was further used to describe the spatial and temporal response characteristics of the neuron. The tested spatial frequencies ranged from 0.025 to 0.4 cycles/degree (c/°) and the temporal frequencies from 0.07 to 37.24 cycles/s (Hz).

4.3 Analysis of recorded data

4.3.1 Estimation of visual receptive fields

The extent of the visual receptive field was determined subjectively by listening the neuronal activity to moving a light spot generated by a handheld lamp. To qualitatively assess the responsiveness within the receptive fields we divided the receptive fields into several subparts (12-20 parts), and projected systematically the preferred stimulus of each neuron over these subparts. At each stimulus site the net firing rate was calculated to quantify the responsiveness as a difference between the peri- and prestimulus activity.

4.3.2 Latency estimation of neuronal responses

The method presented here was specifically developed for the analysis of neuronal activity stored in PSTHs (Eördegh et al., 2005). The original temporal resolution of the recorded data was 1 ms, which was converted to a 5 ms bin width for faster processing. Each PSTH consisted of a prestimulus interval and a peristimulus interval. The prestimulus interval contains the genuine spontaneous activity of a neuron, while the peristimulus interval contains both the spontaneous activity and the responses of a neuron to the stimulation. The duration of the spontaneous activity in the peristimulus interval defines the onset latency of the neuronal response.

4.3.2.1 Response onset allocation via the t test

The first element of this computational method is a double sliding-window technique with repetitive application of t test of dependent samples. A computer program slides two virtual time windows with specific width along the frequency histogram of the activity. The first window called the reference window, slides through the peristimulus histogram in 1 bin steps (5 ms in our analysis), and that portion is selected that represents the maximum frequency (or the minimum frequency if an inhibitory response is investigated) of the peristimulus interval, using a simple sum function (Fig. 2a). The content of this window is declared to be the ‘pure response’ and is applied later as a reference in the t test. The importance of the accurate definition of the length of this reference window is understandable, since too narrow a window may not compensate for the frequency variability inside the response, while too broad a window may include pure spontaneous activity in addition to the responses.

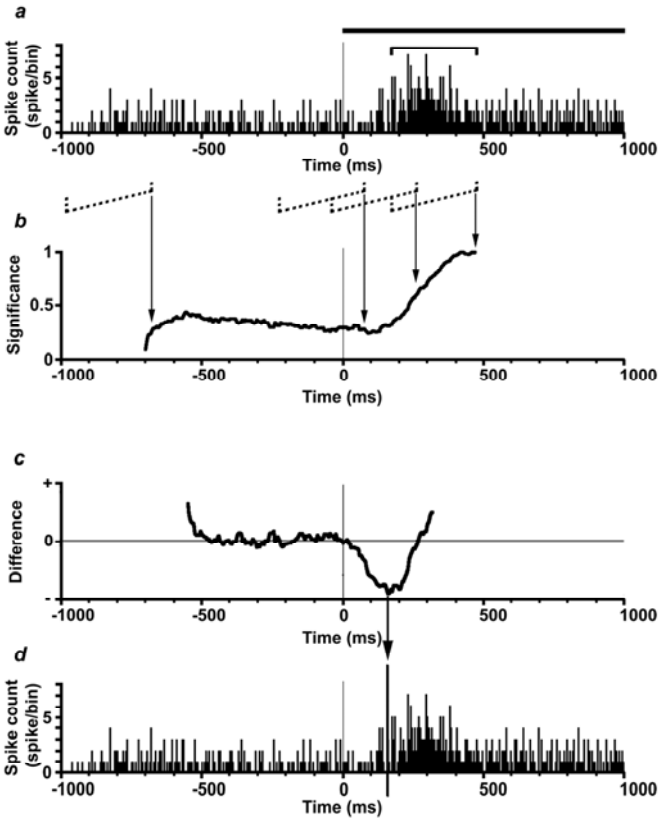

Figure 2.: Estimation of neuronal response onset latency with the double sliding-window technique. **(a)** Peristimulus time histogram (PSTH) of an excitatory neuronal response. The duration of visual stimulation is indicated by a thick horizontal black line above the PSTH. The solid black clamp above the PSTH denotes the position of the reference window. **(b)** Significance curve calculated by the series of t tests. sample windows corresponding to different activity levels of the neuron are indicated by dotted clamps. The ordinate denotes the result of the series of paired t tests between the activity in the reference window and the activity within each step. **(c)** Curve of the second-order difference function (SOD) derived from the significance curve (n = 30). The ordinate demonstrates the positivity or negativity of the SOD results. The minimum point of this curve coincides with the maximum slope change of the significance curve, and thus approximates to the onset of the neuronal response. **(d)** PSTH with marked response onset (thick vertical line). Accordingly, the visual response onset latency of the demonstrated neuron was 160 ms.

A second window, called the sample window, slides from the beginning of the prestimulus period (pure spontaneous activity) to the position of the reference window in 1 bin steps. For each 1 bin step, a paired t test is carried out between the spike rate of the reference and the sample windows, and the level of significance (p value) calculated from the t value is stored and plotted on a graph. This method calculates the similarity between a reference window containing a pure neuronal response and a moving sample window, which at the beginning of the evaluation contains only pure spontaneous activity; later it contains both spontaneous and stimulated activity; and finally only pure stimulated activity is present. Initially, when no response occurred inside the sample window, the similarity is minimal (the significance level is low). Afterwards, the sampling window slides into the response period, finally reaching total equivalence (significance level 1) as the two windows overlap each other. A curve is fitted to the p values, in a theoretical case this being a sigmoid curve (Fig. 2b). The time interval between the start of the stimulation and the first point of the ascending segment of this curve provides the response onset latency.

4.3.2.2 Estimation of the onset of elevation

When a response occurs, the significance curve mentioned above no longer fits to one straight line, but consists of several linear segments, each with a different slope. Each segment of the curve produced by the sliding-window function describes a different period of the neuronal activity, and the slope of each segment gives an estimate of the change in the neuronal discharge rate during that segment according to the fixed reference window. In Fig. 2b, the first segment represents pure spontaneous activity, while the second component represents the time segment when the sample window slides onto the response period and contains spontaneous activity and also neuronal responses. Finally, the third segment represents the stage when the sample window clearly overlaps the response. The slope of the second segment is steeper than that of the first, indicating a 'positive conformity change' between the two window contents. The elevation of the significance curve is indifferent as far as the direction of the neuronal discharge rate change is concerned, thus our method can be used to estimate the onset latency of both excitatory and inhibitory neuronal responses. To estimate the latency quantitatively, a second order difference function (SOD) is calculated from the sliding-window function to determine the first point of the elevating segment of the significance curve. The aim of this function is to locate breaks and discontinuities between linear segments. Eqn. (1) is used to produce such a function according to Falzett et al. (1985):

$$SOD_{(t)} = \quad |(X_{(t-n)} - X_{(t)})| \; - \; |(X_{(t+n)} - X_{(t)})| \qquad (1)$$

where X = the significance level; t = the actual time component of the function; and $n = \Delta t$, an arbitrary time offset. $SOD_{(t)}$ is computed for each point on the significance curve (Fig. 2c).

A zero value of this difference function means that no change occurs in the steepness of the observed curve in the vicinity of moment $X_{(t)}$. The peaks in the SOD curve furnish estimates of the positions of maximal slope change, and thus define the endpoints of each linear segment. The latency of the response can be calculated by subtracting the time of the stimulus onset from the minimum in $SOD_{(t)}$.

In order to eliminate sporadic disturbances in measurement (estimation imprecision in the case of a single n value), the method calculates the response onset latencies as a median of 25 measurements per registration, using 25 selected different parameter combinations that provided the most accurate latencies for our data sample (4 different window widths from 150 to 300 ms, and the corresponding highest possible n values of SOD; Fig. 7a).

For the cell shown in Fig. 2, the maximum possible *n* offset of SOD function (30 bins) was applied (which is equal to half of the t test window width (300 ms, 60 bins) as otherwise the SOD function may run out of the range of the t test results), because this value produced a relatively smooth SOD with well-defined peaks., The analysis began with the 31st point of the significance curve (t = 31; n = 30), and the difference between the 30 locations neighbouring points and the original point was computed ($SOD_{(31)} = |(X_{(1)} - X_{(31)})| - |(X_{(61)} - X_{(31)})|$). The next point of the significance curve to the right of point 31 was then selected and the process was repeated until the entire difference curve had been generated.

4.3.2.3 *Validation of the double sliding-window technique; comparison of effectiveness to other methods*

Subjective visual latency estimation was performed independently by three experienced neurophysiologists (G.B., A.N. and A.B.). The mean of the three quantified latencies was regarded as the as gold standard during the comparison, and estimation error (EE) was calculated for each latency by different techniques applying the following equation:

$$EE = | L_t - L_s | \qquad (2)$$

where L_t is the onset latency acquired by the automated latency estimation method used, and L_s is the visually quantified gold standard value.

The EE results did not indicate a normal distribution according to the Lilliefors test ($p < 0.01$), and the Wilcoxon test for correlated samples was therefore used to compare the EE results of the different calculation methods.

4.3.3 Analysis of temporal frequency modulation of responses – an alternative way to map the hierarchical organization of the tectal visual system

A majority of the CN and AEV neurons exhibited a modulated response to the drifting gratings. For technical reasons and in order to obtain data that could be compared with the findings of our previous studies in the Sg (Paróczy et al., 2006), the SC; (Waleszczyk et al., 2007) and the AEV (Nagy et al., 2003a), we consistently centred the stimulation monitor on the area centralis and stimulated a large central part (with a diameter of 30°) of the receptive fields. The relative modulation index (MI) was calculated as the ratio of the amplitude of the response component at

the fundamental (i.e. the stimulus) temporal frequency (f_1) and the net response of the cell (f_0) (Movshon et al., 1978):

$$MI = f_1/f_0 \quad (3)$$

MI was calculated only for the modulated responses with a clear peak in the spectrogram at frequency f_1. We regarded a spectrogram value at frequency f_1 as a peak when it exceeded the mean amplitude along all of the frequencies in the spectrogram by at least one standard deviation (SD). We applied the procedure of finding peaks to spectrograms averaged over 12 responses to a stimulus with given parameters MI = f_1 / f_0

4.3.4 Analysis of stimulus preference of SNr

4.3.4.1 Estimation of response strength

The data were analyzed with the MATLAB® software (The Mathworks Inc). Since the responses of the SNr neurons to visual stimuli in the anesthetized cats were usually weaker than those of other visually responsive structures in the extrageniculo-extrastriate visual system, and since in some cases we found consecutive increases and decreases in their activity, the commonly used t-test between the pre- and peristimulus periods was not fit to describe the responsiveness correctly. To obtain a parameter which reliably estimates the effect of the applied stimulus over the activity of a neuron on the basis of a relatively low number of recorded trials (due to the numerous conditions), we tested the responses in overlapping narrow time windows with the help of the Kolmogorov-Smirnov (KS) test (Fig. 3). While all of the prestimulus periods during the whole recording of a neuron contained the spontaneous activity, we handled them as a common dataset of the spontaneous activity. Neurons with inhomogeneous spontaneous activity (bursting, fluctuations, etc.) were excluded from the analysis. Two hundred sequences of 200 ms were randomly selected from this dataset, and the firing rates of each 200-ms-long segment were calculated. In the second step, the firing rates in each stimulus combination were estimated separately. The firing rate of each 100-ms-long sequence (with 50% overlap) within the peristimulus period was compared with the previously created dataset (which represented the spontaneous activity) by using the KS test. Those 100-ms-long sequences of the peristimulus time were defined as responses for which the KS test revealed a significant difference from the spontaneous activity. To quantify the strength of a response, we summed the net firing rates (the difference of the stimulated firing rate and the spontaneous firing rate) during the significant sequences of the peristimulus intervals.

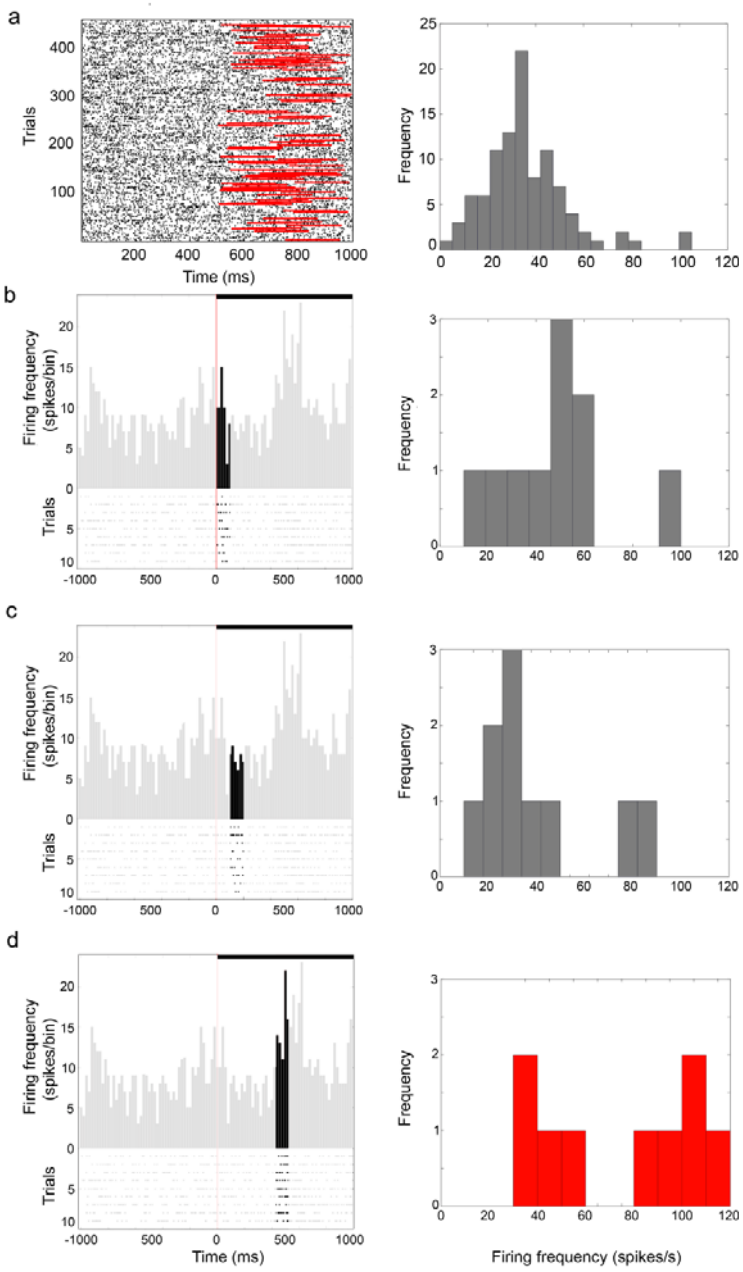

Figure 3.: Analysis of the visual responsivity of SNr neurons.
(**a**) The left panel depicts the raster plot of the spontaneous activity of a SNr neuron across the recorded 480 trials, each 1,000 ms long. The representative dataset for the spontaneous firing rate of the investigated cell are indicated by red lines. The distribution function of this dataset can be seen in the right panel, where the abscissa defines the firing frequency ranges, and the ordinate the frequencies of occurrence of these ranges; (**b, c**) highlight two 100-ms-long segments of the neuronal activity during visual stimulation. The left panel shows the peristimulus time-histogram (PSTH) of a neuron. The time scales are presented on the abscissas (ms). The duration of visual stimulation is denoted by the thick horizontal black line above the PSTH. The ordinates demonstrate the cumulated spike counts in each 25-ms-wide bin. Below the PSTHs, the raster plots of the activities of the 10 trials are delineated. The unshaded part denotes the 100-ms-long segment of the response from which the distribution function in the right panel is calculated. The Kolmogorov-Smirnov test indicates that these distributions in parts b and c are not significantly different from the distribution of the spontaneous activity (part a, right panel); (**d**) depicts a part of the PSTH which contains a visually induced neuronal firing frequency increase; in this segment, the distribution of the firing rates differs significantly from that of the spontaneous activity.

The KS test combined with the calculation of net firing rates proved to be an effective tool for estimation of the strength of a response, because it eliminates the disturbances caused by non-consequent burst-like activities among trials, and also gives a reliable quantification of the strength. We tested our estimation method on numerous negative control recordings, and also on earlier well-characterized neuronal data.

4.3.4.2 Objective classification of response types via artificial neuronal networks

To visualize the stimulus preference of each neuron, two-dimensional colour-coded maps were constructed, where the axes represent the independent stimulus parameters, and the colour scale denotes the responses to the different parameter combinations (Fig. 10). After visual inspection of the response characteristics, we classified the SNr neurons into 8 different tuning types (for details, see the Results section). To classify the recorded neurons into the hypothesized classes, we used an artificial neural network containing 40 joints as an input layer and 10 joints as an output layer (representing the 10 different hypothesized classes), together with 3 hidden layers, each with 400 neurons. The output layer was adjusted to have a log-sigmoid transfer function, and thus the response value of each output component was in the range between 0 and 1. Resilient back-propagation as a self-learning algorithm was embedded in the system, and this method therefore gives the possibility for a properly trained network to recognize correctly inputs they have never seen before. To train the network, we generated artificial response characteristics (40-100 of each tuning type) and presented them to the network over several hundred epochs until the recognition error limit criterion (mean squared error < 10^{-5}) was met. After the training session, the real data for each recorded SNr neuron were presented, and the network provided 10 values representing the probability of fit into the 10 different types of tuning characteristics. The schematic build-up of this artificial neural network is outlined in Fig. 4.

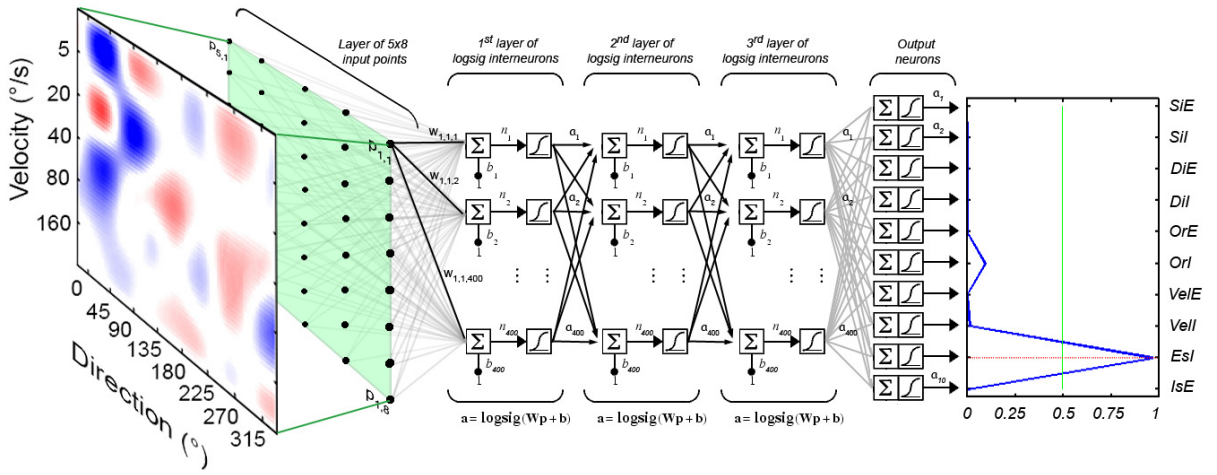

Figure 4.: Scheme of the artificial neural network used for response profile classification.
The figure demonstrates the input dataset containing the response map of a recorded neuron, the layers of the artificial neural network, and the response characteristic profile produced by the network. The colour coding and the conventions are the same as in Figs. 10 and 11. For a detailed explanation of the tuning of artificial neural layers, see the text.

For each automated classification result, we calculated the confidence value as:

$$V_c = 1 - \frac{p_2}{p_1}, \tag{4}$$

where V_c is the calculated confidence value, while p_1 and p_2 denote the probability of the first and second most probable class type, respectively. We accepted a result as well-classified if the probability of the primary class was > 0.5 and its confidence value was also > 0.5.

4.4 Histological control of recording sites

At the end of the experiments, the animals were overanesthetized with pentobarbital (200 mg kg^{-1}, i.v.) and transcardially perfused with 4% paraformaldehyde solution. The brains were removed and sliced into coronal sections of 50 µm. The sections were stained with Neutral Red. The positions of the recorded neurons were identified on the basis of the electrode tracks, and their depths recorded during the experiment were related to the surface of the investigated structure. The position of the uppermost neuron of the given structure (as distinguished from the surrounding structures by considering firing rate) was defined as the dorsal surface of the structure. This was later verified on the basis of the stereotaxic brain atlas of the feline brain.

5 Results

5.1 Visual receptive field properties and coding of spatial visual information

The borders of the receptive fields in each investigated structure were approximated subjectively by listening to the neuronal responses evoked by movements. The extent of visual receptive fields in the Sg, the AEV, the CN and in the SNr were similar: they were extremely large compared to the common receptive field sizes in the geniculo-striate visual system, consistently larger than 1.8 steradian (6000 degree^2). We found that these receptive fields covered a major part of the contralateral hemifield and extended deep into the ipsilateral one, yielding a field that overlapped almost totally the visual field of the contralateral eye (Nagy et al., 2003b, 2005a,b). The receptive fields consistently included the area centralis. No signs of retinotopical organization were observed within either of these structures. The absence of classical topographical organization suggests an alternative coding of spatial visual information in the above mentioned structures. Spatial sensitivity investigation within the Sg, the AEV and the CN demonstrated that the single-cells exhibited different responses to visual stimulation deriving from different parts of their large receptive field. This means that these neurons could code the position of the visual stimulus in their discharge rate. Thus they can serve as panoramic localizers. Moreover, the maximum responsiveness within the visual receptive fields of the AEV, the Sg and the CN neurons varied extensively in the neurons recorded. Some of the units exhibited a preference for a particular stimulus site, while other units were most responsive to other locations. The maximally sensitive sites of the CN neurons, similarly to those of the Sg and the AEV were distributed over the whole visual filed of the investigated eye. Thus, in contrast to the geniculo-striate pathway where the area centralis is overrepresented, there is no such a distinguished part of the visual field in the ascending tectofugal visual system (Fig. 5). We suggest that there should be a distributed population code of spatial visual information in the ascending tectofugal system where populations of maximally active neurons can accurately code the position of the visual stimuli.

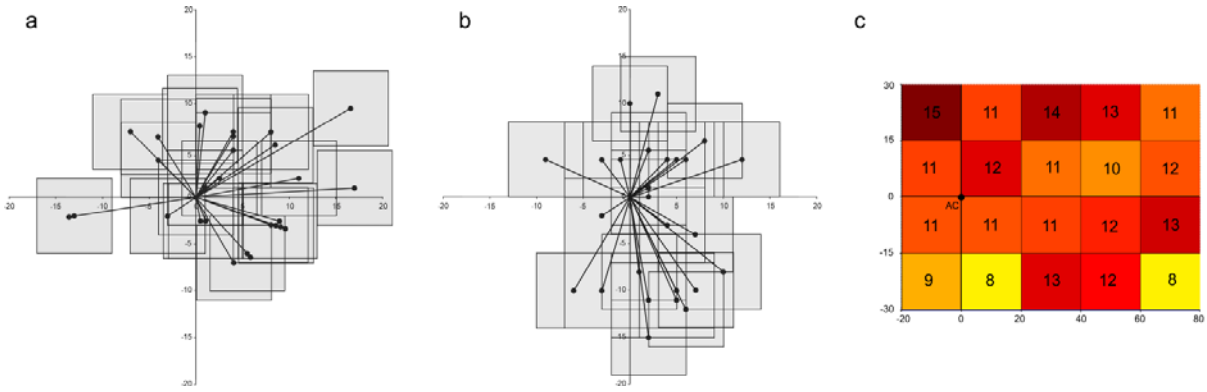

Figure 5.: Position of the site of maximum responsivity in the receptive fields of 32 AEV single-units **(a)**, 35 Sg single-units **(b)** and 228 CN neurons **(c)** determined by the highest firing rate in the respective window. On part a and b every single-unit is represented by an 8°×8° grey window representing the motion of the stimulus and a vector line between the area centralis and the centre of the "window" from where the highest activity was elicited. On part c the distribution of maximal responsive sites are colour coded, and the numbers of single-units preferring each specific location are marked within each stimulated rectangle. Vertical and horizontal meridians are presented as thick lines, with scaling given in degrees.

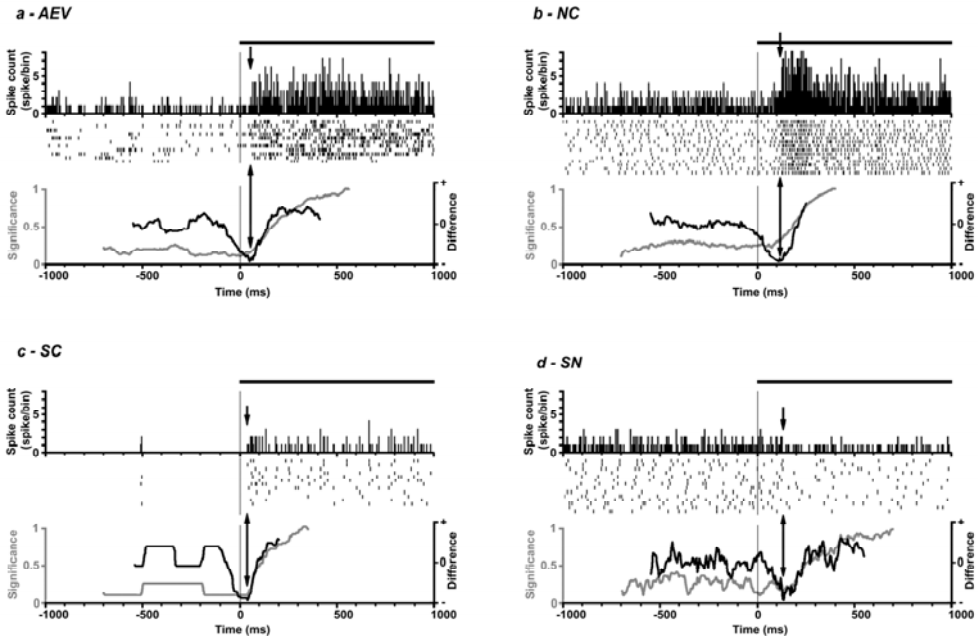

Figure 6.: Application of the double sliding-window technique.
Calculation of the visual onset response latencies of excitatory neuronal responses in the anterior ectosylvian visual area **(a)**, the caudate nucleus **(b)** and the superior colliculus **(c)**, and an inhibitory response in the substantia nigra pars reticulata **(d)**. Each part contains the summed neuronal activity in the form of PSTHs (uppermost part), the trial-by-trial activity in raster form (each row visualizes one trial, where each small dash means one neuronal excitation; middle part) and the two calculated curves (lower part), the significance (gray) and the SOD curve (black). The arrows show the minimum point of the SOD curve that depicts the neuronal response onsets. The conventions are the same as in Fig. 2.

5.2 Effectiveness and validity of the double sliding-window technique

A total of 681 extracellular single-unit recordings (PSTHs) were analyzed using the double sliding-window technique. All these PSTHs were selected from our earlier recordings following two criteria: the PSTH was to demonstrate a significant neuronal response to visual stimulation, and it had to be possible to estimate the response onset latency by subjective visual estimation. Latencies were calculated for each neuronal response subjectively by visual evaluation and by using the double sliding-window technique with 135 different parameters (10 different window widths, from 10 to 100 bins, and the possible corresponding n values in the SOD function, from 2 to 50; Fig. 7a). Figure 6 depicts the characteristics of three different excitatory (Fig. 6a-c) and one inhibitory (Fig. 6d) neuronal response, with their corresponding significance levels and the SOD curves returned by the latency analysis. The automatically determined response onsets are indicated by vertical arrows.

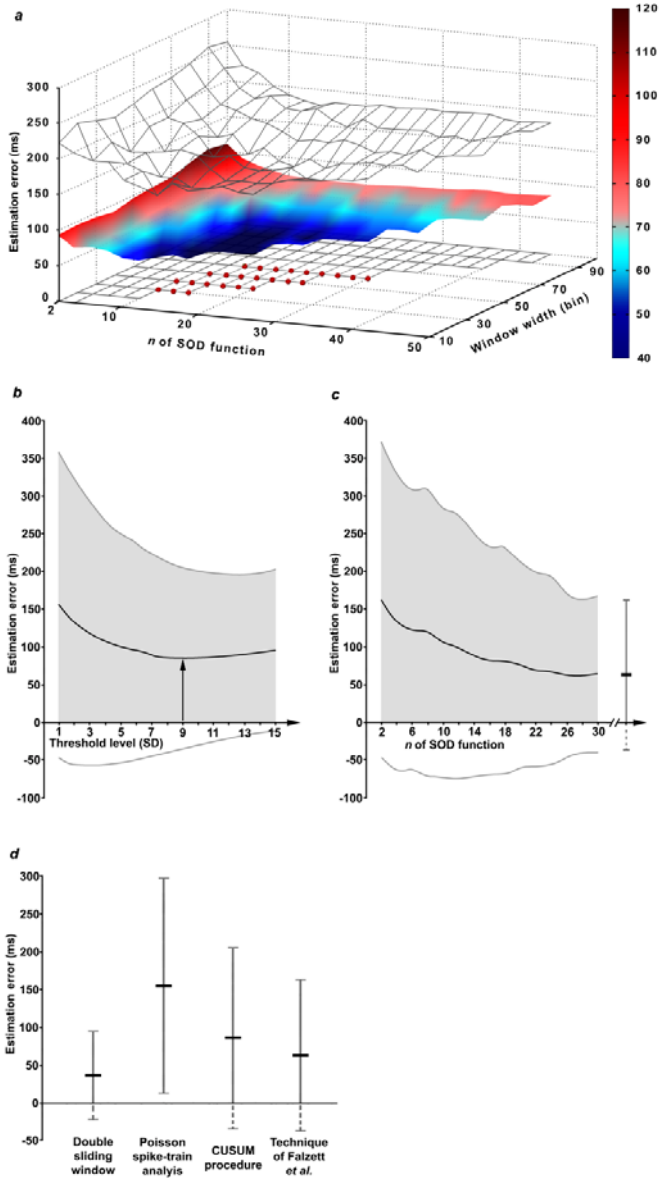

Figure 7.: Effectivities of the four investigated latency estimation methods.
The double sliding-window technique **(a)** was tested by using 135 different parameter combinations on 681 extracellular single-unit recordings. A solid colour-shaded surface was constructed from the means of the estimation errors (EEs) of the 681 neurons as a result of using each 135 parameter combination; the ±1 SD range is marked with the two meshes. The parameter combinations that were constantly used to calculate the mean of the medians of the EEs (see part d) are marked with red dots. The CUSUM method **(b)** was also tested on the same 681 recordings using 15 different threshold values. The technique of Falzett *et al.* **(c)** was tested with 15 different SOD values on the same dataset. The mean of the medians of the EEs is indicated as a discrete range on the right side of the graph. **(d)** Comparison of the effectiveness of the four latency estimation methods, using the most accurate parameter(s) for each method. The ordinate shows the EEs in ms. Thick horizontal lines denote the mean EE, while the whiskers show the ±1 SD EE range for each method.

The difference between the subjectively determined latency and the latency estimated by using the double sliding-window technique was defined as the estimation error (EE) of a measurement. If the n value was higher than a limit (10-12) and the window width was in an appropriate range (30-60 bins) there was not a significant difference between the computed EEs (Fig. 7a). Further, calculation of the median of the acquired onset latencies by using the highest mathematically possible n values with different window widths furnishes higher internal stability, this smoothing leading to the most accurate onset latencies. The use of the median instead of the mean to estimate the central tendency is more accurate in this case, since sporadic disturbances in a dataset (estimation inaccuracy for a single n value) distort the final latencies less. The mean of the medians of the EEs when the double sliding-window technique was used was 35.98 ms (N = 681; SD: ±58.48 ms).

5.2.1 Response onset latency estimation with other automated methods

The visual response onset latencies of the same 681 neuronal recordings (PSTH) were also estimated by using Poisson spike-train analysis, the CUSUM method and the extension described by Falzett et al. (1985). In some cases, Poisson spike-train analysis estimated the response onset before the onset of the stimulus. We excluded these data from our comparison (none of the other methods could provide 'negative' latencies for technical reasons). The mean EE of the Poisson spike-train analysis was 154.41 ms (N = 576; SD: ±141.81 ms; Fig. 7d).

In CUSUM analysis, 1, 2 or 3 SDs above the mean spontaneous activity is usually used as the threshold level for this process (Ouellette and Casanova, 2006; Butler et al., 1992). We found that this method tested with 1-3 SDs thresholds consistently underestimated the latencies. We therefore tested our dataset with 15 different SD parameters (the threshold was varied in the interval 1-15 SDs). The most accurate latencies and therefore the smallest EE could be calculated by using 9 SDs as threshold. Below and above this threshold, the EEs were higher (Fig. 7b, 7d). The mean EE with the most accurate (9 SDs) threshold was 85.26 ms (N = 681; SD: ±120.11 ms).

The method of Falzett et al. combined the advantages of the CUSUM process with the same SOD function as used in our double sliding-window technique. Figure 7c illustrates the mean EEs on the use of different n values of the SODs. Similarly, like the double sliding-window technique, the method of Falzett et al. provides the most accurate response onset latencies when high n values are used (n > 22; Fig. 7c, 7d). The median calculation of the acquired onset latencies using different high n values (n = 22-30) provided the most accurate values. The mean of the medians of the EEs by the method of Falzett et al. was 62.87 ms (N = 681; SD: ±99.98 ms).

5.2.2 Comparison of the confidence of the double sliding-window technique with Poisson spike-train analysis, the CUSUM procedure and the method of Falzett et al.

Since the EE datasets did not reveal a normal distribution, we used the Wilcoxon test for the correlated samples to compare the effectiveness of the double sliding-window technique with that of Poisson spike-train analysis, the CUSUM procedure and the method of Falzett et al. The distributions of the EEs observed when the four investigated techniques were used are presented in Figure 7d. The double sliding-window technique appears to be the most accurate automated latency estimation method in the sense that the EE provided by this technique (mean: 35.98 ms; N = 681; SD: ±58.48 ms) was significantly smaller (in all cases $p < 0.01$) than those resulting from Poisson spike-train analysis (mean: 154.41 ms; N = 576; SD: ±141.81 ms), the CUSUM procedure (mean: 85.26 ms; N = 681; SD: ±120.11 ms) and the advanced method of Falzett et al. (mean: 62.87 ms; N = 681; SD: ±99.98 ms).

5.3 Latencies of visual responses along the extrageniculo-extrastriate pathway

To decide whether the cortico-thalamic or the tecto-thalamo-cortical route has the dominant role in the transmission of visual information to the Sg and the AEV, we compared the visual response latencies of 35 Sg and 32 AEV neurons. Response latency values were calculated with the help of the new double sliding-window technique. The shortest latency in both the Sg and the AEV was similar (35 ms). Statistically, however, the latencies of the responses measured for the AEV units were longer than those for the Sg units. The mean response latency of the Sg neurons (calculated at their maximally responsive sites) was 59.4 ms (N= 35; range: 35–130 ms; S.D.: ± 26.28 ms). The mean latency of the AEV units was 81.7 ms (N= 32; range: 35–185 ms; S.D.: ±42.48 ms).

The distribution of the latencies in the AEV did not reveal normal distribution, presumably reflecting the fact that there is no homogeneous population of units producing this response, and the cortical afferents of these neurons may substantially modify their responsivity by mean of both timing and frequency. Comparison of the cortical and thalamic latencies by the Kruskal–Wallis test revealed that the visual response latencies of the investigated Sg neurons were significantly shorter than the visual response latencies of the AEV neurons ($p = 0.011$).

5.4 Temporal frequency modulation of responses in different structures

Of 89 CN cells the responses of 64 (72%) were considered to be modulated by the applied temporal frequency of the sinusoidal gratings (see Methods, Fig 8a), with clear peaks in the spectrograms at the fundamental frequency f1 derived from the Fourier transforms of the PSTHs (Fig. 8b). MI was calculated for the maximal responses (to the optimal stimulus) of each neuron that displayed a modulated response. The mean MI was 1.12 (N = 64, SD: ±0.79, range: 0.38–5.1). Twenty-eight CN cells were strongly modulated, with MI > 1.0. Figure 8c represents a CN neuron with non-modulated responses.

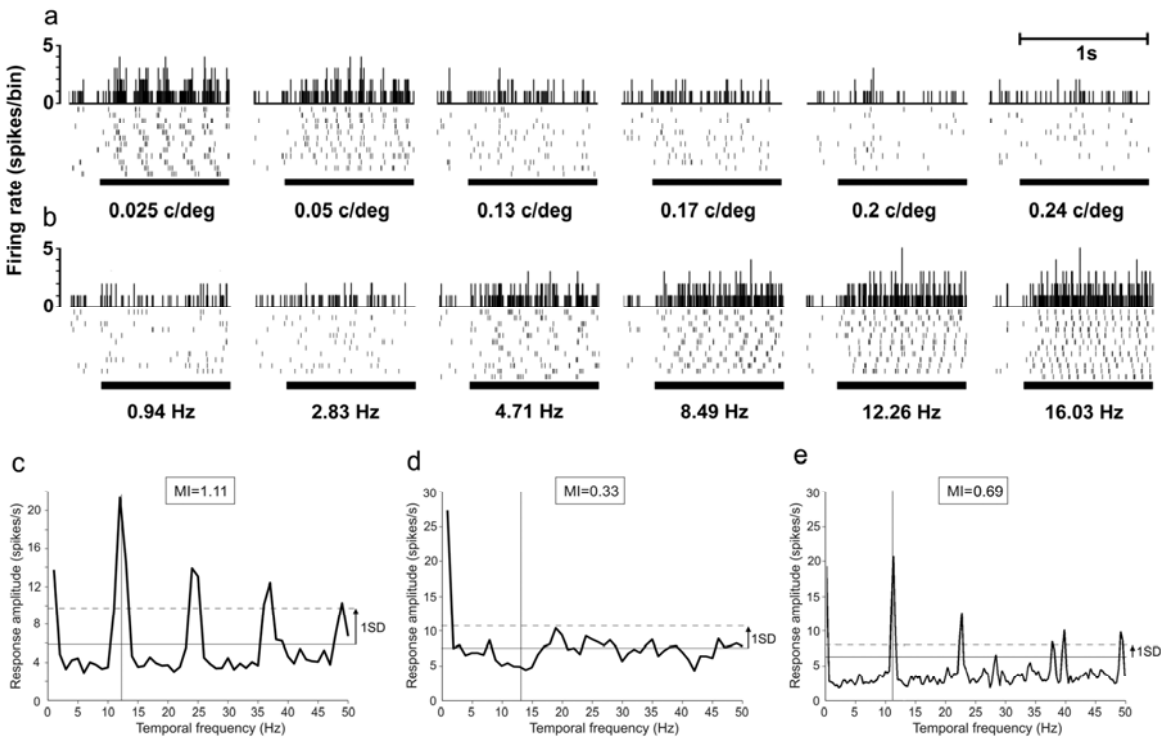

Figure 8.: Examples of modulated responses.
(a) Responses of a CN neuron to six different spatial frequencies (temporal frequency was constant at 5.66 Hz). **(b)** Responses of the same CN neuron to six different temporal frequencies (spatial frequency was constant at 0.025 c/°). Corresponding spatial or temporal frequencies of the sinusoidally modulated drifting gratings are shown under the PSTHs. The ordinate denotes the discharge rate (spikes per bin). The thick black lines under the PSTHs indicate the duration of the stimulation. Averaged spectrograms for CN neurons responding with modulated **(c)** or unmodulated **(d)** activity and for a typical modulated AEV neuron **(e)** are calculated with Fourier transformation. The modulation indices are presented in boxes above the spectrograms. The solid horizontal line denotes the mean amplitude of the spectrogram, and the dashed line is one standard deviation (1SD) above the mean. The vertical line indicates the temporal frequency of the stimulus.

A similar proportion of neurons was found to have modulated responses in the AEV. The mean MI was 1.25 (N = 28, SD = ±0.99, range 0.55-3.94). In contrast to this the non-modulated AEV neurons exhibited a mean MI of 0.37 (N = 13, SD: ±0.13, range: 0.1-0.49). Figure 8d represents the activity of a modulated AEV neuron in the form of a derived Fourier spectrum.

5.5 Directional and velocity sensitivity of neurons in the SNr

5.5.1 Visual responsiveness of the SNr neurons

The visual responses of altogether 312 SNr neurons were analyzed. The recorded units were GABAergic SNr cells with monophasic spikes with waveform lengths of < 1 ms (Grace and Bunney, 1983; Ungless et al., 2004). The spontaneous activity of these neurons was high, with a mean of 27 spikes/s (SD: ±13 spikes/s, range: 17-76 spikes/s).

The majority of the visually active neurons responded optimally to high velocities (>40°/s), but poorly to stationary visual stimulation. There were no particular directions that were preferred by a majority of the SNr neurons. The spontaneous neuronal activity and velocity preference displayed a weak negative correlation. Single units with higher spontaneous firing rate preferred lower stimulus velocities ($R = -0.12$, $p = 0.025$). We found no such correlation concerning the direction sensitivity.

Stimulus conditions evoking the greatest change in neuronal activity were regarded as the preferred conditions of the neurons. There were 132 units with dominantly excitatory responses (an increase in their firing rate during stimulation). Their average firing rate in response to the preferred conditions was 34 spikes/s (SD: ±17 spikes/s, range: 19-84 spikes/s), that is, a 21.1% average increase relative to the spontaneous activity. For the 180 neurons with dominantly inhibitory responses (a decrease in their firing rate during stimulation), the mean firing rate in response to the preferred conditions was 21 spikes/s (SD: ±11 spikes/s, range: 5-68 spikes/s), that is, 18.5% less than the mean spontaneous activity. Comparison of the spontaneous activity of the cells with the visual responses observed under the preferred conditions revealed significant differences for both the excitatory ($p<0.01$) and the inhibitory ($p<0.01$) SNr neurons (Wilcoxon rank-sum test).

5.5.2 Velocity and direction tuning of the SNr visual responses

The major finding of this study is that a population of the visual SNr neurons was not exclusively inhibitory or excitatory in nature, but could elicit either excitatory (increased activity) or inhibitory (decreased activity) visual responses, depending on the stimulus parameters. These SNr cells were uniform in the sense that they were able to respond with a definite increase in activity, but only under certain stimulus conditions. Moreover, even if applying the same stimulus, both excitatory and inhibitory neuronal responses could be observed (Fig. 9).

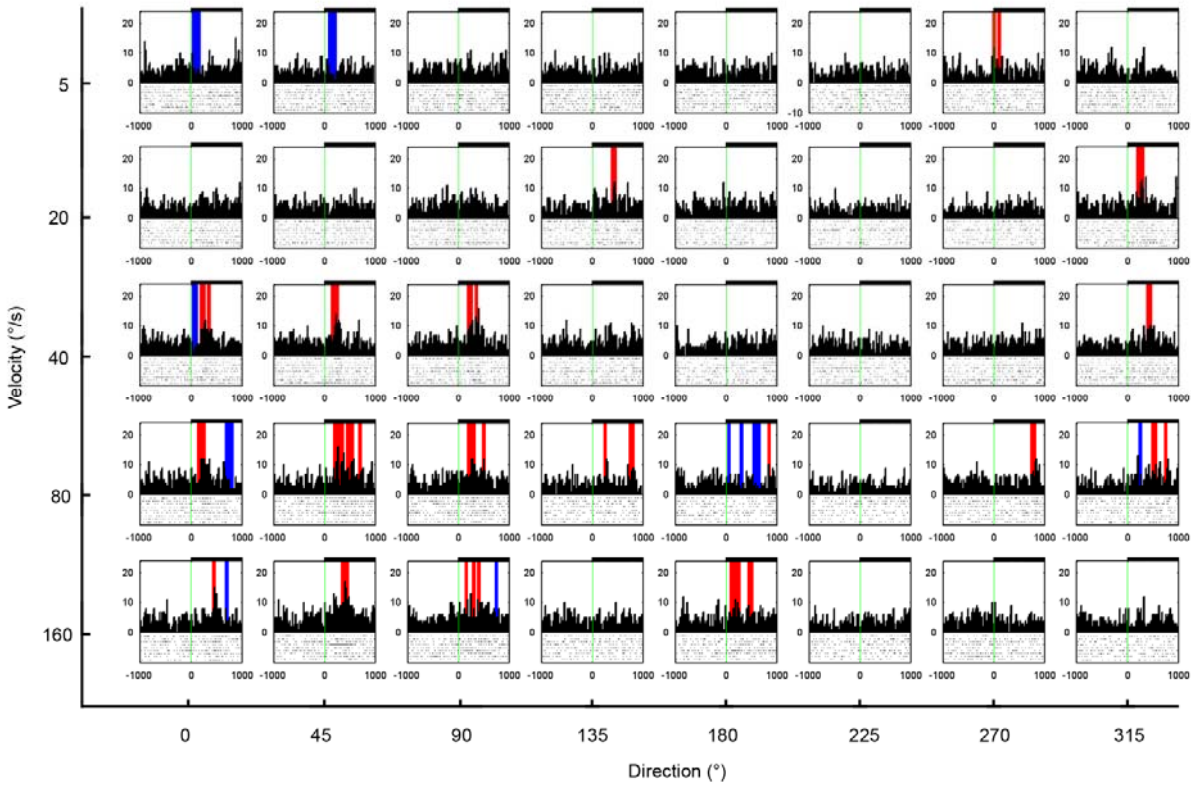

Figure 9.: Visual responses of a SNr neuron.
The 5x8 peristimulus time-histogram (PSTH) represents the responses of a SNr GABAergic neuron during the corresponding stimuli, with the same conventions as in Fig. 3. A significant increase in firing rate in a specific period in response to a given stimulus condition is indicated by a red bar, and a significant decrease by a blue bar. The direction and velocity of the movements of the applied stimuli are shown on the common abscissa and ordinate, respectively.

These response characteristics were utilized to generate a direction/velocity map for each cell. Based upon these maps the neurons were classified into 8 categories (Fig. 10) with the help of an artificial neural network (see Methods). The majority of the neurons (61%, N = 190), referred to as *simple cells,* exhibited a simple stimulus preference, that is, they displayed significant changes in

activity in response to well-defined stimulus combinations. These cells revealed narrow directional and velocity tuning. Eighty-one of these simple neurons responded predominantly with excitation, i.e. with an increase in activity, while 109 underwent a definite inhibition, i.e. a decrease in activity during visual stimulation (Fig. 10a,b).

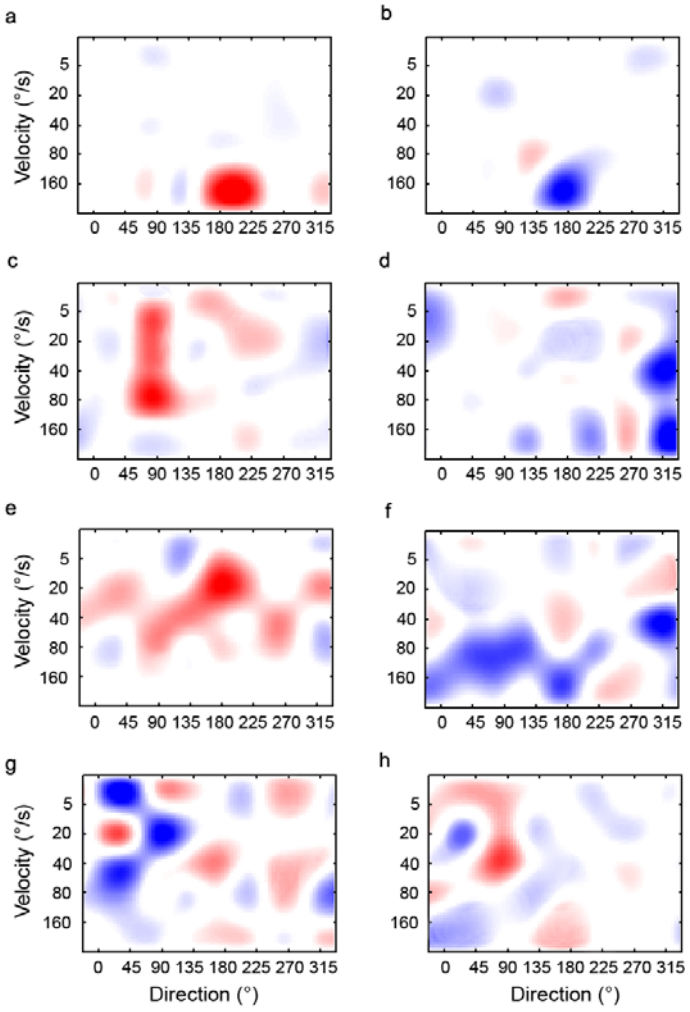

Figure 10.: Examples of visual response tuning maps.
Each stimulus preference map shows the responsiveness of a SNr GABAergic cell with a specific type of preference. The abscissa denotes the 8 different directions of stimulus movement and the ordinate the different velocities. The strength of the response to each specific stimulus parameter combination is colour-coded; inhibitory responses where the firing frequency is decreased during stimulation are in blue, and excitatory responses (increase in firing rate) in red. The intensities of the colours are proportional to the strength of the responses. For better visibility, the colour codes of the preference maps are normalized and smoothed via a bicubic spline technique. The neuronal responses to the applied visual stimuli were classified into 4x2 distinct classes: (**a, b**) simple excitatory and inhibitory, (**c, d**) direction-sensitive excitatory and inhibitory, (**e, f**) velocity-sensitive excitatory and inhibitory and (**g, h**) concentric neurons. For further details concerning the preference classes, see text.

Fifty-seven of the recorded SNr neurons, referred to as *direction-sensitive neurons*, responded to stimuli moving in a particular direction. Seventeen of them exhibited an increase in activity in response to the preferred stimulus, and 40 cells a decrease. No correlation was found between the directions evoking excitation and those evoking inhibition. All directions occurred with the same frequency (Fig. 10c,d).

No orientation sensitive neurons were found in the SNr that preferred both of the opposing pairs of directions of movements.

Twenty of the recorded units were observed to be *velocity-sensitive*. These neurons responded to stimuli moving at a certain velocity, irrespective of their direction. Seven (2%) of the responses were excitatory and 13 (4%) inhibitory (Fig. 10e,f). The distribution of the preferred velocities was not characteristic; all velocities occurred with the same frequency.

The remaining 45 neurons, referred to as *concentric neurons,* exhibited complex response characteristics. Twenty-eight cells responded to a particular stimulus condition with an increase in activity, and to all the neighbouring conditions (both velocity and direction) with a definite decrease. In other words, these neurons exhibited a simple response surrounded by an inhibitory domain. Seventeen cells revealed an inverse characteristic: they responded to a certain stimulus condition with a decrease in activity and to the neighbouring conditions with a definite increase (Fig. 10g,h).

The neurons described above were distributed randomly in the SNr. No spatial clustering of the neuronal stimulus preference types was observed. Similarly, we did not find any correlation between the location of the cells and their velocity or direction preference.

5.5.3 Stimulus size modulation of the responses of the SNr neurons

To address the question of how the size of the stimulus affects the response characteristics of the SNr neurons, light spots of 1° or 5° in diameter were used to elicit visual responses from 139 neurons. Most of the cells exhibited the same visual response tuning, irrespectively of the size of the stimulus; only the strength of the excitatory responses decreased and the strength of the inhibitory responses increased when the 5° stimulus was applied. In response to stimulation with the 5° light spot, there was a mean decrease of 18% in the excitatory response and a mean increase of 40% in the inhibitory response. The excitatory response to the 1° spot was significantly stronger than that to the 5° spot (Mann-Whitney test, $p<0.01$). In contrast, the inhibitory response was significantly stronger ($p<0.01$) to the 5° spot than to the 1° spot. It is noteworthy that the sum of the response strengths remained the same for each cell, irrespectively of the stimulus size. Only the ratio of the excitatory and inhibitory responses changed. With the use of the smaller spot as visual stimulus, 57% excitatory and 43% inhibitory responses were observed within the overall neuron population, while with the larger spot as stimulus, 41% of the total neuronal responses were excitatory and 59% inhibitory.

6 Discussion

6.1 Comparing the double sliding-window technique with other latency estimation methods

Our novel method, the double sliding-window technique, allows a rapid, reproducible, accurate and automated estimation of the neuronal response onset latency. The double sliding-window technique yields more accurate latency data than Poisson spike-train analysis (Legéndy and Salcman, 1985), the CUSUM procedure (Ellaway, 1978) or the method of Falzett et al. (1985) as signified by the fact that the EEs of the latencies calculated by the double sliding-window technique are significantly smaller than those of these most commonly used methods. Furthermore, the double sliding-window technique seems to make it possible to determine the latency of both excitatory and inhibitory neuronal responses since it detects conformity changes between two datasets regardless of the direction of change.

Poisson distribution (Legéndy and Salcman, 1985) expresses the probability of a number of rare events occurring in a fixed period of time if these events occur with a known average rate, and are independent of the time since the last event. The weakness of Poisson spike-train analysis, i.e. the overestimation of the response latency, may occur for several reasons. The neuronal excitations in a spike train are not independent of each other, and if the spontaneous activity of a single unit is relatively high, and thus the estimated parameter λ of the method is higher than a particular limit, the Poisson spike-train analysis may not work properly. Poisson spike-train analysis is suitable only for the calculation of onset latencies of neurons with low or no spontaneous activity. However, a noteworthy population of neurons has high spontaneous activity, and for these, Poisson spike-train analysis returns inaccurate latencies.

As for the CUSUM method (Ellaway, 1978), it appears that the most commonly used 1 or 2 SDs above the main spontaneous discharge rate chosen as threshold level is not sufficient to calculate the response onset latency. The mean + 9 SD threshold level allows an estimation of the most accurate onset latencies whereas the mean + 2 SD threshold level results in an underestimation of the response onset latencies. However, even if we choose a statistically extremely high 9 SD threshold level, the CUSUM method is still a poorly reliable technique. In the modification of the CUSUM procedure (method of Falzett et al., 1985) the most sensitive problem is the choice of the

appropriate n value for the SOD. A 100 ms binwidth and n = 3-5 were chosen in the original publication of Falzett et al. as producing the most reliable onset latencies. In our analysis we used 5 ms binwidth, and found that n = 22-30 is the most appropriate parameter with which to calculate the response onset latencies in the method of Falzett et al. Thus it seems that the correct level of n has to be chosen for the binwidth. Despite the arbitrarily chosen n value, the method of Falzett et al. still appears to be the most reliable of the three techniques discussed above for numerous neuronal response characteristics.

In order to exclude the subjective, arbitrary selection of the parameters, the n value of the SOD and the window width, the double sliding-window technique calculates the latencies by using a series of constant parameters, and the median of the latencies estimated using 25 constant parameter combinations (see Results) defines the response onset latency of a single neuron.

The double sliding-window method therefore offers an alternative to subjective visual estimation, Poisson spike-train analysis, the CUSUM procedure and the method of Falzett et al. for estimation of the response onset latency. The solidity and reproducibility of the double sliding-window method makes it appropriate to be used in the daily, routine analysis of neuronal response onset latencies.

6.2 Direction of information flow in the tectal visual system - Morphological and functional correlates

The function of the thalamus in the mammalian brain is based on the existence of two types of relays (Sherman and Guillery, 1998, 2002). Thalamic first-order relays receive their driving afferents from ascending pathways and transmit messages to the cortex that the cortex has not received before. Higher-order relays bring driver messages to the thalamus from the cortex for transmission from one cortical area to another. This duality stresses the importance of the cortico-thalamic and the thalamo-cortical pathways. The distinction between the two types of relays, however, is not always unequivocal. There are thalamic nuclei that receive drive from both the cortex and lower centres. The best-known nuclei of this kind are the pulvinar and the lateral posterior nuclei, which receive driving afferents from the visual cortex, and there is an additional tectal input to them (Casanova et al., 2001; Merabet et al., 1998). Similarly, Sommer and Wurtz (2004) described that the medial dorsal nucleus of the thalamus, that innervates the frontal eye field, receives drive from both the cortex and the intermediate and deep layers of the SC, but its main

drive arrives from the tectal region. These thalamic nuclei process messages that have already reached the cortex and have been processed in at least one cortical area, and at the same time they serve the role of first-order relays receiving signals from the ascending pathways. A similar ambiguity seems to characterize the role of the Sg and its connections with the cortex along the AES. The Sg receives heavy afferentation both from the intermediate and deep layers of the SC (Katoh and Benedek, 1995) and from the visual associative cortex along the AES (Hicks et al., 1986). Thus, it could serve either as a higher-order relay nucleus or as a simple first-order relay of tectal information. Our data suggest that the visual information flows bidirectionally between the Sg and the AES cortex. However, further investigations are necessary to clarify whether the thalamo-cortical and corticothalamic axons are drivers or modulators.

6.2.1 The gain of latency estimation in visual experiments

The results of our latency studies provide data on the sequence of volleys of excitation between the cortex and the thalamus. We found that there was no difference between the shortest latency values of the thalamic and the cortical units. Both structures responded to visual motion with a minimum latency of 35 ms. The mean response latency of the Sg units, however, is significantly shorter than the mean latency of the AEV neurons. These results might suggest that both the thalamo-cortical and the cortico-thalamic route are active between the extrageniculate visual thalamus and the visual associative cortex. There are thalamic nuclei that receive drive from both the cortex and lower centres. Beside the pulvinar, the lateral posterior and the medial dorsal nuclei, the Sg also receives driving afferents from the extrastriate visual cortex, and there is an additional tectal input to them. Thus, the Sg could serve either as a higher-order relay nucleus or as a simple first-order relay of tectal information. However, the statistically shorter latencies in the Sg might indicate that the visual information flows predominantly from the Sg to the AEV.

6.2.2 Panoramic localizers

The size of the receptive fields in the AEV described by Olson and Graybiel (1987) and later by Scannel et al. (1996) were considerably smaller than that described by us. This discrepancy could originate from the different types of anaesthesia used or in the obvious difficulties in describing these huge receptive fields. Both Olson and Graybiel (1987) and Scannell et al. (1996) concentrated on finding the locations of the most intense areas, while we attempted to find the

border between the responsive and absolutely non-responsive areas and sought the locations of the regions of maximum sensitivity. The majority of the Sg and the AEV units in our experiments proved to be selective for the stimulus location; they exhibited significantly different responses to stimuli from different spatial locations. These indicate that as it has been described earlier for the AES units (Benedek et al., 2004), the Sg units have similar abilities to serve as panoramic localizers (Middlebrooks et al., 1994, 1998). The regions of maximal sensitivity within the investigated part of the visual field are widely distributed for both the AEV (Benedek et al., 2004) and the Sg neurons. These observations point to the possible existence of a distributed population code of visual information in both the Sg and the AEV (Benedek et al., 2004), based on panoramic localizer neurons (Middlebrooks et al., 1994, 1998, 2002). Similarly to the Sg and the AEV neurons the CN neurons also possessed spatial selectivity within their huge receptive field. We provide evidence of the distributed population code of spatial visual information in the CN where the single visual neurons have also panoramic localizing ability. It is important to note, that by the investigation of the distribution of maximally preferred stimulus sites among neuronal populations (based on the analysis of large number of neuronal recordings) we found that these locations showed a nearly uniform spatial distribution, opposing to the receptive field location distributions along the geniculo-striate visual system, where a massive area centralis/foveal overrepresentation exists. This latter observation emphasizes the functional difference between the two systems: While the main function of the geniculo-striate system is to detect the smooth details and colour of objects which can be considered as static properties, the tectal visual system is responsible for motion and novelty detection in which case the object may appear more likely at the periphery of the visual field than focused on the area centralis. The loss of central overrepresentation occurs at early stage of processing, which explains the similar distributed population code in the AEV, the Sg and the CN.

6.2.3 Temporal modulation of responses along the tectal visual system

It is an interesting phenomenon that the drifting gratings strongly modulated the responses of the majority of the CN neurons. AEV neurons also exhibit strong temporal frequency modulated discharges. To decide whether cortex modulates the responses of the CN or vice versa, one might look for the source of this modulation. While the SC and Sg neurons responded to drifting gratings with a weakly modulated or unmodulated increase in activity (Paróczy et al., 2006; Waleszczyk et al., 2007), and the primary visual cortex sends efferents through the PMLS toward the AES cortex,

we assume that this latter structure may be the origin of the modulation in the CN, and thus the cortico-caudate direction of information flow does exist, and it has functional consequences. This result is somewhat confusing, since there is no direct anatomical evidence for a cortico-caudate connection; the indirect connection exists through the Sg, which structure does not elicit modulated responses to visual stimulation.

We argue that the Sg, CN and AEV neurons are good candidates for tasks involved in the perception of motion and probably in the perception of changes in the visual environment during self-motion (Morrone et al., 1986; Brosseau-Lachaine et al., 2001), with their extremely large receptive fields (Nagy et al., 2003b), their preferences for low spatial frequencies, and their fine spatial and temporal tuning. It has been reported in human psychophysical investigations that all motion detectors are apparently finely tuned to temporal and spatial frequencies (Anderson and Burr, 1985; Burr and Ross, 1986; Burr et al., 1986). These properties suggest that Sg, CN and AEV play an important role in detecting movements of the visual environment relative to the body, and participate in the adjustment of motor behaviour to environmental challenges.

6.3 The role of the SN in saccade initiation and novelty detection, intra-nigral connections

We highlight here the modulatory effect of moving visual stimuli as regards the presence of excitatory and inhibitory responses of the SNr neurons in anesthetized, immobilized cats. This is a suitable model for investigation of the visual information-processing function of the SN without the numerous direct and indirect non-sensory influencing factors (e.g. reward prediction, unexpectedness and motor processes) present during behavioural paradigms (Sato and Hikosaka, 2002; Dommett et al., 2005; Hikosaka, 2007). Below, we speculate on the role of this dualistic behaviour of the SNr, and propose a sequence of information coding with which the SNr may control the visuomotor functions of the SC.

On the basis of their neurotransmitters, the cells of the SNr can be classified mainly into dopaminergic (DAergic) and GABAergic classes. Within this structure there are also a relatively small number of non-DAergic-non-GABAergic cells, whose transmitters have not yet been clarified. Ficalora and Mize (1989) demonstrated that the nigrotectal tract consists of the axons of GABAergic neurons. We selected the GABAergic cells from the neuronal population during recording by considering two properties: GABAergic cells have narrow spike forms (~1 ms) in

extracellular recordings, and can therefore be reliably differentiated from DAergic cells producing broad spikes of over 2 ms, which are usually coupled into spike doublets or triplets (Grace and Bunney, 1983; Ungless, 2004); additionally, GABAergic cells have indirectly been shown to be fast-firing type II cells, in contrast to the slow-firing type I DAergic cells (Guyenet and Aghajanian, 1978). Earlier studies suggested that the GABAergic SNr neurons responded to visual stimuli with strong inhibition, while a smaller proportion increased its firing rate (Handel and Glimcher, 1999; Basso and Wurtz, 2002; Comoli et al., 2003). The most noteworthy finding of our study is that the SNr GABAergic neurons can elicit either excitation or inhibition, depending on the stimulus conditions applied. Accordingly, we propose a classification of SNr neurons based on their visual response tuning characteristics. As for the localization of cells with different characteristics in the SNr, we did not detect any clustering or correlation between their position, direction or velocity preference, which supports the notion that this structure does not involve any topographical organization: neither direct retinotopy nor any other more complex type.

A shift of attention toward novel stimuli in the surrounding space requires an analysis of the movement parameters of the object by the saccade control system. With the functional support of the novelty detector dopaminergic SN pars compacta units (Martin and Waszczak, 1994, 1996; Rice et al., 1997; Radnikow and Misgeld, 1998; Comoli et al., 2003; Dommett et al., 2005; Redgrave and Gurney, 2006), the SNr has the ability to command the saccadic functions appropriately. The fact that we found an equally represented preference for every stimulus direction and velocity combination suggests that despite the absence of a topographical organization in the SNr, there may be some special functional organization there. The Wurtz group (Hikosaka and Wurtz, 1986; Basso and Wurtz, 2002) postulated the existence of a higher-order topographical organization between the visual stimulus site and the centre of the receptive fields. This kind of coding sequence may be insufficient for accurate control of the smooth gating of saccades. We suggest that each SNr neuron might be connected to its corresponding SC cell in such a way that it can activate or block the saccade that is specifically related to it (McIlwain, 1990). The SC, on the other hand, receives a retinotopically highly-ordered input both from the retina (Graybiel, 1975; Ogawa and Takahashi, 1981; Beckstead and Frankfurter, 1983) and from the cortical visual areas (McIlwain, 1977; Berson and McIlwain, 1983; Berson, 1987). These two projections presumably overlap on the SC neurons, and this furnishes a special retinotopic organization of the SC neurons, which ordering also meets the aims of saccade generation (McIlwain, 1990). The simple SNr cells may activate or inhibit the

specific saccade that would drive the attention toward the position where the stimulus is predicted to be at the moment the saccade is carried out. The functional relation between the SNr and SC in pursuit eye movements and saccade generation is known, but the code behind the information transmission remains controversial. Both of the competing theories about the meaning of population activity code in the SC (Van Gisbergen et al., 1987; Lee et al., 1988; Van Opstal and Van Gisbergen, 1989) suggest that the activity of each of the ensembles determines a vector of eye movement with a definite amplitude and direction, which means that the SC expresses an integrated signal, taking into account both the actual eye position and gait (McIlwain, 1990), and the required future position. This output signal (which is a dynamic sum of the 'mini-vectors' represented by the single units of the active population) is suitable for direct driving of the oculomotor centres (Anderson et al., 1998). The vectorial response profiles of both the build-up and burst cells assume two sources: one is a feedback signal reflecting the actual eye position while the other informs about the position of the point of interest. These might be either integrated within the SC, or, it also seems possible that an external structure serves as an integrative centre, and the SC therefore receives dynamic vector-based input signals instead of static descriptive ones. The latter is supported by the fact that both of the above-mentioned SC cell types receive common inputs from the SNr (Liu and Basso, 2008), though it is likely that both mechanisms play a role in the final saccade commands. Li et al. (2006) concluded that the mutual inhibition among the populations of neurons will shape the sum gross response profile of the SC as a dynamic balance between inhibitions and exhibitions. The inhibitory-type nigrotectal pathway helps to sharpen this response map either by disinhibiting SC units via the decreased firing rate of inhibitory nigral neurons or by inhibiting them by increasing the GABAergic influence. That the functional role of the SNr signal is at least partially to modify saccade direction was verified recently by Liu and Basso (2008). They found that electrical activation of the GABAergic SNr cells profoundly modified the amplitude and direction of saccades in behaving paradigms, and the stimulation influenced both cell types in the SC. We speculate here that the various direction- and velocity-dependent integrative responses of the SNr cells may dynamically form the response profile of the SC intermediate and deep layers through vector-based commands, further integration taking place with the aid of the intracollicular visual retinotopic inputs (Ozen et al., 2000).

The direction- and velocity-sensitive neurons may reflect a higher level of organization. They may receive multiple inputs from different simple cells and thereby they integrate their preference

maps. This would also explain the existence of concentric preference maps, where the response to a simple condition is surrounded by inverse responses. In an attempt to find evidence in support of this theory, we compared the stimulus preference maps of the neurons by applying different stimulus sizes. We hypothesized that, if the position of a novel stimulus is ambiguous (the brain having difficulties in defining an exact location to focus on), the saccade can not be defined as obvious either. As a consequence, the SN is expected to elicit more intensive inhibition in response to a larger stimulus, which should allow more saccades, each with a slightly different property. This hypothesis was supported by the observation that increase of the stimulus size was accompanied by an increase in the proportion of inhibitory responses (which disinhibits the SC for saccadic information). On the other hand, increase of the stimulus size also resulted in a strong decrease in the excitatory responses, while the amount of total responses remained at the same level.

To summarize, we provide a model of how visual information may modulate the activity of the SNr neurons. The spatio-temporally represented visual information may determine the sensorimotor integrative function of the SNr. We suggest that the SNr could control the activity of the SC through nigrotectal connections, and could enhance or inhibit the reflexive initiation of complex and accurate saccades.

7 Summary

Extracellular single-cell recordings were carried out via tungsten microelectrodes at different stages of the ascending tectofugal visual system in anesthetized, paralyzed, artificially respirated adult cats. We analyzed the correlation between the morphologically verified network and the functional relationship of the investigated structures. To determine the way of information flow and coding algorithm between the groups of neurons we made an attempt to analyze their response properties from different aspects by applying visual stimuli. Two specific parts of the tectal visual system was investigated in detail:

1. the pathways between the Sg of the posterior thalamus, the CN and the visual cortical area along the AES,
2. the nigrotectal pathway, which projects saccade initiative information from the SNr toward the SCi and SCd.

To investigate the direction of the information flow between the Sg and the AEV, we measured the response onset latencies of neurons within both structures during standardized visual stimulation. In order to enhance the quality and objectivity of the onset latency estimation, we developed a novel method, the so-called ‘double sliding-window’ technique, which combines the advantages of mathematical methods with the reliability of standard statistical ones. This method is based on a repetitive series of statistical probes between two virtual time windows. The layout of the significance curve reveals the starting points of changes in neuronal activity in the form of break-points between linear segments. A second-order difference function is applied to determine the position of maximum slope change, which corresponds to the onset of the response. To validate our novel method, we have tested the reliability of the automatically estimated latencies on a large number of neuronal recordings. We found that the results returned by this method are in good agreement with the subjectively obvious latencies acquired by visual inspection. In comparison with Poisson spike-train analysis, the cumulative sum technique and the method of Falzett et al., this ‘double sliding-window’ technique seems to be a more accurate automated procedure to calculate the response onset latency of a broad range of neuronal response characteristics. The mean visual response latency of the Sg units was found to be significantly shorter than the mean latency of the AEV neurons, but there was no difference between the shortest latency values of the thalamic and

the cortical single-units. This suggests that the visual information flows predominantly from the Sg to the AEV, though the cortico-thalamic route is also active.

The lack of retinotopical organization within the Sg, AEV and the CN suggest the possibility of an alternative neuronal code of spatial visual information in these structures. The majority of the AEV, Sg and CN units can provide information via their discharge rate at the site of the visual stimulus within their large receptive fields. This suggests that they may serve as panoramic localizers. The sites of maximum responsivity of the CN, AEV and Sg neurons are distributed over the whole investigated part of the visual field. Our results provided evidence on the distributed population code of spatial visual information based on panoramic CN, Sg and AEV neurons. It is noteworthy that the spatial locations of maximum sensitivity in the AEV, Sg, and CN neurons had uniform distributions, with a homogenous representation of the area centralis and the peripheral visual field in contrast to the members of the geniculo-striate system, where the fovea is strongly overrepresented. This homogenous spatial sensitivity helps the detection of peripheral events. An additional functional similarity between the AEV and the NC is that both of them contain neuronal subpopulations in which moving sinusoidal grating stimuli elicit temporally strongly modulated responses. The source and the pathway which transmits this modulation between the AEV and NC have not yet been discovered, however, the absence of modulated responses in the Sg and in the SC suggests a cortical origin of temporal modulation in the CN.

The striking similarities in visual response properties of different structures along the tectal visual system suggest that the transmitted information about the visual environment is rather stable. Since many of these structures play a key role in the motor feedback actions as members of the basal ganglia circuitry, it seems that the visually perceived changes in the environment have a massive impact on the ongoing motoric patterns. This may help to adjust the motor behaviour to environmental challenges including oculomotor processes such as novelty detection, and foveation.

The orientation of spatial attention via saccades is controlled by the nigrotectal tract, which enhances the ability to respond to novel stimuli. However, the algorithm whereby the substantia nigra pars reticularis (SNr) translates the visual input to saccade-driving information is still unknown. We recorded the responses of 312 SNr neurons to moving visual stimuli. Depending on the size, velocity and direction of the visual signal, SNr units responded by either increasing or decreasing their firing rate. Using artificial neuronal networks, visual SNr neurons could be classified into distinct groups. Some of the units showed a clear preference for one specific

combination of direction and velocity (*simple neurons*), while other SNr neurons were sensitive to the direction (*direction tuned neurons*) or the velocity (*velocity tuned neurons*) of the movement. Furthermore, we could record visually active SNr neurons that exhibited a narrow inhibitory/excitatory domain in the velocity/direction dimension with an opposing surround (*concentric neurons*). According to our results, the spatio-temporally represented visual information may determine the discharge pattern of the SNr. We suggest that the SNr utilizes the spatio-temporal properties of the visual information to generate vector-based commands. In this way, the SNr might control the activity of the SC through nigrotectal connections and enhance or inhibit the reflexive initiation of complex and accurate saccades.

8 Acknowledgement

I respectfully thank Professor György Benedek and Dr. Attila Nagy who have served as my mentors and supervisors and for the opportunity that I could work with them. I greatly appreciate their helpful and instructive guidance. I express my gratitude to Professor Gábor Jancsó for allowing me to work in the Neuroscience PhD Program. My special thanks go to Dr. Zita Márkus, Dr. Zsuzsanna Paróczy, Dr. Alice Rokszin, Dr Ágnes Farkas, Péter Gombkötő, Gábor Braunitzer and Dr. Gabriella Eördegh for their help and friendship. I would like to acknowledge the help of Andrea Pető, Wioletta Waleszczyk and Marek Wypych, too.

I express my most sincere gratitude to Gabriella Dósai for her valuable technical assistance and for the preparation of high-quality figures for my thesis. Many thanks are due to Péter Liszli for his expert help in solving hardware and software problems.

I would like to express my thanks to all colleagues in the Department of Physiology for their support and kindness. It was nice to work with them in this department.

My deepest thanks are due to my wife, Dr. Kinga Dékány, my parents, Dr. Zoltán Berényi and Dr. Rita Komáromy, and my brother, Zoltán Berényi, for their continuous love and help in my life.

Our experiments were supported by OTKA/Hungary grant F048396, OTKA/Hungary grant 42610.

9 References

Anderson RW, Keller EL, Gandhi NJ, Das S. Two-dimensional saccade-related population activity in superior colliculus in monkey. *J. Neurophysiol.* (1998) **80**:798-817

Anderson SJ, Burr DC. Spatial and temporal selectivity of the human motion detection system. *Vision Res.* (1985) **25**:1147-1154

Basso MA, Wurtz RH. Neuronal activity in substantia nigra pars reticulata during target selection. *J. Neurosci.* (2002) **22**:1883-1894

Beckstead RM, Frankfurter A. A direct projection from the retina to the intermediate gray layer of the superior colliculus demonstrated by anterograde transport of horseradish peroxidase in monkey, cat and rat. *Ex.p Brain Res.* (1983) **52**:261-268

Benedek G, Eördegh G, Chadaide Z, Nagy A. Distributed population coding of multisensory spatial information in the associative cortex. *Eur. J. Neurosci.* (2004) **20**:525-529

Benedek G, Fischer-Szatmári L, Kovács G, Perényi J, Katoh YY. Visual, somatosensory and auditory modality properties along the feline suprageniculate-anterior ectosylvian sulcus/insular pathway. *Prog. Brain Res*. (1996) **112**:325-334

Benedek G, Jang EK, Hicks TP. Physiological properties of visually responsive neurones in the insular cortex of the cat. *Neurosci. Lett.* (1986) **64**:269-274

Benedek G, Mucke L, Norita M, Albowitz B, Creutzfeldt OD. Anterior ectosylvian visual area (AEV) of the cat: physiological properties. *Prog. Brain Res.* (1988) **75**:245-255

Berson DM, McIlwain JT. Visual cortical inputs to deep layers of cat's superior colliculus. *J. Neurophysiol.* (1983) **50**:1143-1155

Berson DM. Retinal W-cell input to the upper superficial gray layer of the cat's superior colliculus: a conduction-velocity analysis. *J. Neurophysiol.* (1987) **58**:1035-1051

Brecht M., Engel AK. Cortico-tectal interactions in the cat visual system. Artificial Neural Networks (1996) pp. 395-399

Brosseau-Lachaine O, Faubert J, Casanova C. Functional sub-regions for optic flow processing in the posteromedial lateral suprasylvian cortex of the cat. *Cereb. Cortex*. (2001) **11**:989-1001

Burr DC, Ross J. Visual processing of motion *Trends in Neurosci*. (1986) **9**:304-307

Burr DC, Ross J, Morrone MC. Seeing objects in motion. *Proc. R. Soc. Lond. B. Biol. Sci.* (1986) **227**:249-265

Butler EG, Horne MK, Hawkins NJ. The activity of monkey thalamic and motor cortical neurones in a skilled, ballistic movement. *J. Physiol*. (1992) **445**:25-48

Carew TJ. Behavioral Neurobiology: the Cellular Organization of Natural Behavior. Sinauer Associates., (2000)

Casanova C, Merabet L, Desautels A, Minville K. Higher-order motion processing in the pulvinar. *Prog. Brain Res.* (2001) **134**:71-82

Comoli E, Coizet V, Boyes J, Bolam JP, Canteras NS, Quirk RH, Overton PG, Redgrave P. A direct projection from superior colliculus to substantia nigra for detecting salient visual events. *Nat. Neurosci.* (2003) **6**:974-980

Dommett E, Coizet V, Blaha CD, Martindale J, Lefebvre V, Walton N, Mayhew JE, Overton PG, Redgrave P. How visual stimuli activate dopaminergic neurons at short latency. *Science*. (2005) **307**:1476-1479

Dreher B, Sefton AJ. Properties of neurons in cat's dorsal lateral geniculate nucleus: a comparison between medial interlaminar and laminated parts of the nucleus. *J. Comp. Neurol.* (1979) **183**:47-64

Ellaway PH. Cumulative sum technique and its application to the analysis of peristimulus time histograms. *Electroencephalogr. Clin. Neurophysiol.* (1978) **45**:302-304

Eördegh G, Nagy A, Berényi A, Benedek G. Processing of spatial visual information along the pathway between the suprageniculate nucleus and the anterior ectosylvian cortex. *Brain Res. Bull.* (2005) **67**:281-289

Falzett M, Moore RK, Petry HM, Powers MK. A method for determining threshold from single-unit neural activity. *Brain Res.* (1985) **347**:127-131

Ficalora AS, Mize RR. The neurons of the substantia nigra and zona incerta which project to the cat superior colliculus are GABA immunoreactive: a double-label study using GABA immunocytochemistry and lectin retrograde transport. *Neuroscience.* (1989) **29**:567-581

Freygang WH. An analysis of extracellular potentials from single neurons in the lateral geniculate nucleus of the cat. *J. Gen. Physiol.* (1958) **41**:543-564

Gehring WJ. New Perspectives on Eye Development and the Evolution of Eyes and Photoreceptors: The Evolution of Eyes and Brain. *J. Heredity* (2005) **96**:171–184

Grace AA, Bunney BS. Intracellular and extracellular electrophysiology of nigral dopaminergic neurons--1. Identification and characterization. *Neuroscience.* (1983) **10**:301-315

Grant S, Shipp S. Visuotopic organization of the lateral suprasylvian area and of an adjacent area of the ectosylvian gyrus of cat cortex: a physiological and connectional study. *Vis. Neurosci*. (1991) **6**:315-338

Graybiel AM. Anatomical organization of retinotectal afferents in the cat: an autoradiographic study. *Brain Res.* (1975) **96**:1-23

Guyenet PG, Aghajanian GK. Antidromic identification of dopaminergic and other output neurons of the rat substantia nigra. *Brain Res.* (1978) **150**:69-84

Handel A, Glimcher PW. Quantitative analysis of substantia nigra pars reticulata activity during a visually guided saccade task. *J. Neurophysiol.* (1999) **82**:3458-3475

Harting JK, Updyke BV, Van Lieshout DP. Striatal projections from the cat visual thalamus. *Eur. J. Neurosci.* (2001(a)) **14**:893-896

Harting JK, Updyke BV, Van Lieshout DP. The visual-oculomotor striatum of the cat: functional relationship to the superior colliculus. *Exp. Brain Res.* (2001(b)) **136**:138-142

Hicks TP, Benedek G, Thurlow GA. Modality specificity of neuronal responses within the cat's insula. *J. Neurophysiol.* (1988(a)) **60**:422-437

Hicks TP, Benedek G, Thurlow GA. Organization and properties of neurons in a visual area within the insular cortex of the cat. *J. Neurophysiol.* (1988(b)) **60**:397-421

Hicks TP, Stark CA, Fletcher WA. Origins of afferents to visual suprageniculate nucleus of the cat. *J. Comp. Neurol.* (1986) **246**:544-554

Hikosaka O, Wurtz RH. Visual and oculomotor functions of monkey substantia nigra pars reticulata. I-IV. *J. Neurophysiol.* (1983) **49**:1230-1301

Hikosaka O. Basal ganglia mechanisms of reward-oriented eye movement. *Ann. N. Y. Acad. Sci.* (2007) **1104**:229-249

Hoshino K, Nagy A, Eördegh G, Benedek G, Norita M. Two types of neuron are found within the PPT, a small percentage of which project to both the LM-SG and SC. *Exp. Brain Res.* (2004) **155**:421-426

Isa T, Saito Y. The direct visuo-motor pathway in mammalian superior colliculus; novel perspective on the interlaminar connection. *Neurosci. Res.* (2001) **41**:107-113

Jiang H, Stein BE, McHaffie JG. Opposing basal ganglia processes shape midbrain visuomotor activity bilaterally. *Nature.* (2003) **423**:982-986

Katoh YY, Benedek G. Organization of the colliculo-suprageniculate pathway in the cat: a wheat germ agglutinin-horseradish peroxidase study. *J. Comp. Neurol.* (1995(a)) **352**:381-397

Katoh YY, Benedek G, Deura S. Bilateral projections from the superior colliculus to the suprageniculate nucleus in the cat: a WGA-HRP/double fluorescent tracing study. *Brain Res*. (1995(b)) **669**:298-302

Katoh YY, Benedek G. Cerebellar fastigial neurons send bifurcating axons to both the left and right superior colliculus in cats. *Brain Res*. (2003) **970**:246-249

Katzner S, Nauhaus I, Benucci A, Bonin V, Ringach DL, Carandini M. Local origin of field potentials in visual cortex. *Neuron.* (2009) **61**:35-41

Lee C, Rohrer WH, Sparks DL. Population coding of saccadic eye movements by neurons in the superior colliculus. *Nature.* (1988) **332**:357-360

Legéndy CR, Salcman M. Bursts and recurrences of bursts in the spike trains of spontaneously active striate cortex neurons. *J. Neurophysiol.* (1985) **53**:926-939

Lennie P. The physiological basis of variations in visual latency. *Vision Res.* (1981) **21**:815-824

Li X, Kim B, Basso MA. Transient pauses in delay-period activity of superior colliculus neurons. *J. Neurophysiol.* (2006) **95**:2252-2264

Liu P, Basso MA. Substantia nigra stimulation influences monkey superior colliculus neuronal activity bilaterally. *J. Neurophysiol.* (2008) **100**:1098-1112

Loe PR, Benevento LA. Auditory-visual interaction in single units in the orbito-insular cortex of the cat. *Electroencephalogr. Clin. Neurophysiol.* (1969) **26**:395-398

Lokwan SJ, Overton PG, Berry MS, Clark D. Stimulation of the pedunculopontine tegmental nucleus in the rat produces burst firing in A9 dopaminergic neurons. *Neuroscience.* (1999) **92**:245-254

Magariños-Ascone C, García-Austt E, Buño W. Polymodal sensory and motor convergence in substantia nigra neurons of the awake monkey. *Brain Res.* (1994) **646**:299-302

Martin LP, Waszczak BL. D1 agonist-induced excitation of substantia nigra pars reticulata neurons: mediation by D1 receptors on striatonigral terminals via a pertussis toxin-sensitive coupling pathway. *J. Neurosci.* (1994) **14**:4494-4506

McIlwain JT. Topography of eye-position sensitivity of saccades evoked electrically from the cat's superior colliculus. *Vis. Neurosci.* (1990) **4**:289-298

McIlwain JT. Topographic organization and convergence in corticotectal projections from areas 17, 18, and 19 in the cat. *J. Neurophysiol.* (1977) **40**:189-198

Merabet L, Desautels A, Minville K, Casanova C. Motion integration in a thalamic visual nucleus. *Nature.* (1998) **396**:265-268

Middlebrooks JC, Clock AE, Xu L, Green DM. A panoramic code for sound location by cortical neurons. *Science.* (1994) **264**:842-844

Middlebrooks JC, Xu L, Eddins AC, Green DM. Codes for sound-source location in nontonotopic auditory cortex. *J. Neurophysiol.* (1998) **80**:863-881

Middlebrooks JC, Xu L, Furukawa S, Macpherson EA. Cortical neurons that localize sounds. *Neuroscientist.* (2002) **8**:73-83

Morrone MC, Di Stefano M, Burr DC. Spatial and temporal properties of neurons of the lateral suprasylvian cortex of the cat. *J. Neurophysiol.* (1986) **56**:969-986

Movshon JA, Thompson ID, Tolhurst DJ. Spatial summation in the receptive fields of simple cells in the cat's striate cortex. *J. Physiol.* (1978) **283**:53-77

Mucke L, Norita M, Benedek G, Creutzfeldt O. Physiologic and anatomic investigation of a visual cortical area situated in the ventral bank of the anterior ectosylvian sulcus of the cat. *Exp. Brain Res.* (1982) **46**:1-11

Nagy A, Eördegh G, Benedek G. Spatial and temporal visual properties of single neurons in the feline anterior ectosylvian visual area. *Exp. Brain Res.* (2003(a)) **151**:108-114

Nagy A, Eördegh G, Norita M, Benedek G. Visual receptive field properties of neurons in the caudate nucleus. *Eur. J. Neurosci.* (2003(b)) **18**:449-452

Nagy A, Eördegh G, Norita M, Benedek G. Visual receptive field properties of excitatory neurons in the substantia nigra. *Neuroscience.* (2005(a)) **130**:513-518

Nagy A, Paróczy Z, Norita M, Benedek G. Multisensory responses and receptive field properties of neurons in the substantia nigra and in the caudate nucleus. *Eur. J. Neurosci*. (2005(b)) **22**:419-424

Nagy A, Eördegh G, Paróczy Z, Márkus Z, Benedek G. Multisensory integration in the basal ganglia. *Eur. J. Neurosci.* (2006) **24**:917-924

Norita M, McHaffie JG, Shimizu H, Stein BE. The corticostriatal and corticotectal projections of the feline lateral suprasylvian cortex demonstrated with anterograde biocytin and retrograde fluorescent techniques. *Neurosci. Res.* (1991) **10**:149-155

Norita M, Mucke L, Benedek G, Albowitz B, Katoh Y, Creutzfeldt OD. Connections of the anterior ectosylvian visual area (AEV). *Exp. Brain Res.* (1986) **62**:225-240

Ogawa T, Takahashi Y. Retinotectal connections within the superficial layers of the cat's superior colliculus. *Brain Res.* (1981) **217**:1-11

Olson CR, Graybiel AM. An outlying visual area in the cerebral cortex of the cat. *Prog. Brain Res.* (1983) **58**:239-245

Olson CR, Graybiel AM. Ectosylvian visual area of the cat: location, retinotopic organization, and connections. *J. Comp. Neurol.* (1987) **261**:277-294

Ouellette BG, Casanova C. Overlapping visual response latency distributions in visual cortices and LP-pulvinar complex of the cat. *Exp. Brain Res.* (2006) **175**:332-341

Ozen G, Augustine GJ, Hall WC. Contribution of superficial layer neurons to premotor bursts in the superior colliculus. *J. Neurophysiol.* (2000) **84**:460-471

Paróczy Z, Nagy A, Márkus Z, Waleszczyk WJ, Wypych M, Benedek G. Spatial and temporal visual properties of single neurons in the suprageniculate nucleus of the thalamus. *Neuroscience.* (2006) **137**:1397-1404

Radnikow G, Misgeld U. Dopamine D1 receptors facilitate GABAA synaptic currents in the rat substantia nigra pars reticulata. *J. Neurosci.* (1998) **18**:2009-2016

Redgrave P, Gurney K. The short-latency dopamine signal: a role in discovering novel actions? *Nat. Rev. Neurosci.* (2006) **7**:967-975

Redgrave P, Mitchell IJ, Dean P. Descending projections from the superior colliculus in rat: a study using orthograde transport of wheatgerm-agglutinin conjugated horseradish peroxidase. *Exp. Brain Res*. (1987) **68**:147-167

Rice ME, Cragg SJ, Greenfield SA. Characteristics of electrically evoked somatodendritic dopamine release in substantia nigra and ventral tegmental area in vitro. *J. Neurophysiol.* (1997) **77**:853-862

Rodríguez M, Abdala P, Obeso JA. Excitatory responses in the 'direct' striatonigral pathway: effect of nigrostriatal lesion. *Mov. Disord.* (2000) **15**:795-803

Rosenquist AC. Connections of visual cortical areas in the cat. Cerebral Cortex Volume 3 Visual Cortex. In: Peters A, Jones EG(eds.) (1985) New York Plenum Press, New York pp.81-117

Saint-Cyr JA, Ungerleider LG, Desimone R. Organization of visual cortical inputs to the striatum and subsequent outputs to the pallido-nigral complex in the monkey. *J. Comp. Neurol.* (1990) **298**:129-156

Sato M, Hikosaka O. Role of primate substantia nigra pars reticulata in reward-oriented saccadic eye movement. *J. Neurosci.* (2002) **22**:2363-2373

Scannell JW, Sengpiel F, Tovée MJ, Benson PJ, Blakemore C, Young MP. Visual motion processing in the anterior ectosylvian sulcus of the cat. *J. Neurophysiol.* (1996) **76**:895-907

Schwarz M, Sontag KH, Wand P. Sensory-motor processing in substantia nigra pars reticulata in conscious cats. *J. Physiol.* (1984) **347**:129-147

Sherman SM, Guillery RW. On the actions that one nerve cell can have on another: distinguishing "drivers" from "modulators". *Proc. Natl. Acad. Sci. U.S.A.* (1998) **95**:7121-7126

Sherman SM, Guillery RW. The role of the thalamus in the flow of information to the cortex. *Philos. Trans. R. Soc. Lond. B. Biol. Sci.* (2002) **357**:1695-1708

Sommer MA, Wurtz RH. What the brain stem tells the frontal cortex. I. Oculomotor signals sent from superior colliculus to frontal eye field via mediodorsal thalamus. *J. Neurophysiol.* (2004) **91**:1381-1402

Stein BE, Meredith MA. The merging of the senses. Cambridge MA, MIT Press, Cambridge (1993)

Tokuno H, Takada M, Ikai Y, Mizuno N. Direct projections from the deep layers of the superior colliculus to the subthalamic nucleus in the rat. *Brain Res.* (1994) **639**:156-160

Ungless MA, Magill PJ, Bolam JP. Uniform inhibition of dopamine neurons in the ventral tegmental area by aversive stimuli. *Science.* (2004) **303**:2040-2042

van Gisbergen JA, van Opstal AJ, Tax AA. Collicular ensemble coding of saccades based on vector summation. *Neuroscience.* (1987) **21**:541-555

van Opstal AJ, van Gisbergen JA. A model for collicular efferent mechanisms underlying the generation of saccades. *Brain. Behav. Evol.* (1989) **33**:90-94

Waleszczyk WJ, Nagy A, Wypych M, Berényi A, Paróczy Z, Eördegh G, Ghazaryan A, Benedek G. Spectral receptive field properties of neurons in the feline superior colliculus. *Exp. Brain Res.* (2007) **181**:87-98

Wang C, Dreher B, Assaad N, Ptito M, Burke W. Excitatory convergence of Y and non-Y channels onto single neurons in the anterior ectosylvian visual area of the cat. *Eur. J. Neurosci*. (1998) **10**:2945-2956

Wurtz RH, Hikosaka O. Role of the basal ganglia in the initiation of saccadic eye movements. *Prog. Brain Res.* (1986) **64**:175-190

I.

BRAIN RESEARCH 1178 (2007) 141–148

available at www.sciencedirect.com

www.elsevier.com/locate/brainres

BRAIN RESEARCH

Research Report

Double sliding-window technique: A new method to calculate the neuronal response onset latency

*Antal Berényi, György Benedek, Attila Nagy**

Department of Physiology, Faculty of Medicine, Albert Szent-Györgyi Medical and Pharmaceutical Center, University of Szeged, Dóm tér 10, H-6720 Szeged, Hungary

ARTICLE INFO

Article history:
Accepted 13 August 2007
Available online 24 August 2007

Keywords:
Latency
Automation
Second-order difference function
PSTH

ABSTRACT

Neuronal response onset latency provides important data on the information processing within the central nervous system. In order to enhance the quality of the onset latency estimation, we have developed a 'double sliding-window' technique, which combines the advantages of mathematical methods with the reliability of standard statistical processes. This method is based on repetitive series of statistical probes between two virtual time windows. The layout of the significance curve reveals the starting points of changes in neuronal activity in the form of break-points between linear segments. A second-order difference function is applied to determine the position of maximum slope change, which corresponds to the onset of the response. In comparison with Poisson spike-train analysis, the cumulative sum technique and the method of Falzett et al., this 'double sliding-window, technique seems to be a more accurate automated procedure to calculate the response onset latency of a broad range of neuronal response characteristics.

1. Introduction

Peristimulus time histograms (PSTHs; developed by Gerstein and Kiang, 1960) are commonly used to visualize the effect of a stimulus on the neuronal activity in extracellular recordings. Estimation of the neuronal response onset latency may provide important data concerning the information flow within the central nervous system (Berson, 1987; Dreher and Sefton, 1979). Despite the fact that the response onset latency comprises a source of data with which to resolve the information coding in the central nervous system alternative to the well-discussed properties of neuronal responses, i.e. the neuronal firing frequency, response duration and stimulus threshold, only a small proportion of neuronal recordings are generally analyzed from this aspect, possibly because of the weakness of automated latency estimation methods.

In the automation of the estimation of latency, a basic problem is to extract a signal from the spontaneous activity, which is determined by environmental and physiological noise. Mathematically, two solutions exist: counting the number of impulses discharged in some fixed interval (counting method) and detecting the time for the discharge of a fixed number of impulses (timing method) (Wandell, 1977). Poisson spike-train analysis is currently the most frequently applied method of latency estimation (Legéndy and Salcman, 1985). The neuronal response onset is calculated by averaging the time positions of some arbitrarily chosen bursts in the proven trials. The cumulative sum (CUSUM) technique was the first method in which the latency of neuronal responses was calculated via the analysis of PSTHs (Ellaway, 1978). The value of this method lies in the detection of change in the mean level of the activity. Since the change in

* *Corresponding author*. Department of Physiology, University of Szeged, Dóm tér 10, H-6720 Szeged, POB 427, Hungary. Fax: +36 62 545842.
E-mail address: nagya@phys.szote.u-szeged.hu (A. Nagy).
Abbreviations: CUSUM, cumulative sum; EE, estimation error; PSTH, peristimulus time histogram; SOD, second-order difference

0006-8993/$ – see front matter © 2007 Elsevier B.V. All rights reserved.
doi:10.1016/j.brainres.2007.08.041

the mean could be small relative to the variation in the individual values, an arbitrary threshold level (usually 1, 2 or 3 standard deviations (SD) above the mean of the spontaneous activity condition) is often chosen to quantify the start-point of the increment in the CUSUM curve (Ouellette and Casanova, 2006). The CUSUM technique has the weakness that it is not possible to determine precisely which temporal component of the response should be analyzed. Accordingly, Falzett et al. (1985) introduced a combination of the CUSUM technique with a second-order difference (SOD) function. However, despite the numerous methods proposed (Table 1), none of them can be applied reassuringly as a universal latency estimation method.

Is it possible to develop an estimation method for onset latency whereby the estimation becomes a clear objective statistical procedure? Can this new statistical function contribute to the applicability and reliability of automated latency estimation? Is it possible to keep the computational time-cost low? In an attempt to answer these questions, we have developed a 'double sliding-window' technique with which to calculate the neuronal response onset latencies. The double sliding-window technique analyzes trial-by-trial data on PSTHs and combines the advantages of mathematical methods with the reliability of standard statistical processes. In order to check on the validity of the technique, we calculated the visual response onset latencies of neuronal responses obtained in a large number of extracellular single-unit recordings and compared them with visually quantified latencies and with the latencies provided by Poisson spike-train analysis, the CUSUM technique, and the advanced method of Falzett et al.

2. Results

For measurement of the latency of neuronal response onsets, we developed a software program, the double sliding-window

Table 1 – Methods for estimating neuronal response onset latencies

χ^2-test within a different time window	(Fournier et al., 1986; Marque et al., 2001)
Significance level set to a specific threshold of spontaneous activity	(Tamura and Tanaka, 2001; Edwards et al., 2003)
Cumulative sum technique (CUSUM)	(Ellaway, 1978; Butler et al., 1992; Forlano et al., 1993; Rolls et al., 1993; Ouellette and Casanova, 2006)
Advanced CUSUM (method of Falzett et al.)	(Falzett et al., 1985; Day and Sibbald, 1989; Akeyson et al., 1990; Knuepfer and Holt, 1991; Holt et al., 1991; Drew et al., 1996; Hernandez et al., 2002)
CUSUM with Monte Carlo technique	Ushiba et al. (2002)
Poisson spike-train analysis	(Legéndy and Salcman, 1985; Hanes et al., 1995; Sáry et al., 2006)
Maximum likelihood estimation	(Seal et al., 1983; DiCarlo and Maunsell, 2005)
Artificial neuronal network	Churchward et al. (1997)

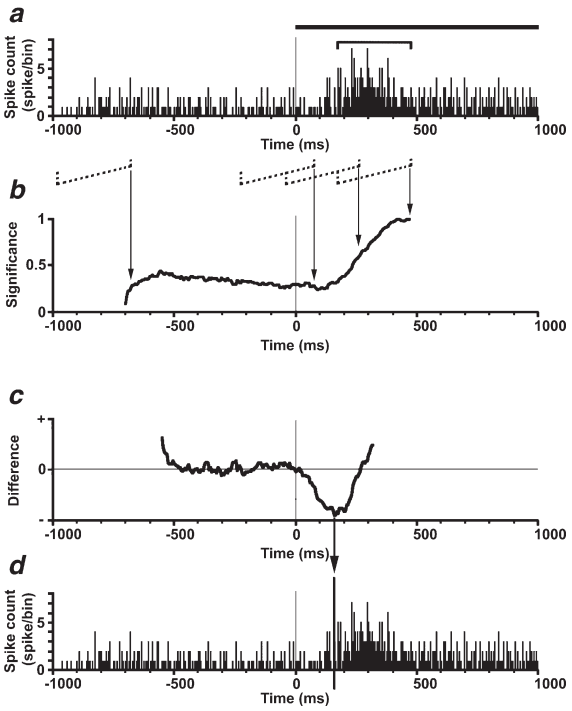

Fig. 1 – Estimation of neuronal response onset latency with the double sliding-window technique. (a) Peristimulus time histogram (PSTH) of an excitatory neuronal response. A PSTH consists of a prestimulus and a peristimulus period; the time-scale is presented on the abscissa (ms). The duration of visual stimulation is indicated by a thick horizontal black line above the PSTH. The beginning of visual stimulation is the zero time point. The ordinate demonstrates the cumulated spike count in each 5 ms wide bin. The solid black clamp above the PSTH denotes the position of the 300 ms wide reference window, where it overlaps the highest neuronal activity. (b) Significance curve calculated by the series of t tests. Four specific positions of the 300 ms wide sample window corresponding to different activity levels of the neuron are indicated by dotted clamps, while the arrows denote the corresponding significance values. The first two positions relate to cases when the sample window contains only pure spontaneous activity, while the third contains the transition between the pure spontaneous activity and the neuronal response to visual stimulation. The fourth marker shows the final position, when the reference and the sample windows overlap each other (the significance level of the t test is 1). The ordinate denotes the result of the series of paired t tests between the activity in the reference window (shown in part A) and the activity within each actual sample window in 5 ms (one bin) steps. (c) Curve of the second-order difference function (SOD) derived from the significance curve ($n=30$). The ordinate demonstrates the positivity or negativity of the SOD results. The minimum point of this curve coincides with the maximum slope change of the significance curve, and thus approximates to the onset of the neuronal response. (d) PSTH with marked response onset (thick vertical line). Accordingly, the visual response onset latency of the demonstrated neuron was 160 ms.

technique, which slides two windows along the PSTHs. The first window (reference window) slides through the peristimulus period in 1 bin steps, and selects the portion that represents the maximum (or the minimum) frequency (depending on the excitatoric or inhibitoric characteristic of the neuronal response). A second window (sample window) then slides through, also in 1 bin steps. After each step, the program calculates the significance level between the spike frequencies of the two windows with the *t* test. The latency of the responses is calculated from the time function of these *p* values. A curve is fitted to the *p* values, and the response onset latency is provided as the time interval between the start of the stimulation and the first point of the rising segment of the p curve, which is estimated by a SOD function (Fig. 1).

2.1. *Response onset latency estimation using the double sliding-window technique*

A total of 681 extracellular single-unit recordings (PSTHs) were analyzed by using the double sliding-window technique. All these PSTHs were selected from among our earlier recordings with regard to two criteria: the PSTH had to demonstrate a significant neuronal response to visual stimulation, and the response onset latency from the PSTH could be determined by subjective visual estimation. Latencies were calculated for each neuronal response subjectively by visual evaluation and by using the double sliding-window technique with 135 different parameters (10 different window widths, from 10 to 100 bins, and the possible corresponding *n* values in the SOD function, from 2 to 50; Fig. 3a). Fig. 2 depicts the characteristics of three different excitatory (Figs. 2a–c) and one inhibitory (Fig. 2d) neuronal response, with their associated significance and the SOD curves produced by the latency analysis. The automatically determined response onsets are indicated by vertical arrows.

The difference between the subjectively determined latency and the latency estimated by using the double sliding-window technique was defined as the estimation error (EE) of a measurement. If the *n* value was higher than a limit (10–12) and the window width was in an appropriate range (30–60 bins), there was not a significant difference between the computed EEs (Fig. 3a). Furthermore, calculation of the median

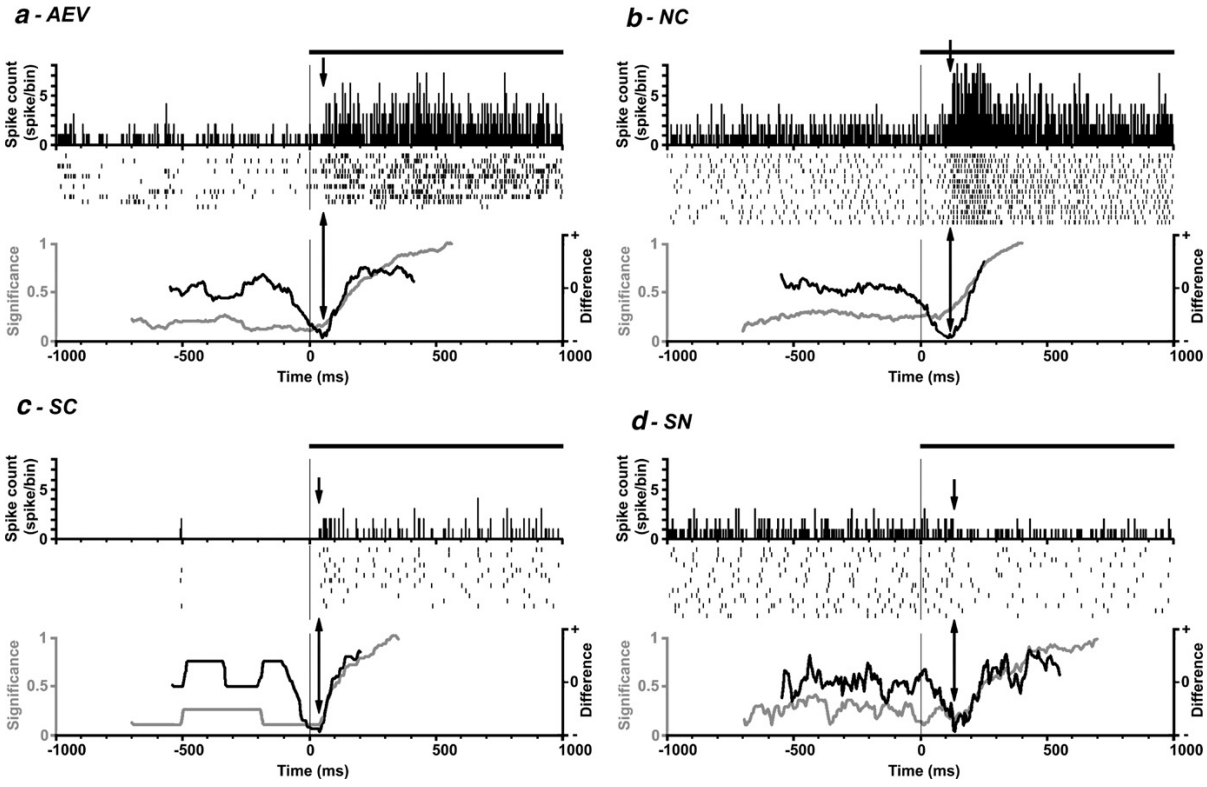

Fig. 2 – Application of the double sliding-window technique. Calculation of the visual onset response latencies of excitatory neuronal responses in the anterior ectosylvian visual area (a), the caudate nucleus (b) and the superior colliculus (c), and an inhibitory response in the substantia nigra pars reticulata (d). Each part contains the summed neuronal activity in the form of PSTHs (uppermost part), the trial-by-trial activity in raster form (each row visualizes one trial, where each small dash means one neuronal excitation; middle part) and the two calculated curves (lower part), the significance (gray) and the SOD curve (black). The arrows show the minimum point of the SOD curve that depicts the neuronal response onsets. The conventions are the same as in Fig. 1.

of the acquired onset latencies by using the highest mathematically possible *n* values with different window widths furnishes higher internal stability, this smoothing leading to the most accurate onset latencies. Use of the median instead of the mean to estimate the central tendency is more accurate in this case, since sporadic disturbances in a data set (estimation inaccuracy for a single *n* value) distort the final latencies less. The mean of the medians of the EEs when the double sliding-window technique was used was 35.98 ms ($n=681$; SD: ±58.48 ms).

2.2. *Response onset latency estimation with other automated methods*

The visual response onset latencies of the same 681 neuronal recordings (PSTH) were also estimated by using Poisson spike-

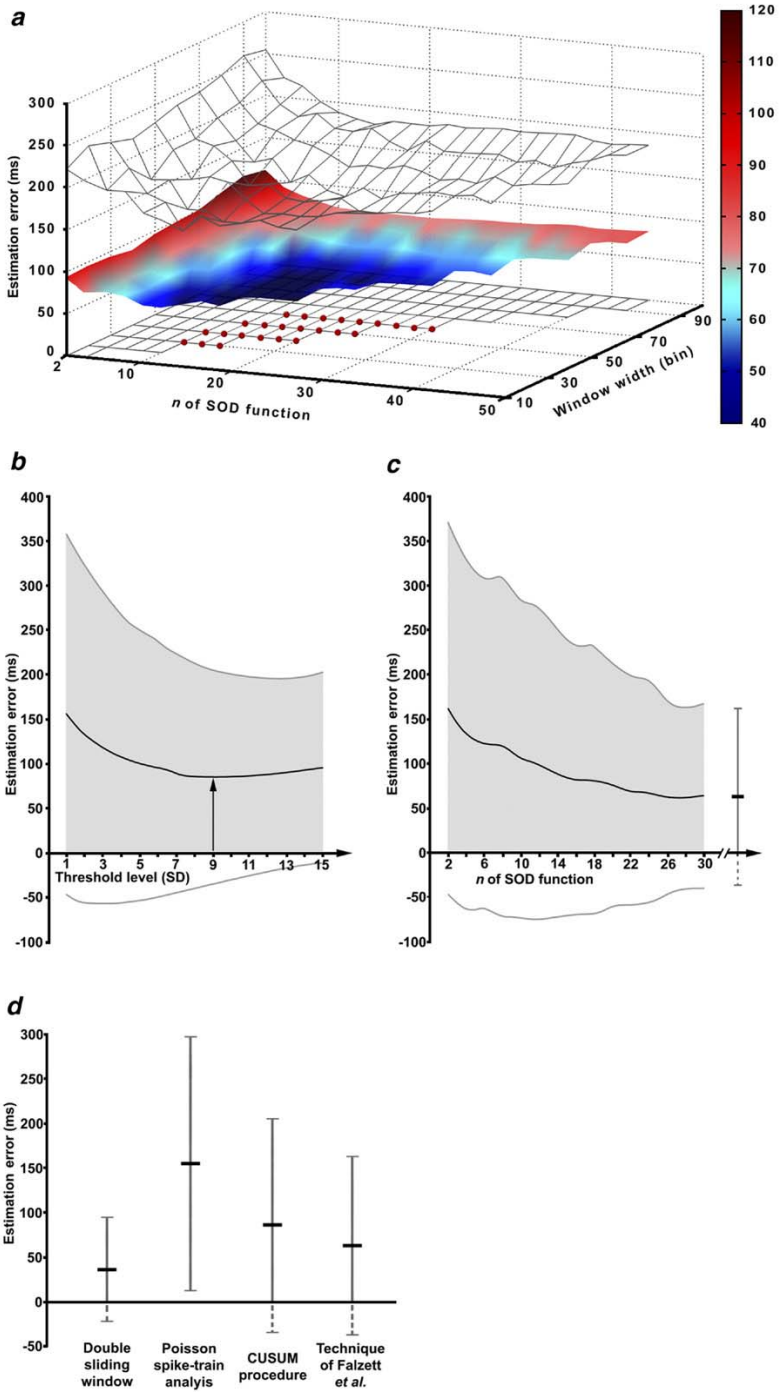

Fig. 3 – Effectivities of the four investigated latency estimation methods. The double sliding-window technique (a) was tested by using 135 different parameter combinations (10 different window widths from 10 to 100 bins and the corresponding possible SOD parameters) on 681 extracellular single-unit recordings. A solid color-shaded surface was constructed from the means of the estimation errors (EEs) of the 681 neurons as a result of using each 135 parameter combination; the ±1 SD range is marked with the two meshes (the lowest limit for this range was defined as 0 since the result of the EE calculation equation cannot be negative). The measurement parameter combinations that were constantly used to calculate the mean of the medians of the EEs (see part d) are marked with red dots. The CUSUM method (b) was also tested on the same 681 recordings using 15 different parameters 1–15 SDs above the mean firing rate as threshold level. The mean+9 SD threshold level (denoted by an arrow) provided the most accurate latency values. The technique of Falzett et al. (c) was tested with 15 different SOD parameters on 681 recordings, and a continuous graph was constructed from the calculated average EE values of the acquired data in ms. The mean of the medians of the EEs (when $n=22$–30 was applied, which yielded the most accurate latency result) is indicated as a discrete range on the right side of the graph. (d) Comparison of the effectiveness of the four latency estimation methods, using the most accurate parameter(s) for each method. The ordinate shows the EEs in ms. Thick horizontal lines denote the mean EE. From left to right, the EEs of the double sliding-window technique, Poisson spike-train analysis, the CUSUM procedure and the technique of Falzett et al. are presented, while the whiskers show the ±1 SD EE range for each method.

train analysis, the CUSUM method and the extension described by Falzett et al. (1985). In some cases, Poisson spike-train analysis estimated the response onset before the onset of the stimulus. We excluded these registrations from our comparison (none of the other methods could provide 'negative' latencies for technical reasons). The mean EE of the Poisson spike-train analysis was 154.41 ms (n=576; SD: ±141.81 ms; Fig. 3d).

In CUSUM analysis, 1, 2 or 3 SDs above the mean spontaneous activity are usually used as the threshold level for this process (Ouellette and Casanova, 2006; Butler et al., 1992). We found that this method tested with 1–3 SDs thresholds consistently underestimated the latencies. We therefore tested our data set with 15 different SD parameters (the threshold was varied in the interval 1–15 SDs). The most accurate latencies and therefore the smallest EE could be calculated by using 9 SDs as threshold. Below and above this threshold, the EEs were higher (Figs. 3b, d). The mean EE with the most accurate (9 SDs) threshold was 85.26 ms (n=681; SD: ±120.11 ms).

The method of Falzett et al. combined the advantages of the CUSUM process with the same SOD function as used in our double sliding-window technique. Fig. 3c illustrates the mean EEs on the use of different n values of the SODs. Similarly as with the double sliding-window technique, the method of Falzett et al. provides the most accurate response onset latencies when high n values are used (n>22; Figs. 3c, d). The median calculation of the acquired onset latencies using different high n values (n=22–30) provided the most accurate values. The mean of the medians of the EEs by the method of Falzett et al. was 62.87 ms (n=681; SD: ±99.98 ms).

2.3. *Comparison of the confidence of the double sliding-window technique with Poisson spike-train analysis, the CUSUM procedure and the method of Falzett et al.*

Since the EE data sets did not reveal normal distribution, we used the Wilcoxon test for the correlated samples to compare the effectiveness of the double sliding-window technique with that of Poisson spike-train analysis, the CUSUM procedure and the method of Falzett et al. The distributions of the EEs observed when the four investigated techniques were used are presented in Fig. 3d. The double sliding-window technique appears to be the most accurate automated latency estimation method in the sense that the EE provided by this technique (mean: 35.98 ms; n=681; SD: ±58.48 ms) was significantly smaller (in all cases p<0.01) than those resulting from Poisson spike-train analysis (mean: 154.41 ms; n=576; SD: ±141.81 ms), the CUSUM procedure (mean: 85.26 ms; n=681; SD: ±120.11 ms) and the advanced method of Falzett et al. (mean: 62.87 ms; n=681; SD: ±99.98 ms).

3. Discussion

The new method described here, the double sliding-window technique, allows the rapid, reproducible, accurate and automated estimation of the neuronal response onset latency. Our results show that the double sliding-window technique can yield more accurate latency data than Poisson spike-train analysis (Legéndy and Salcman, 1985), the CUSUM procedure (Ellaway, 1978) and the method of Falzett et al. (1985) in the sense that the EEs of the latencies calculated by the double sliding-window technique are significantly smaller than those of these most commonly used methods. Furthermore, the double sliding-window technique seems to be able to determine the latency of both excitatory and inhibitory neuronal responses since it detects conformity changes between two data sets regardless of the direction of change.

Poisson distribution (Legéndy and Salcman, 1985) expresses the probability of a number of rare events occurring in a fixed period of time if these events occur with a known average rate, and are independent of the time since the last event. The weakness of Poisson spike-train analysis, i.e. the overestimation of the response latency, may occur for several reasons. The neuronal excitations in a spike train are not independent of each other, and if the spontaneous activity of a single unit is relatively high, and thus the estimated parameter λ of the method is higher than a particular limit, the Poisson spike-train analysis may not work properly. Poisson spike-train analysis is suitable only for the calculation of onset latencies of neurons with low or no spontaneous activity. However, a noteworthy population of neurons has high spontaneous activity, and for these, Poisson spike-train analysis furnishes inaccurate latencies.

As concerns the CUSUM method (Ellaway, 1978), it appears that the most commonly used 1 or 2 SDs above the main spontaneous discharge rate chosen as threshold level is not sufficient to calculate the response onset latency. The mean +9 SD threshold level allows an estimation of the most accurate onset latencies whereas the mean+2 SD threshold level results in an underestimation of the response onset latencies. However, even if we choose a statistically abnormal high 9 SD threshold level, the CUSUM method is still a poorly reliable technique. In the modification of the CUSUM procedure (method of Falzett et al., 1985), the most sensitive problem is the choice of the appropriate n value for the SOD. A 100 ms binwidth and n=3–5 were chosen in the original publication of Falzett et al. as producing the most reliable onset latencies. In our analysis we used a 5 ms binwidth, and found that n=22–30 is the most appropriate parameter with which to calculate the response onset latencies by the method of Falzett et al. Thus, it seems that the correct level of n has to be chosen for the binwidth. Despite the arbitrarily chosen n value, the method of Falzett et al. still appears to be the most reliable of the three techniques discussed above for numerous neuronal response characteristics.

In order to exclude the subjective, arbitrary selection of the parameters, the n value of the SOD and the window width, the double sliding-window technique calculates the latencies by using a series of constant parameters, and the median of the latencies estimated for 25 constant parameter combinations (see Results) defines the response onset latency of a single neuron. It should be noted that the optimal parameter combination set used here to calculate the response onset latency may be valid only for this particular study and may differ from the optimal parameter combinations for other areas of the central nervous system. Another weakness of automated response onset latency estimation procedures is that the arithmetical accuracy of latency value does not correlate with the uncertainty of the estimation. In order to reduce such false

estimations, preliminary visual inspection of the recordings or preliminary, basic statistical probes are recommended.

With regard to its advantages and disadvantages, the double sliding-window method offers a practical alternative to other methods, such as subjective visual estimation, Poisson spike-train analysis, the CUSUM procedure and the method of Falzett et al. (1985). The reliability and reproducibility of the double sliding-window method allow its use in the daily, routine calculation of neuronal response onset latencies.

4. Experimental procedures

The method presented here was specifically developed for the analysis of neuronal activity stored in PSTHs (Eördegh et al., 2005). The original temporal resolution of the recoded data was 1 ms, which was converted to a 5 ms binwidth for faster processing. Each PSTH consisted of a prestimulus interval and a peristimulus interval. The prestimulus interval contains the genuine spontaneous activity of a neuron, while the peristimulus interval contains both the spontaneous activity and the responses of a neuron to the stimulation. The duration of the spontaneous activity in the peristimulus interval defines the onset latency of the neuronal response.

4.1. *Response onset allocation via the t test*

The first element of this computational method is a double sliding-window technique with repetitive application of the *t* test for dependent samples. A computer program slides two virtual time windows with specific width along the spike frequency histogram. The first window, called the reference window, slides through the peristimulus histogram in 1 bin steps (5 ms in our analysis), and the portion is selected where the difference between the content of the reference window and the average activity during the prestimulus period is the highest. The reference window in this specific position represents the maximum frequency (or the minimum frequency if an inhibitory response is investigated) of the peristimulus interval (Fig. 1a). The content of this window is declared to be the 'pure response' and is applied later as a reference in the *t* test. A second window, called the sample window, slides from the beginning of the prestimulus period (pure spontaneous activity) to the position of the reference window in 1 bin steps. For each 1 bin step, a paired *t* test is carried out between the spike rate of the reference and the sample windows, and the level of significance (*p* value) calculated from the *t* value is stored and plotted on a graph. The accurate definition of the lengths of the windows is reasonable, since a too narrow reference window may not compensate the frequency variability inside the spontaneous activity (i.e. a stochastic simultaneous excitation in several trials may lead to an erroneous response identification when the sample window is too narrow to compensate it), while a too broad sample window may include pure spontaneous activity in addition to the response (especially when the window width is broader than the duration of the neuronal response).

This method calculates the similarity between a reference window containing a pure neuronal response and a moving sample window, which at the beginning of the evaluation contains only pure spontaneous activity; later, it contains both spontaneous and stimulated activity; and finally only pure stimulated activity is present. Initially, when no response occurs inside the sample window, the similarity is minimal (the significance level is low). Afterwards, the sampling window slides into the response period, finally reaching total equivalence (significance level 1) as the two windows overlap each other. A curve is fitted to the *p* values, in a theoretical case this being a sigmoid curve (Fig. 1b). The time interval between the start of the stimulation and the first point of the ascending segment of this curve provides the response onset latency.

4.2. *Estimation of the onset of elevation*

When a response occurs, the significance curve mentioned above no longer fits one straight line, but consists of several linear segments, each with a different slope. Each segment of the curve produced by the sliding-window function describes a different period of the neuronal activity and the slope of each segment gives an estimate of the change in the neuronal discharge rate during that segment according to the fixed reference window. In Fig. 1b, the first segment represents pure spontaneous activity, while the second component represents the time segment when the sample window slides onto the response period and contains spontaneous activity and also neuronal responses. Finally, the third segment represents the stage when the sample window clearly overlaps the response. The slope of the second segment is steeper than that of the first, indicating a 'positive conformity change' between the two window contents. The elevation of the significance curve is indifferent as regards the direction of the neuronal discharge rate change, and thus our method can be used to estimate the onset latency of both excitatory and inhibitory neuronal responses. To estimate the latency quantitatively, a SOD is calculated from the sliding-window function to determine the first point of the elevating segment of the significance curve. The aim of this function is to locate breaks and discontinuities between linear segments.

Eq. (1) is used to produce such a function according to Falzett et al. (1985):

$$SOD_{(t)} = |(X_{(t-n)} - X_{(t)})| - |(X_{(t+n)} - X_{(t)})| \quad (1)$$

where X = the significance level; *t* = the actual time component of the function; and $n = \Delta t$, an arbitrary time offset. $SOD_{(t)}$ is computed for each point on the significance curve (Fig. 1c).

A zero value of this difference function means that no change occurs in the steepness of the observed curve in the vicinity of moment $X_{(t)}$. The peaks in the SOD curve furnish estimates of the positions of maximal slope change, and thus define the endpoints of each linear segment. The latency of the response can be calculated by subtracting the time of the stimulus onset from the minimum in $SOD_{(t)}$.

In order to eliminate sporadic disturbances in measurement (estimation imprecision in the case of a single *n* value), the method calculates the response onset latencies as a median of 25 measurements per registration, using 25 selected different parameter combinations that provided the most

accurate latencies for our data sample (4 different window widths from 150 to 300 ms, and the corresponding highest possible n values of SOD; Fig. 3a).

For the cell shown in Fig. 1, the maximum possible n offset of SOD function (30 bins) was applied (which is equal to half of the t test window width (300 ms, 60 bins) as otherwise the SOD function may run out of the range of the t test results), because this value produced a relatively smooth SOD with well-defined peaks. The analysis began with the 31st point of the significance curve ($t=31$; $n=30$), with computation as defined by the equation $(SOD_{(31)}=|(X_{(1)}-X_{(31)})|-|(X_{(61)}-X_{(31)})|)$. The next point of the significance curve to the right of point 31 was then selected and the process was repeated until the entire difference curve had been generated $(SOD_{(32)}=|(X_{(2)}-X_{(32)})|-|(X_{(62)}-X_{(32)})|)$.

4.3. *Statistical evaluation of onset latencies*

Visual latency estimation was performed independently by all three authors (experienced neurophysiologists). The mean of the three subjectively quantified latencies was regarded as the gold standard during the comparison, and EE was calculated for each latency by different techniques via the following equation:

$$EE = |L_t - L_s| \quad (2)$$

where L_t is the onset latency acquired by the automated latency estimation method used, and L_s is the visually quantified gold standard value.

The EE results did not indicate a normal distribution according to the Lilliefors test ($p<0.01$), and the Wilcoxon test for correlated samples was therefore used to compare the EE results of the different calculation methods.

4.4. *Recording and stimulation*

The visual responses of 681 neurons (10 in the suprageniculate nucleus, 238 in the anterior ectosylvian visual area, 20 in the caudate nucleus, 228 in the substantia nigra, 80 in the superior colliculus and 105 in the primary visual cortex) of the feline brain were analyzed in this study. The animal preparation, the surgery and the other details of data collection were described in our earlier papers (Eördegh et al., 2005; Nagy et al., 2005; Paróczy et al., 2006).

Acknowledgments

The authors express their gratitude to Gabriella Dósai Molnár and Kálmán Hermann for their valuable technical assistance and to Péter Liszli for his expert help. The data-collecting activities of Zita Márkus and Zsuzsanna Paróczy are gratefully appreciated. This work was supported by OTKA/Hungary grants T 042610 and F 048396.

Appendix A. Supplementary data

Supplementary data associated with this article can be found, in the online version, at doi:10.1016/j.brainres.2007.08.041.

REFERENCES

Akeyson, E.W., Knuepfer, M.M., Schramm, L.P., 1990. Splanchnic input to thoracic spinal neurons and its supraspinal modulation in the rat. Brain Res. 536, 30–40.

Berson, D.M., 1987. Retinal W-cell input to the upper superficial gray layer of the cat's superior colliculus: a conduction-velocity analysis. J. Neurophysiol. 58, 1035–1051.

Butler, E.G., Horne, M.K., Hawkins, N.J., 1992. The activity of monkey thalamic and motor cortical neurones in a skilled, ballistic movement. J. Physiol. 445, 25–48.

Churchward, P.R., Butler, E.G., Finkelstein, D.I., Aumann, T.D., Sudbury, A., Horne, M.K., 1997. A comparison of methods used to detect changes in neuronal discharge patterns. J. Neurosci. Methods 76, 203–210.

Day, T.A., Sibbald, J.R., 1989. A1 cell group mediates solitary nucleus excitation of supraoptic vasopressin cells. Am. J. Physiol. 257, R1020–R1026.

DiCarlo, J.J., Maunsell, J.H., 2005. Using neuronal latency to determine sensory-motor processing pathways in reaction time tasks. J. Neurophysiol. 93, 2974–2986.

Dreher, B., Sefton, A.J., 1979. Properties of neurons in cat's dorsal lateral geniculate nucleus: a comparison between medial interlaminar and laminated parts of the nucleus. J. Comp. Neurol. 183, 47–64.

Drew, T., Cabana, T., Rossignol, S., 1996. Responses of medullary reticulospinal neurones to stimulation of cutaneous limb nerves during locomotion in intact cats. Exp. Brain Res. 111, 153–168.

Edwards, R., Xiao, D., Keysers, C., Foldiak, P., Perrett, D., 2003. Color sensitivity of cells responsive to complex stimuli in the temporal cortex. J. Neurophysiol. 90, 1245–1256.

Ellaway, P.H., 1978. Cumulative sum technique and its application to the analysis of peristimulus time histograms. Electroencephalogr. Clin. Neurophysiol. 45, 302–304.

Eördegh, G., Nagy, A., Berenyi, A., Benedek, G., 2005. Processing of spatial visual information along the pathway between the suprageniculate nucleus and the anterior ectosylvian cortex. Brain Res. Bull. 67, 281–289.

Falzett, M., Moore, R.K., Petry, H.M., Powers, M.K., 1985. A method for determining threshold from single-unit neural activity. Brain Res. 347, 127–131.

Forlano, L.M., Horne, M.K., Butler, E.G., Finkelstein, D., 1993. Neural activity in the monkey anterior ventrolateral thalamus during trained, ballistic movements. J. Neurophysiol. 70, 2276–2288.

Fournier, E., Meunier, S., Pierrot-Deseilligny, E., Shindo, M., 1986. Evidence for interneuronally mediated Ia excitatory effects to human quadriceps motoneurones. J. Physiol. 377, 143–169.

Gerstein, G.L., Kiang, N.Y., 1960. An approach to the quantitative analysis of electrophysiological data from single neurons. Biophys. J. 1, 15–28.

Hanes, D.P., Thompson, K.G., Schall, J.D., 1995. Relationship of presaccadic activity in frontal eye field and supplementary eye field to saccade initiation in macaque: Poisson spike train analysis. Exp. Brain Res. 103, 85–96.

Hernandez, A., Zainos, A., Romo, R., 2002. Temporal evolution of a decision-making process in medial premotor cortex. Neuron 33, 959–972.

Holt, I.L., Akeyson, E.W., Knuepfer, M.M., 1991. Medial medullary contribution to tonic descending inhibition of visceral input. Am. J. Physiol. 261, R727–R737.

Knuepfer, M.M., Holt, I.L., 1991. Effects of electrical and chemical stimulation of nucleus raphe magnus on responses to renal nerve stimulation. Brain Res. 543, 327–334.

Legéndy, C.R., Salcman, M., 1985. Bursts and recurrences of bursts in the spike trains of spontaneously active striate cortex neurons. J. Neurophysiol. 53, 926–939.

Marque, P., Nicolas, G., Marchand-Pauvert, D., Gautier, J., Simonetta-Moreau, M., Pierrot-Deseilligny, E., 2001. Group I projections from intrinsic foot muscles to motoneurones of leg and thigh muscles in humans. J. Physiol. 536, 313–327.

Nagy, A., Paróczy, Z., Norita, M., Benedek, G., 2005. Multisensory responses and receptive field properties of neurons in the substantia nigra and in the caudate nucleus. Eur. J. Neurosci. 22, 419–424.

Ouellette, B.G., Casanova, C., 2006. Overlapping visual response latency distributions in visual cortices and LP-pulvinar complex of the cat. Exp. Brain Res. 175, 332–341.

Paróczy, Z., Nagy, A., Márkus, Z., Waleszczyk, W.J., Wypych, M., Benedek, G., 2006. Spatial and temporal visual properties of single neurons in the suprageniculate nucleus of the thalamus. Neuroscience 137, 1397–1404.

Rolls, E.T., Cahusac, P.M., Feigenbaum, J.D., Miyashita, Y., 1993. Responses of single neurons in the hippocampus of the macaque related to recognition memory. Exp. Brain Res. 93, 299–306.

Sáry, G., Köteles, K., Chadaide, Z., Tompa, T., Benedek, G., 2006. Task-related modulation in the monkey inferotemporal cortex. Brain Res. 1121, 76–82.

Seal, J., Commenges, D., Salamon, R., Bioulac, B., 1983. A statistical method for the estimation of neuronal response latency and its functional interpretation. Brain Res. 278, 382–386.

Tamura, H., Tanaka, K., 2001. Visual response properties of cells in the ventral and dorsal parts of the macaque inferotemporal cortex. Cereb. Cortex 11, 384–399.

Ushiba, J., Tomita, Y., Masakado, Y., Komune, Y., 2002. A cumulative sum test for a peri-stimulus time histogram using the Monte Carlo method. J. Neurosci. Methods 118, 207–214.

Wandell, B.A., 1977. Speed-accuracy tradeoff in visual detection: applications of neural counting and timing. Vis. Res. 17, 217–225.

II.

ELSEVIER

Brain Research Bulletin 67 (2005) 281–289

BRAIN
RESEARCH
BULLETIN

www.elsevier.com/locate/brainresbull

Processing of spatial visual information along the pathway between the suprageniculate nucleus and the anterior ectosylvian cortex

Gabriella Eördegh, Attila Nagy, Antal Berényi, György Benedek *

Department of Physiology, Faculty of Medicine, Albert Szent-Györgyi Medical and Pharmaceutical Centre, University of Szeged, Dóm tér 10, H-6720 Szeged, Hungary

Received 6 January 2005; received in revised form 5 May 2005; accepted 21 June 2005
Available online 19 August 2005

Abstract

This study describes the visual information coding ability of single neurons in the suprageniculate nucleus (Sg), and provides new data concerning the visual information flow in the suprageniculate/anterior ectosylvian pathways of the feline brain. The visual receptive fields of the Sg neurons have an internal structure rather similar to that described earlier in the anterior ectosylvian visual area (AEV). The majority of the Sg units can provide information via their discharge rate at the site of the visual stimulus within their large receptive fields. This suggests that they may serve as panoramic localizers. The sites of maximum responsivity of the Sg neurons are distributed over the whole investigated part of the visual field. There is no significant difference between the distributions of spatial location of maximum sensitivity of the AEV and the Sg neurons. The mean visual response latency of the Sg units was found to be significantly shorter than the mean latency of the AEV neurons, but there was no difference between the shortest latency values of the thalamic and the cortical single-units. This suggests that the visual information flows predominantly from the Sg to the AEV, though the cortico-thalamic route is also active. The Sg seems to represent a thalamic nucleus rather similar in function to both the first-order relays and the higher-order thalamic nuclei. These results, together with the fact that the superior colliculus provides the common ascending source of information to the suprageniculate/anterior ectosylvian pathway, suggest a unique function of the AEV and the Sg in sensorimotor integration.

Keywords: Suprageniculate nucleus; AEV; Panoramic localizers; Spatial coding; Latency; Visual

1. Introduction

The existence of the visual areas along the anterior ectosylvian sulcus (AES) of the feline brain was described in the 1980s [3,11,21,25]. Morphological studies revealed that these areas receive visual information bypassing the geniculo-striate system, through a cortical route via the lateral suprasylvian visual areas and through a tecto-thalamic route via the suprageniculate nucleus (Sg) and the lateral posterior nucleus pars medialis (LPm) of the thalamus [24,23]. The physiological properties of the LPm and its connections have been studied fairly widely [1,6,13,15,16,28,33]. The Sg, however, has attracted much less interest during the last 25 years, although the neurons in this thalamic nucleus exhibit special physiological properties. While the lateral geniculate nucleus (LGN) relays the retinal input towards the primary visual cortex without causing any fundamental modification in the size of the receptive fields, the visual receptive fields in the Sg are rather dissimilar to those of the neurons of the intermediate and deep layers of the superior colliculus (SC) from where they receive their tectal visual afferentation. The receptive fields of the Sg neurons uniformly cover the whole extent of the visual field of the stimulated eye [4,12]. These receptive field properties can appear for two reasons. The strong convergence of the collicular fibres on the Sg [14] could be responsible for the representation of the whole visual field. The Sg might mediate this information to the cortex, and thus the similarly huge receptive fields of the neurons along the AES [3,11,21] could be a consequence

* Corresponding author. Tel.: +36 62 545098; fax: +36 62 545842.
E-mail address: benedek@phys.szote.u-szeged.hu (G. Benedek).

0361-9230/$ – see front matter © 2005 Elsevier Inc. All rights reserved.
doi:10.1016/j.brainresbull.2005.06.036

of the thalamic relaying of this convergence. On the other hand, the activity of the pathway between the visual associative cortex (AEV) and the Sg [12,33] could also result in the large receptive fields of Sg neurons. This raises at least two important questions concerning the visual information processing and flow between the AES cortex and the Sg: is the internal organization of the large receptive fields of the Sg units similar to or different from that of the AEV [2,5]? Then, as regards the direction of the information flow, are the cortico-thalamic and thalamo-cortical routes equally active during visual information processing?

We attempted to aquire data which would clarify these problems by recording single-unit responses to visual stimulation both in the AEV and in the Sg of the feline brain. The stimulation was performed by moving a randomly selected portion of a large visual white-noise pattern in front of the animal. Earlier use of the same stimulation set-up revealed that within each visual receptive field of the neurons in the AES cortex there is a "hot-spot", i.e. a region which is preferentially sensitive to visual stimulation [5]. The location of this region varies among the neurons, providing a possibility for a non-traditional spatial coding of signals in the visual field [2,5]. In the present study, we investigated the distribution of sites of maximum sensitivity within the large receptive fields of the Sg neurons and compared the organization of the receptive fields in the AEV and the Sg. We further calculated the latencies of the AEV and the Sg visual responses. Comparison of the AEV and Sg latencies could possibly shed light on the direction of information flow between the AEV and the Sg and may provide an indication as to whether the cortico-thalamic volley first reaches the thalamus, or whether the SC causes the initial excitation in the neurons of the Sg.

2. Materials and methods

2.1. Animal preparation and surgery

The experiments were performed on 19 adult cats ranging in weight from 2.4 to 4.0 kg. The experimental protocol had been accepted by the Ethical Committee for Animal Research of the University of Szeged. The anaesthesia was initiated with ketamine hydrochloride (30 mg/kg, i.m.). After cannulation of the femoral vein and the trachea, the animals were placed in a stereotaxic headholder. The wound edges and pressure points were treated generously with procaine hydrochloride (1%). The anaesthesia was continued with halothane (1.6% during surgery and 0.8% during recordings). The depth of anaesthesia was monitored by repeated checks of pupil size on the non-treated side, and checking electrocorticogram and electrocardiogram recordings. All of the parameters controlled revealed the general anaesthesia of the animals throughout the whole of the experiments. The animals were immobilized with gallamine triethiodide (Flaxedyl, 20 mg/kg i.v.). During the experiment, a solution containing gallamine (8 mg/(kg h)), glucose (10 mg/(kg h)) and dextran (50 mg/(kg h)) in Ringer's solution was infused continuously at a rate of 3 ml/h. Atropine (0.1%, 0.2 ml) was administered subcutaneously. The end-tidal CO_2 level and

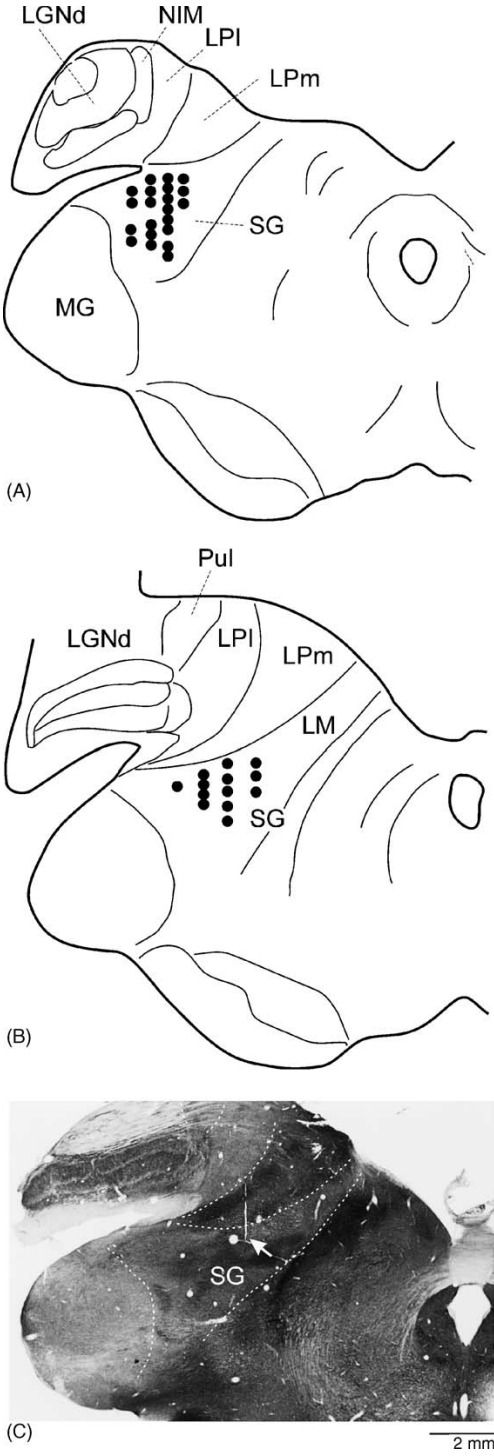

the rectal temperature were monitored continuously and kept constant at 3.8–4.2% and 37–38 °C, respectively. The skull was opened with a dental drill to allow a vertical approach to the Sg and the AEV. The dura was covered with a 4% solution of agar dissolved in Ringer solution. The eye contralateral to the cortical recording was treated with phenylephrine (10%) and atropine (0.1%), and was equipped with a +2 dioptre contact lens. The ipsilateral eye was covered during stimulation. A subcutaneous injection of 0.2 ml 0.1% atropine was administered preoperatively. The retinal landmarks and major retinal blood vessels were projected routinely twice daily onto a tangent screen, using a fiberoptic light source [26]. In some cases, the area centralis could be seen directly, in others, it was plotted by reference to the optic disc 14.6° medially and 6.5° below the centre of optic disc [7].

2.2. Recording

Electrophysiological recordings were performed extracellularly with tungsten microelectrodes (AM System Inc. USA, 2–4 MΩ). Single-unit discrimination was made with a spike-separator system (SPS-8701, Australia). Vertical penetrations were performed to reach the Sg between the Horsley–Clarke coordinates anterior 4.5–6.5 and lateral 4–7 in the stereotaxic depths in the interval 10–13 mm. The AEV neurons were recorded between the co-ordinates anterior 11–14 and lateral 12–14 in the stereotaxic depths in the interval 13–19 mm. At the end of the experiments, the animals were deeply anaesthetized with pentobarbital and perfused transcardially with paraformaldehyde solution (4%). The brains were removed, cut in coronal sections of 50 μm and stained with neutral red or for acetylcholine-esterase. Electrolytic lesions marked the locations of successful electrode penetrations. All of the recorded neurons were located either in the Sg (Fig. 1) or in the AEV.

2.3. Stimulation and data evaluation

The visual responsivity of the neurons was tested subjectively by the generation of moving visual stimuli with a hand-held lamp. Whenever a single-unit was found to be sensitive to moving visual stimulation, computer-controlled visual noise patterns were used to estimate its visual response properties. For computer-controlled visual stimulation, an 18-in. computer monitor (refresh rate—60 Hz) was placed 57 cm in front of the animal. A stationary visual noise stimulus (grain size: 0.2–1.5°) was presented to the animal in an area of 24° × 32° around the area centralis. The mean luminance of the screen was 17 cd/m^2. We divided this area into 12 parts each of 8° × 8°. To avoid stationary problems, the stimuli were randomized in position over trials. The randomly selected 8° × 8° portion of the elements comprising the pattern was then moved for 2500 ms at a speed of 10°/s. We investigated the responses to eight different moving directions of the visual noise pattern along four axes (0–315° at 45° increments) to find the preferred moving direction of each single neuron. Neuronal activities were then recorded and correlated with the movement of the visual noise pattern in the preferred direction. They were stored for further analysis as peristimulus time histograms (PSTHs). The original binwidth was 62 ms, while binwidths of 1, 2, 5 and 10 ms were used to calculate the visual response latencies. The prestimulus time (during which a stationary visual noise pattern stimulus was shown) was 500 ms and the peristimulus time (while the visual noise pattern stimulus was moving) was 2500 ms. At least four trials were run in each 8° × 8° window. The interstimulus interval was 1 s.

We defined the net firing rate in each 8° × 8° window as the response when a paired *t*-test demonstrated a significant difference ($p < 0.05$) between the prestimulus and peristimulus firing rates. While the visual receptive field of the AEV and the Sg neurons are extremely large [4,22], we considered a cell to be visually responsive if it was responsive in each 8° × 8° window. The spatial selectivity of each responsive cell was investigated with one-way ANOVA. We defined a neuron as spatially selective if the net firing rate of at least one window was significantly different from the mean of the others. As maximum site, we considered the stimulus location at which the net firing rate was highest. We estimated the distance of the maximum responsive site from the area centralis and the angle of the vector connecting the maximum responsive site and the area centralis. We compared these values between the AEV and the Sg neurons. The comparison was performed either with the *t*-test, if the values exhibited normal distribution, or with the Kruskal–Wallis test, if the distribution of the values was not normal.

To measure the latency of the responses, we used a software program developed in our laboratory. This was based on a sliding-window technique. The program slid two 350 ms windows along the frequency histogram of the responses. The first window slid through the peristimulus firing rate in 5 ms steps, and selected the 350 ms wide portion that represented the maximum frequency. Then, a second window was slid in 5 ms steps, and after each step the program calculated the significance level between the spike frequency values of the two windows with the *t*-test. The latency of the responses was calculated from the time function of these *p* values. A curve was fitted to the *p* values, and the time interval between the start of the stimulation and the inflection point provided the response latency.

Fig. 1. Histological reconstruction of the recording sites and the recorded units in the Sg. (A and B) Positions of the recorded visually responsive neurons (black dots) in the Sg. The drawings depict coronal sections of the Sg in the cat brain in A5 and A6 according to the stereotaxic atlas of Reinoso-Suarez [27]. (C) An acethylcholine–esterase stained section of the Sg within the position of the recording electrode marked by the white arrowhead. Bars in the right bottom corner provide size calibration and orientation in the dorso-ventral and medio-lateral aspect. *Abbreviations*: LGNd, lateral geniculate nucleus; LPl, lateral division of the nucleus lateralis posterior; LPm, medial division of the nucleus lateralis posterior; LM, nucleus lateralis medialis; Sg, suprageniculate nucleus; MG, medial geniculate nucleus.

3. Results

Altogether 35 visually responsive single-units were recorded extracellularly in the Sg and 32 visual responsive units in the AEV. The information processing and coding abilities of these units were analysed in detail. Fig. 1 demonstrates the histological reconstruction of the recording tracks and the positions of the analysed Sg units (A and B) a Sg section with the electrode penetration (C).

The extent of the visual receptive field was estimated subjectively by listening to the neuronal responses to movements of a light spot generated by a hand-held lamp. Similarly to earlier results, the visual receptive fields in both the extrageniculate thalamus and the visual associative cortex were extremely large (consistently larger than 6000 degree^2): they covered a major part of the contralateral hemifield and extended deep into the ipsilateral one, yielding a field that overlapped almost totally with the visual field of the right eye [4,21]. The receptive fields consistently included the area centralis. No signs of retinotopical organization were observed within either the AEV or the Sg. The visual receptive fields of both the Sg and the AEV neurons were definitely larger than the computer monitor used for visual stimulation. Thus, we could investigate the information coding abilities of the AEV and the thalamic neurons only in a restricted, though large central part of their visual receptive fields.

3.1. Spatial selectivity of the AEV and the Sg neurons

The distributions of the preferred directions of the 35 Sg and the 32 AEV units were very similar. Only small proportions of the AEV (3/32) and the Sg neurons (4/35) exhibited optimum responsivity to movement along the horizontal axis (90° and 270° directions). The preferences for the other six directions were distributed evenly among the neurons. The data obtained for the optimum directions were used for the further analysis.

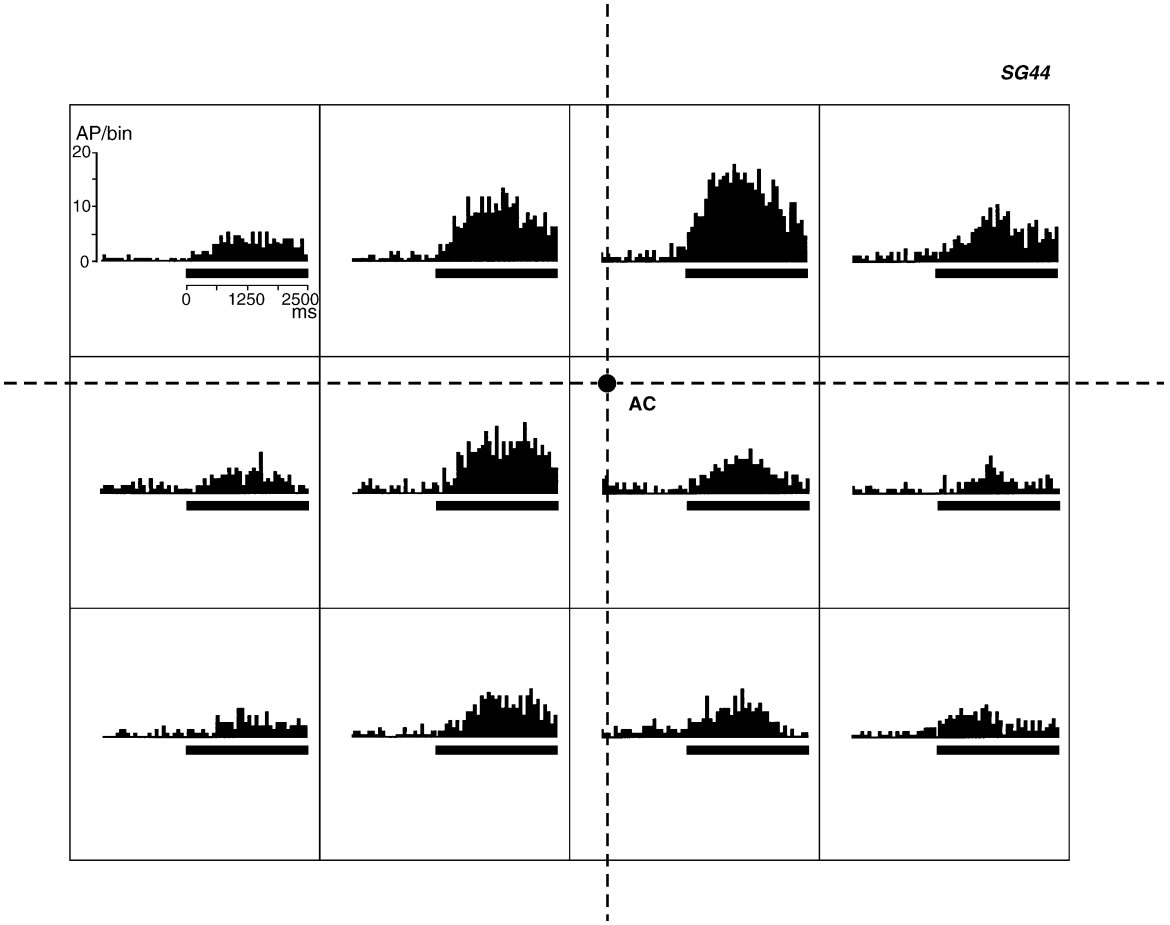

Fig. 2. Receptive field organization of a panoramic suprageniculate nucleus neuron, *SG44*. Peristimulus histograms are presented that were recorded during the motion of visual noise in the respective part of the visual field. Every window represents a 8° × 8° portion of the receptive field. In each window, the abscissa indicates time. The ordinate denotes number of action potential/binwidth values (binwidth = 62 ms). The thick black line indicates the motion of the visual noise for 2500 ms.

Spatial sensitivity towards moving stimulation within the restricted part of the receptive field was estimated by comparing the response intensities by means of one-way ANOVA. This indicated that the majority of the visually responsive neurons in both the Sg (26/35; 73.7%) and the AEV (24/32) were sensitive to the location of the moving visual stimulus (Figs. 2 and 3). Similarly to earlier results on the AEV [2,5], the site of maximum responsivity within the visual receptive fields of the Sg neurons varied extensively in the neurons recorded. For the most of the units, the visual field did not appear to contain an exclusive site. Some of the units exhibited a preference for a particular stimulus site, while other units were most responsive to other locations. Thirteen Sg units had a preference in the contralateral upper, 14 in the contralateral lower, 4 in the ipsilateral lower and 4 in the ipsilateral upper quadrant of the investigated central visual field. Our results revealed that the maximum responsive sites of the Sg neurons, similarly to those of the AEV that were described earlier [5], were distributed throughout the whole of the investigated area. Maximum responsive sites were found in each quadrant of the visual field (Fig. 4). Since recent results have demonstrated that the maximum responsive sites of the AEV neurons are distributed in the whole visual field of the right eye [2], we cannot exclude the possibility that some Sg neurons exhibit maximum responsivity to stimulation sites outside the investigated region. No inhibitory responses were recorded at all.

We estimated the distances of the maximum responsive sites from the area centralis of the AEV and the Sg neurons. The mean distance of the maximum sensitive sites of the AEV neurons from the area centralis was 7.99° ($N = 32$; range: 0–20°; S.D.: ±4.29°). The mean distance of the maximum sensitive sites of the Sg neurons from the area centralis was 8.27° ($N = 35$; range: 2–18°; S.D.: ±3.67°). Since the distribution of the distances did not satisfy the criterion of normality, we used the Kruskal–Wallis test to compare them. The test demonstrated that there was no significant difference between the distances of the maximum responsive sites from the area centralis of the cortical and that of the thalamic neurons ($p = 0.55$). Similar results were obtained as

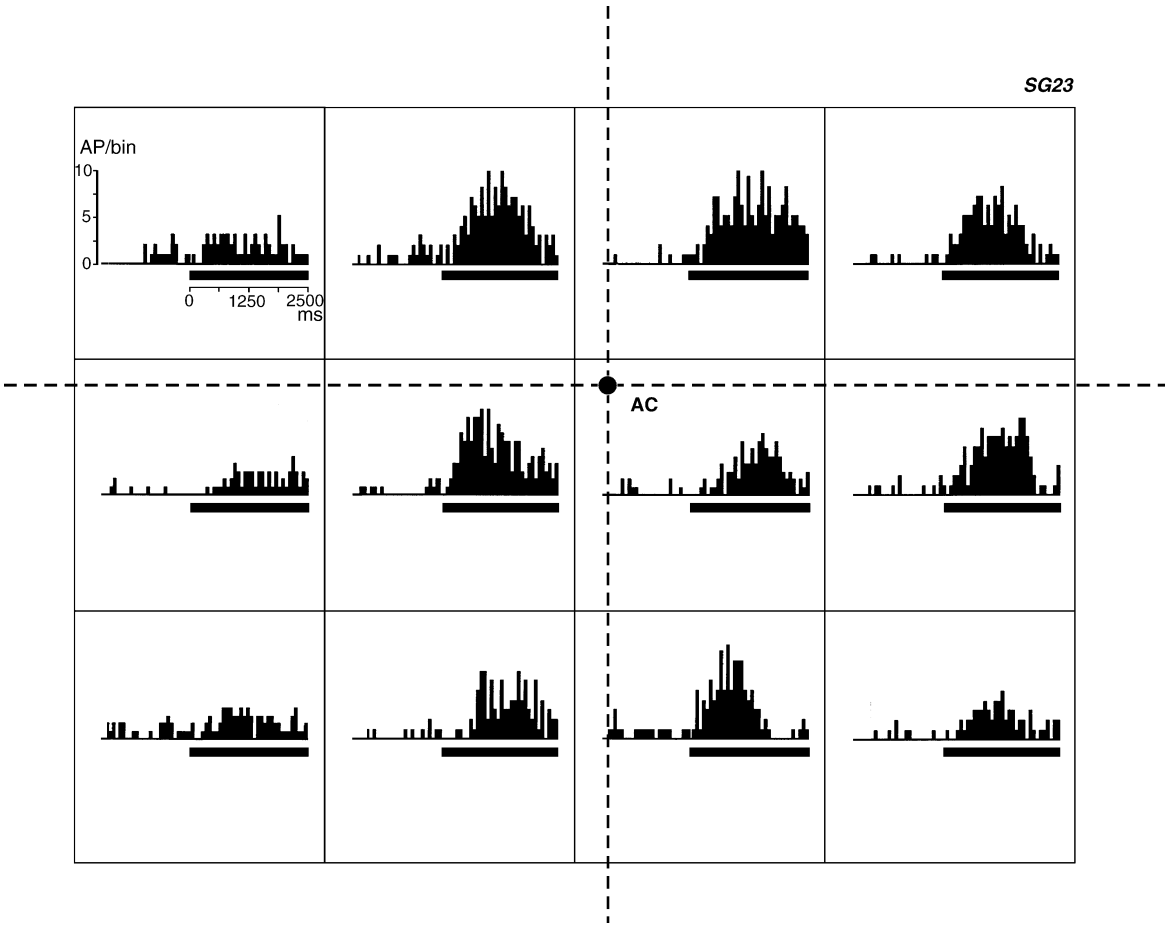

Fig. 3. Receptive field organization of another panoramic suprageniculate nucleus neuron, *SG23,* recorded in another cat. The arrangement here is the same as that in Fig. 2.

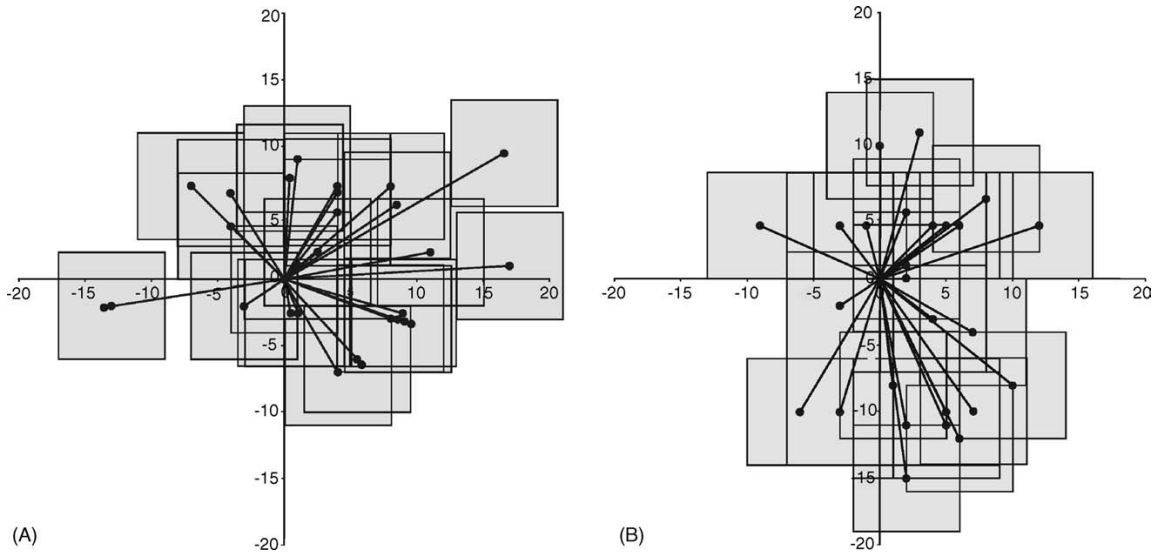

Fig. 4. Position of the site of maximum responsivity in the receptive fields of 32 AEV single-units (A) and 35 Sg single-units (B) determined by the highest firing rate in the respective window. Every single-unit is represented by an 8° × 8° grey window representing the motion of the visual noise and a vector line between the area centralis and the centre of the "window" from where the highest activity was elicited. Vertical and horizontal meridians are presented as thick lines, with scaling given in degrees.

concerns the direction of the line connecting the maximum responsive sites to the area centralis relative to the horizontal meridian. The distributions of the directions for the AEV neurons (mean = 136.5°; $N = 32$; range: 0–345°; S.D.: ±118.0°) and that for the Sg neurons (mean = 146.7°; $N = 35$; range: 0–350°; S.D.: ±114.9°) were very similar. Both displayed a normal distribution. The *t*-test showed no difference between the directions of the sites of maximum sensitivity from the area centralis of the AEV and the Sg neurons ($p = 0.87$). These results indicate that the maximum responsive sites of the AEV and the Sg neurons are distributed similarly in the investigated central part of the visual field.

3.2. Response latencies of the AEV and the Sg neurons

We calculated and compared the visual response latencies of the 35 investigated Sg and 32 AEV units to assess whether the cortico-thalamic or the thalamo-cortical information processing route has a temporal priority between the Sg and the AEV (Fig. 5). The shortest latency in both the Sg and the AEV was 35 ms. Generally, however, the latencies of the responses measured for the AEV units were longer than those for the Sg units. The mean latency of the response of the Sg neurons (calculated at their maximum responsive sites) was 59.4 ms ($N = 35$; range: 35–130 ms; S.D.: ± 26.28 ms). The mean latency of the AEV units was 81.7 ms ($N = 32$; range: 35–185 ms; S.D.: ±42.48 ms). The distribution of the latencies did not reveal normal distribution, presumably reflecting the fact that there is no homogeneous population of units producing this response. Comparison of the cortical and thalamic latencies by means of the Kruskal–Wallis test revealed that the visual response latencies of the investigated Sg neurons were significantly shorter than the visual response latencies of the AEV neurons ($p = 0.011$).

4. Discussion

Our results demonstrated that the visual receptive fields of the Sg neurons have an internal structure which resembles that described earlier in the AEV [2,5]. We found that the visual receptive fields of the neurons in both structures are similar; they consistently cover the whole visual field of the stimulated eye [4,22]. The size of the receptive fields found in the AEV by Olson and Graybiel [25] and later by Scannel et al. [29] was considerably smaller than that described by us. This discrepancy could originate from the different types of anaesthesia used or in the obvious difficulties in drawing these huge receptive fields. Both Olson and Graybiel [25] and Scannell et al. [29] concentrated on finding the locations of the most intense areas, while we attempted to find the border between the responsive and absolutely non-responsive areas and sought the locations of the regions of maximum sensitivity. The majority of the Sg and the AEV units in our experiments proved selective to the stimulus location; they exhibited significantly different responses to stimuli from different spatial locations. These indicate that as it has been described earlier for the AES units [2], the Sg units have similar abilities to serve as panoramic localizers [18,19]. The regions of maximal sensitivity within the investigated central part of the visual field are widely distributed for both the AEV [2] and the Sg neurons. This is in agreement with the report

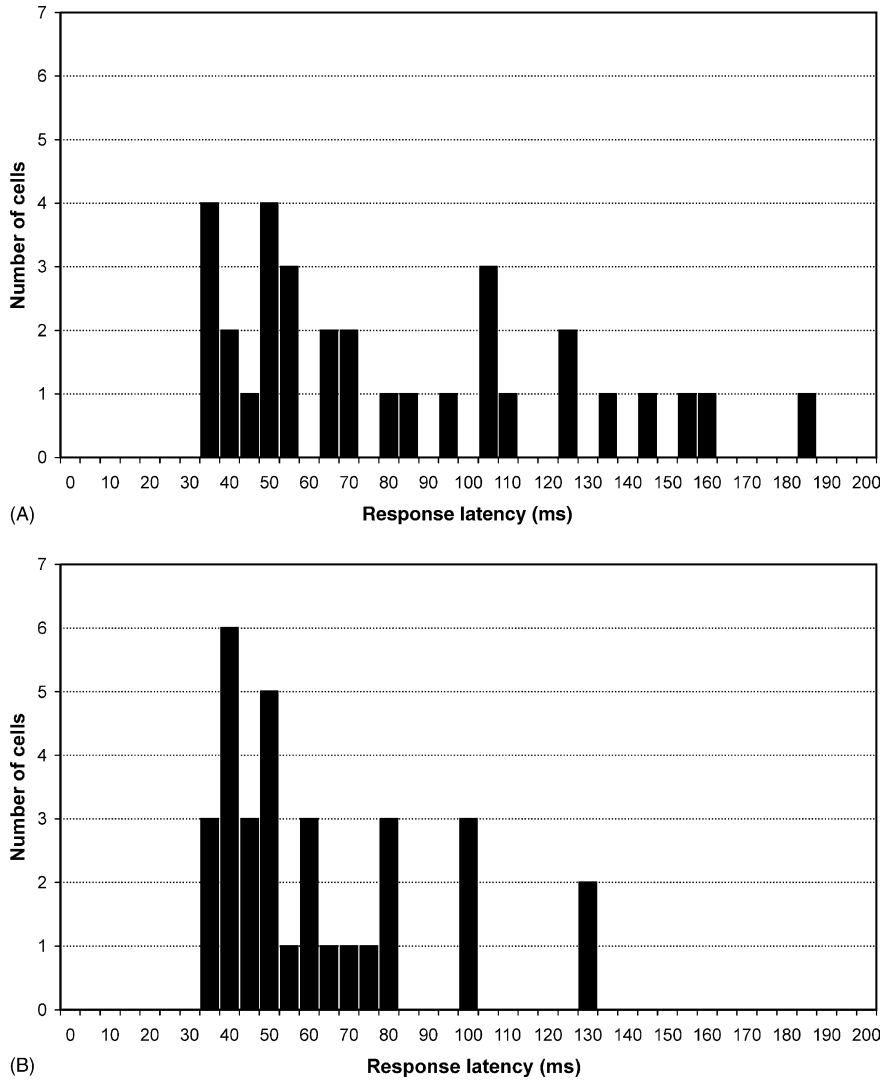

Fig. 5. Frequency distributions of AEV (A) and Sg (B) cells according to their response latency to a visual noise moving in their receptive fields. The abscissa shows the latency of the single-unit activity response in milliseconds. The ordinate indicates the numbers of units with the respective latency values.

from the AEV of Scannell et al. [29], who found the sites of the most intense responses within the same areas of the receptive fields. These observations point to the possibility of a distributed population code of visual information in the Sg, similarly as in the AEV [2], based on panoramic localizer cells [18–20]. The very high similarity of the receptive fields of the Sg and the AES cortex points to the existence of a very intense exchange of information between the two stages of visual processing.

The results of our latency studies provide interesting data on the sequence of volleys of excitation between the cortex and the thalamus. Latency studies are not widely used in the investigation of thalamo-cortical relations, most probably because of the technical limitations in calculating spike latency values amidst considerable spontaneous activity. We found that there was no difference between the shortest latency values of the thalamic and the cortical single-units. Both structures responded to visual motion with a minimum latency of 35 ms. The mean response latency of the Sg units, however, is significantly shorter than the mean latency of the AEV neurons. These results might suggest that both the thalamo-cortical and the cortico-thalamic route are active between the extrageniculate visual thalamus and the visual associative cortex. The generally shorter latencies in the thalamus might indicate that the visual information flows predominantly from the thalamic nucleus to the AEV. The fact that there is a temporal priority of the thalamus over the cortex, however, does not prove the superiority of the thalamo-cortical volleys over the cortico-thalamic ones. We cannot exclude the possibility either that the information

concerning the receptive field properties reaches the Sg (albeit with a delay) through a cortico-thalamic route.

The function of the thalamus in the mammalian brain is based on the existence of two types of relays [30,31]. Thalamic first-order relays receive their driving afferents from ascending pathways and transmit messages to the cortex that the cortex has not received before. Higher-order relays bring driver messages to the thalamus from the cortex for transmission from one cortical area to another. This ambiguity stresses the importance of the cortico-thalamic and the thalamo-cortical pathways. The distinction between the two types of relays, however, is not always equivocal. There are thalamic nuclei that receive driving from both the cortex and lower centres. The best-known such nuclei are the pulvinar and the lateralis posterior nuclei, which receive driving afferents from the visual cortex, and there is an additional tectal input to them [8,17]. Similarly, Sommer and Wurtz [32] described that the medial dorsal nucleus of the thalamus that innervates the frontal eye field receives drive from both the cortex and the intermediate and deep layers of the SC, but its main drive arrives from the tectal region. These thalamic nuclei process messages that have already reached the cortex and been processed in at least one cortical area, and at the same time they serve the role of first-order relays receiving signals from the ascending pathways. A similar ambiguity seems to characterize the role of the Sg of the thalamus and its connections with the cortex along the AES. The Sg receives heavy afferentation both from the intermediate and deep layers of the SC [14] and from the visual associative cortex along the AES [12]. Thus, it could serve either as a higher-order relay nucleus or as a simple first-order relay of tectal information. Since our data suggest that visual information flows bidirectionally between the Sg and the AES cortex, further investigations are necessary to elucidate whether the thalamo-cortical and cortico-thalamic axons are drivers or modulators, and to determine the direction of information flow between the Sg and the AES cortex. Antidromic microstimulation of the AES cortex or the Sg can help reveal direct connections between the responses of the neurons in each area, and neuronal lesions of the Sg or the AES cortex can demonstrate any interdependence of the investigated AES cortex or Sg neuronal activities.

To summarize, our data suggest that the Sg takes part in visual information processing through complex cortico-thalamo-cortical loops. It seems, therefore, that it represents a thalamic nucleus rather similar in function to the pulvinar or lateral posterior nuclei, structures that have been described as higher-order thalamic nuclei [8,17]. Because of the paucity of morphological data available, it is difficult to support this conclusion with histological evidence concerning the same arrangement of cortico-thalamic synapses in the Sg as that described for both the pulvinar and the lateral posterior nuclei [9,10]. The similarities of the physiological responses of all three structures, however, together with the fact that the SC provides their common ascending source of information, suggest a common function for them in the process of sensorimotor integration.

Acknowledgements

The authors thank Gabriella Dósai and Kálmán Hermann for their valuable technical assistance, and Péter Liszli for his expert help in solving software and hardware problems. The data-collecting work of Gyula Kovács, Katalin Kóródi and László Sztriha is highly appreciated. This work was supported by OTKA/Hungary grant T 042610 and FKFP/Hungary grant 0455/2000.

References

[1] B.P. Abramson, L.M. Chalupa, Multiple pathways from the superior colliculus to the extrageniculate visual thalamus of the cat, J. Comp. Neurol. 271 (1988) 397–418.
[2] G. Benedek, G. Eordegh, Z. Chadaide, A. Nagy, Distributed population coding of multisensory spatial information in the associative cortex, Eur. J. Neurosci. 20 (2004) 525–529.
[3] G. Benedek, L. Mucke, M. Norita, B. Albowitz, O.D. Creutzfeldt, Anterior ectosylvian visual area (AEV) of the cat: physiological properties, Prog. Brain Res. 75 (1988) 245–255.
[4] G. Benedek, J. Perenyi, G. Kovacs, L. Fischer-Szatmari, Y.Y. Katoh, Visual, somatosensory, auditory and nociceptive modality properties in the feline suprageniculate nucleus, Neuroscience 78 (1997) 179–189.
[5] G. Benedek, L. Sztriha, G. Kovács, Coding of spatial co-ordinates on neurones of the feline visual association cortex, Neuroreport 11 (2000) 1–4.
[6] D.M. Berson, A.M. Graybiel, Organization of the striate-recipient zone of the cats lateralis posterior-pulvinar complex and its relations with the geniculostriate system, Neuroscience 9 (1983) 337–372.
[7] P.O. Bishop, W. Kozak, G.J. Vakkur, Some quantitative aspects of the cat's eye: axis and plane of reference, visual field coordinates and optics, J. Physiol. (Lond.) 163 (1962) 466–502.
[8] C. Casanova, L. Merabet, A. Desautels, K. Minville K., Higher-order motion processing in the pulvinar, Prog. Brain Res. 134 (2001) 71–82.
[9] R.W. Guillery, S.L. Feig, D.P. Van Lieshout, Connections of higher order visual relays in the thalamus: a study of corticothalamic pathways in cats, J. Comp. Neurol. 438 (2001) 66–85.
[10] R.W. Guillery, S.M. Sherman, Thalamic relay functions and their role in corticocortical communication: generalizations from the visual system, Neuron 33 (2002) 163–175.
[11] T.P. Hicks, G. Benedek, G.A. Thurlow, Organization and properties of neurons in a visual area within the insular cortex of the cat, J. Neurophysiol. 60 (1988) 397–421.
[12] T.P. Hicks, C.A. Stark, W.A. Fletcher, Origins of afferents to visual suprageniculate nucleus of the cat, J. Comp. Neurol. 246 (1986) 544–554.
[13] B. Hutchins, B.V. Updyke, Retinotopic organization within the lateral posterior complex of the cat, J. Comp. Neurol. 285 (1989) 350–398.
[14] Y.Y. Katoh, G. Benedek, Organization of the colliculo-suprageniculate pathway in the cat: a wheat germ agglutinin-horseradish peroxidase study, J. Comp. Neurol. 352 (1995) 381–397.
[15] R. Mason, Differential responsiveness of cells in the visual zones of the cat's LP-pulvinar complex to visual stimuli, Exp. Brain Res. 43 (1981) 25–33.
[16] R. Mason, G.A. Groos, Cortico-recipient and tecto-recipient visual zones in the rat's lateral posterior (pulvinar) nucleus: an anatomical study, Neurosci. Lett. 25 (1981) 107–112.

[17] L. Merabet, A. Desautels, K. Minville, C. Casanova, Motion integration in a thalamic visual nucleus, Nature 396 (1998) 265–268.
[18] J.C. Middlebrooks, A.E. Clock, L. Xu, D.M. Green, A panoramic code for sound location by cortical neurones, Science 264 (1994) 842–844.
[19] J.C. Middlebrooks, L. Xu, A.C. Eddins, D.M. Green, Codes for sound-source location in nontonotopic auditory cortex, J. Neurophysiol. 80 (1998) 863–882.
[20] J.C. Middlebrooks, L. Xu, S. Furukawa, E.A. Macpherson, Cortical neurones that localize sounds, Neuroscientist 8 (2002) 73–83.
[21] L. Mucke, M. Norita, G. Benedek, O.D. Creutzfeldt, Physiologic and anatomic investigation of a visual cortical area situated in the ventral bank of the anterior ectosylvian sulcus of the cat, Exp. Brain Res. 46 (1982) 1–11.
[22] A. Nagy, G. Eordegh, G. Benedek, Extents of visual, auditory and bimodal receptive fields of single neurons in the feline visual associative cortex, Acta Physiol. Hung. 90 (2003) 305–312.
[23] M. Norita, T.P. Hicks, G. Benedek, Y. Katoh, Organization of cortical and subcortical projections to the feline insular visual area, IVA, J. Hirnforsch. 32 (1991) 119–134.
[24] M. Norita, L. Mucke, G. Benedek, B. Albowitz, Y. Katoh, O.D. Creutzfeldt, Connections of the anterior ectosylvian visual area (AEV), Exp. Brain Res. 62 (1986) 225–240.
[25] C.R. Olson, A.M. Graybiel, Ectosylvian visual area of the cat: location, retinotopic organization, and connections, J. Comp. Neurol. 261 (1987) 277–294.
[26] J.D. Pettigrew, M.L. Cooper, G.G. Blasdel, Improved use of tapetal reflection for eye-position monitoring, Invest. Ophthalmol. Vis. Sci. 18 (1979) 490–495.
[27] F. Reinoso-Suarez, Topographischer Hirnatlas der Katze für experimental-physiologische Untersuchungen, Meck AG, Darmstadt, 1961.
[28] M.L. Rodrigo-Angulo, F. Reinoso-Suarez, Topographical organization of the brainstem afferents to the lateral posterior-pulvinar thalamic complex in the cat, Neuroscience 7 (1982) 1495–1508.
[29] J.W. Scannell, F. Sengpiel, M.J. Tovee, P.J. Benson, C. Blakemore, M.P. Young, Visual motion processing in the anterior ectosylvian sulcus of the cat, J. Neurophysiol. 76 (1996) 895–907.
[30] S.M. Sherman, R.W. Guillery, On the actions that one nerve cell can have on another: distinguishing "drivers" from "modulators", Proc. Natl. Acad. Sci. U.S.A. 95 (1998) 7121–7126.
[31] S.M. Sherman, R.W. Guillery, The role of the thalamus in the flow of information to the cortex, Philos. Trans. R. Soc. Lond. B. Biol. Sci. 357 (2002) 1695–1708.
[32] M.A. Sommer, R.H. Wurtz, What the brain stem tells the frontal cortex. I. Oculomotor signals sent from superior colliculus to frontal eye field via mediodorsal thalamus, J. Neurophysiol. 91 (2004) 1381–1402.
[33] B.V. Updyke, Projections from visual areas of the middle suprasylvian sulcus onto the lateral posterior complex and adjacent thalamic nuclei in cat, J. Comp. Neurol. 201 (1981) 477–506.

III.

European Journal of Neuroscience, Vol. 27, pp. 1801–1808, 2008 doi:10.1111/j.1460-9568.2008.06137.x

Drifting grating stimulation reveals particular activation properties of visual neurons in the caudate nucleus

Attila Nagy,[1] Zsuzsanna Paróczy,[1] Zita Márkus,[1] Antal Berényi,[1] Marek Wypych,[2] Wioletta J. Waleszczyk[2] and György Benedek[1]
[1]Department of Physiology, Faculty of Medicine, Albert Szent-Györgyi Medical and Pharmaceutical Center, University of Szeged, Dóm tér 10., H-6720 Szeged, Hungary
[2]Department of Neurophysiology, Nencki Institute of Experimental Biology, 3 Pasteur St., 02-093 Warsaw, Poland

Keywords: basal ganglia, cat, motion detection, spatial and temporal frequency tuning, temporal modulation

Abstract

The role of the caudate nucleus (CN) in motor control has been widely studied. Less attention has been paid to the dynamics of visual feedback in motor actions, which is a relevant function of the basal ganglia during the control of eye and body movements. We therefore set out to analyse the visual information processing of neurons in the feline CN. Extracellular single-unit recordings were performed in the CN, where the neuronal responses to drifting gratings of various spatial and temporal frequencies were recorded. The responses of the CN neurons were modulated by the temporal frequency of the grating. The CN units responded optimally to gratings of low spatial frequencies and exhibited low spatial resolution and fine spatial frequency tuning. By contrast, the CN neurons preferred high temporal frequencies, and exhibited high temporal resolution and fine temporal frequency tuning. The spatial and temporal visual properties of the CN neurons enable them to act as spatiotemporal filters. These properties are similar to those observed in certain feline extrageniculate visual structures, i.e. in the superior colliculus, the suprageniculate nucleus and the anterior ectosylvian cortex, but differ strongly from those of the primary visual cortex and the lateral geniculate nucleus. Accordingly, our results suggest a functional relationship of the CN to the extrageniculate tecto-thalamo-cortical system. This system of the mammalian brain may be involved in motion detection, especially in velocity analysis of moving objects, facilitating the detection of changes during the animal's movement.

Introduction

The caudate nucleus (CN) is the main structure receiving sensory–motor information incoming to the basal ganglia in the mammalian brain. It is involved in visuomotor behavior and contributes to the control of visually guided oculomotor and skeletomotor functions (Lynd-Balta & Haber, 1994; Barneoud *et al*., 2000; Hikosaka *et al*., 2000). Accordingly, a number of studies have been performed to clarify the role of the CN in visual information processing (Pouderoux & Freton, 1979; Rolls *et al*., 1983; Strecker *et al*., 1985; Hikosaka *et al*., 1989; Kolomiets, 1993; Brown *et al*., 1995; Nagy *et al*., 2003b). The CN neurons have been found to possess particular visual receptive field properties. Extracellular recordings in anesthetized cats revealed extremely large visual receptive fields that cover almost the whole of the approachable visual field of the eye, and consequently there is an absence of retinotopical organization (Pouderoux & Freton, 1979; Nagy *et al*., 2003b, 2005). These receptive field properties are in no way in accordance with those described in the neurons of the geniculostriate pathway. This supports the notion that the visual neuronal mechanisms of the basal ganglia represent particular dynamic properties differing from those of the primary visual cortex. Although visual information processing depends critically upon the integration of spatial and temporal information, no study has yet been performed concerning the responses of the CN neurons to sinewave drifting gratings. The sinusoidally modulated grating is an elementary component of the visual scene in the sense that any two-dimensional visual object can be represented by an appropriate combination of these gratings (De Valois *et al*., 1979; Pinter & Harris, 1981). Responses of neurons to drifting gratings of different spatial and temporal frequencies can be interpreted in terms of the dimensions and distribution of spatially and temporally summed excitatory and inhibitory components within their receptive fields (Enroth-Cugell & Robson, 1966; Zumbroich *et al*., 1988). Thus, a description of the hitherto unknown spatiotemporal filter properties of the CN neurons can contribute to an understanding of the role of the striatum in visual information processing and the connected behavioral sensorimotor actions.

Correspondence: Dr A. Nagy, as above.
E-mail: nagya@phys.szote.u-szeged.hu

Received 6 August 2007, revised 6 February 2008, accepted 7 February 2008

Materials and methods

Animal preparation and surgery

The experiments were carried out on six adult cats of either sex weighing from 2.5 to 4.0 kg. All procedures were carried out so as to minimize the number of animals used and followed the European Communities Council Directive of 24 November 1986 (S6609 EEC) and the National Institutes of Health Guidelines for the Care and Use of Animals for Experimental Procedures. The experimental protocol had been accepted by the Ethical Committee for Animal Research at Albert Szent-Györgyi Medical and Pharmaceutical Center at the University of Szeged.

The animals were initially anesthetized with ketamine hydrochloride (30 mg/kg, i.m., Calypsol). An s.c. injection of 0.2 mL 0.1% atropine sulfate was administered preoperatively to reduce salivation and

bronchial secretion. The trachea and the femoral vein were cannulated and the animals were placed in a stereotaxic head holder. All wound edges and pressure points were treated appropriately with procaine hydrochloride (1%). Anesthesia was maintained with halothane (1.6% during surgery and 0.8% during recordings). The depth of anesthesia was monitored by continuous reading of the end-tidal halothane values and by repeated checks of the electroencephalogram (EEG) and the electrocardiogram. There was continuous high-amplitude, low-frequency EEG activity, and we checked repeatedly whether interventions or forceful pressing of the forepaws induced desynchronization. The minimum alveolar anesthetic concentration values calculated from the end-tidal halothane readings always lay in the range given by Villeneuve & Casanova (2003). The animals were then immobilized with gallamine triethiodide (20 mg/kg i.v., Flaxedyl). During recording sessions, a liquid containing gallamine triethiodide (8 mg/kg/h), glucose (10 mg/kg/h) and dextran (50 mg/kg/h) in Ringer's lactate solution was infused at a rate of 3 mL/kg/h. End-tidal CO_2 level and rectal temperature were monitored continuously, and were maintained approximately constant, at 3.8–4.2% and 37–38 °C, respectively. The skull was opened to allow a vertical approach to the CN. The dura was removed and the cortical surface was covered with a 4% solution of agar dissolved in Ringer's solution. The eye contralateral to the recording was treated with phenylephrine (10%) and atropine (0.1%), and was equipped with a +2 diopter contact lens. The ipsilateral eye was covered during stimulation. The retinal landmarks and major retinal blood vessels were projected routinely twice daily onto a tangent screen, using a fiberoptic light source (Pettigrew *et al*., 1979). In some cases, the area centralis could be imaged directly; in others, it was plotted by reference to the optic disk, 14.6° medially and 6.5° below the center of the optic disk (Bishop *et al*., 1962).

Recording

Electrophysiological recordings of single units were carried out extracellularly via tungsten microelectrodes (AM System Inc., USA; 2–4 MΩ). Vertical penetrations were performed between the Horsley-Clarke coordinates anterior: 12–16, lateral: 4–6.5 in the stereotaxic depths 12–19, to record CN single-units. At the end of the experiments, the animals were deeply anesthetized with pentobarbital (200 mg/kg i.v.) and transcardially perfused with 4% paraformaldehyde solution. The brains were removed and cut into 50-μm coronal sections, and the sections were stained with Neutral Red. Recording sites were localized on the basis of the marks of the electrode penetrations. The recorded neurons were located in the dorsolateral aspect of the CN.

Visual stimulation and data analysis

For visual stimulation, an 18-inch computer monitor (refresh rate, 85 Hz) was placed 42.9 cm in front of the animal. The diameter of the stimulation screen was 22.5 cm, and the cat therefore saw it under 30° (if the stimulus diameter on a tangent screen is 22.5 cm and the distance between the eye and the centre point of the screen is 42.9 cm the viewing angle of the stimulus is 30 degrees). The mean luminance of the screen was 23 cd/m^2. For studies of the spatiotemporal characteristics of the cells, high-contrast (96%) drifting sinusoidal gratings were used. The sinusoidal gratings were moved along four different axes in eight different directions (0–315° at 45° increments) to find the optimal moving direction of each unit. The optimal direction of each unit was further used to describe its spatial and temporal characteristics. The tested spatial frequencies ranged from 0.025 to 0.4 cycles/° (c/°) and the temporal frequencies from 0.07 to 37.24 cycles/s (Hz). Stimuli were presented in a pseudo-random sequence in a series consisting of eight spatiotemporal frequency combinations of moving gratings. Each spatiotemporal frequency combination was presented at least 12 times. The interstimulus interval was consistently 1 s. Individual action potentials were distinguished with the help of a spike-separator system (SPS-8701; Australia). The number and temporal distribution of the action potentials recorded during stimulation were stored as peristimulus time histograms (PSTHs, 10-ms bin) and analysed off line. The duration of the prestimulus time (a stationary sinusoidal grating was shown) was 1000 ms, similar to the peristimulus time (a drifting sinusoidal grating was shown). The net discharge rate, calculated as the difference between the mean firing rates of the cell obtained during stimulus movement and the background activity corresponding to the mean activity during the 200 ms preceding movement in the prestimulus period, was used to characterize the response amplitude of the CN neurons. To estimate the extent of direction selectivity, a direction selectivity index (*DI*) similar to that proposed by Dreher *et al*. (1993) was calculated by using the formula:

$$DI = 100 \times (R_p - R_{np})/R_p$$

where R_p and R_{np} are the net discharge rates in the preferred and nonpreferred (opposite) directions, respectively.

A majority of the CN neurons exhibited a modulated response to the drifting gratings. The relative modulation index (*MI*) was calculated as the ratio of the amplitude of the response component at the fundamental (i.e. the stimulus) temporal frequency (f_1) and the net response of the cell (f_0) (Movshon *et al*., 1978a):

$$MI = f_1/f_0$$

MI was calculated only for the modulated responses with a clear peak in the spectrogram at frequency f_1. We regarded a spectrogram value at frequency f_1 as a peak when it exceeded the mean amplitude along all of the frequencies in the spectrogram by at least one standard deviation (SD). We applied the procedure of finding peaks to spectrograms averaged over 12 responses to a stimulus with given parameters $MI = f_1/f_0$ (see Fig. 1).

Results

The activities of 101 visually responsive neurons were recorded in the dorsolateral aspect of the CN in response to drifting sinusoidally modulated gratings. The spectral spatiotemporal visual responses and filter properties of 89 neurons were analyzed in detail. As with earlier findings, our subjective estimation of the extent of the visual receptive fields by recording the neuronal responses to the movements of a light spot generated by a hand-held lamp demonstrated that the visual receptive fields were extremely large: they covered a major part of the contralateral hemifield and extended deep into the ipsilateral hemifield, yielding a receptive field that overlapped almost totally with the visual field of the contralateral eye (Pouderoux & Freton, 1979; Nagy *et al*., 2003b, 2005). For technical reasons and in order to obtain data that could be compared with the findings of our previous studies in the lateral–medial suprageniculate nuclei complex (LM-Sg) of the posterior thalamus (Paróczy *et al*., 2006), the superior colliculus (SC; Waleszczyk *et al*., 2007) and the cortex along the sulcus ectosylvius anterior (AES cortex; Nagy *et al*., 2003a), we consistently centered the stimulation monitor on the area centralis and stimulated a large central part (with a diameter of 30°) of the receptive fields. As the CN visual receptive fields are homogeneous in the sense that the

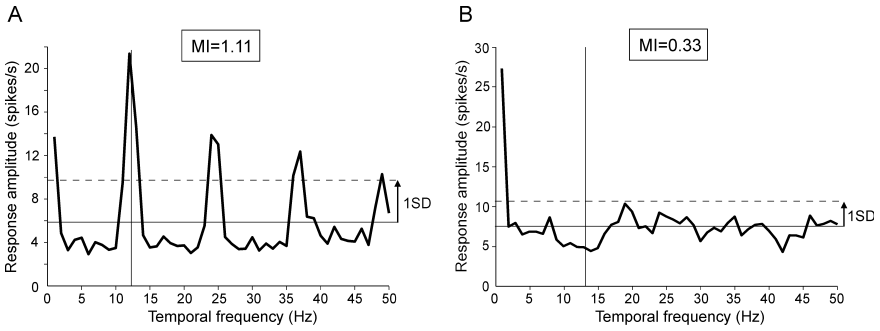

FIG. 1. Determination of the temporal frequency modulation of CN neuron responses (see Materials and methods). Averaged (from 12 trials) spectrograms calculated for neurons responding with modulated (A) or unmodulated (B) activity. The modulation indices are presented in boxes above the spectrograms. The solid horizontal line denotes the mean amplitude of the spectrogram, and the dashed line is one standard deviation (1SD) above the mean. The vertical line indicates the temporal frequency of the stimulus. When the response amplitude in the averaged spectrogram at the fundamental temporal frequency of the stimulus (f_1) exceeded the mean amplitude of the spectrogram by > 1SD, the response was classified as modulated.

site of the stimulation within the receptive field has no effect on the velocity, direction or stimulus size preference of a single cell – only the magnitude of the responses can be modulated – (Nagy *et al.*, 2003b) stimulation of this large central part of the receptive fields may faithfully describe the spatio-temporal characteristics of the CN.

The mean spontaneous activity of the CN neurons was 9 spikes/s ($n = 101$; SD ± 7.4 spikes/s; range 0–32 spikes/s). The CN neurons responded to the drifting gratings with a modulated or unmodulated increase in their discharge rate, although the activities of certain neurons were suppressed for some spatiotemporal frequency combinations and/or directions of the moving gratings.

The responses of 64 (72%) of the 89 CN cells were considered to be modulated by the gratings (see Methods), with clear peaks in the spectrograms at the fundamental frequency f_1 derived from the Fourier transforms of the PSTHs (Fig. 1). *MI* was calculated for the maximal responses (to the optimal stimulus) of each neuron that displayed a modulated response. The mean *MI* was 1.12 ($n = 64$, SD = 0.79, range 0.38–5.1). Twenty-eight CN cells were strongly modulated, with *MI* > 1.0.

Direction selectivity and direction tuning function of the caudate neurons

The direction sensitivity and tuning functions of the CN neurons were determined on the basis of their responses to drifting sinusoidal gratings moving in eight different directions (four different axes of movement). The direction sensitivity of the cells was characterized by using a *DI* (Dreher *et al.*, 1993). A majority of the CN neurons (63/101, 62%) exhibited a *DI* of < 50%, and these units were therefore classified as non-direction-sensitive cells. However, 26 of the 101 CN neurons (26%) had *DI* > 70% and were classified accordingly as direction-selectives, while 12 CN neurons (12%) had *DI*s between 50 and 70% and were direction-sensitive (Fig. 2A). The direction tuning of the direction-sensitive and direction-selective CN neurons was characterized by using the direction tuning width, which was defined as the range of directions over which the magnitude of the responses was at least half of the maximal repsonse. The average direction tuning width was 93° ($n = 38$; SD ± 51°, range 19–233°, Fig. 2B). The distribution of the direction of the drifting grating that induced the maximal response of the single neurons is presented in Fig. 2C. The direction varied considerably in the cells recorded, but given the moderate number of direction-selective and sensitive cells, it is premature to draw conclusions about the possible rule of distribution in direction preference (Fig. 2C).

Spatial frequency tuning of the CN neurons

The spatial frequency tuning function of the CN neurons was determined on the basis of their responses to drifting sinusoidal gratings moving in the optimal direction with optimal temporal

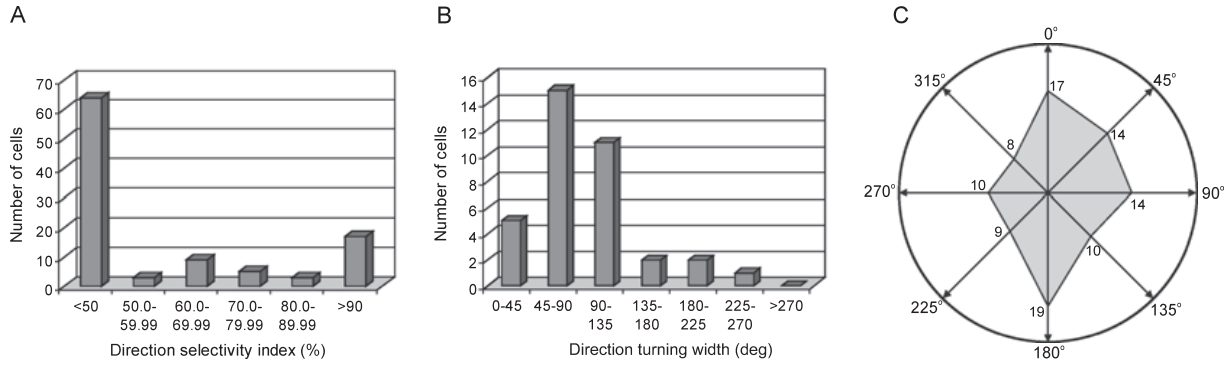

FIG. 2. Direction sensitivity and tuning function of the CN neurons. (A) Distribution of the direction selectivity indices. It should be noted that most of the CN neurons were not direction-sensitive, with *DI*s of < 50%. (B) Direction tuning widths of the direction-sensitive and selective CN units. (C) Distribution of drifting grating directions (indicated by the arrows) that elicited the maximal response amplitude.

frequency. Figure 3A demonstrates the responses of a CN cell to different spatial frequencies. Similarly to this neuron, all of the investigated CN neurons displayed strong responses to very low spatial frequencies. The mean optimal spatial frequency of the CN neurons was 0.05 c/° ($n = 89$, SD ± 0.03 c/°, range 0.025–0.18 c/°; Fig. 4A). The mean optimal spatial frequency may well be overestimated as for 42 neurons the optimal spatial frequency was the lowest (0.025 c/°) tested. The spatial high-frequency cut-off was defined as the frequency at which the net response (after subtraction of the spontaneous activity) of the cell fell to one-tenth of the maximum (Saul & Humphrey, 1990; Waleszczyk *et al*., 2007). This was regarded as a measure of the spatial resolution. The spatial resolution could be calculated for 42 CN units. In this CN neuronal population, the spatial high-frequency cut-off was consistently very low, with a mean of 0.1 c/° ($n = 42$, SD ± 0.05 c/°, range 0.039–0.20 c/°). In contrast to this finding, the responses of the remaining 47 CN neurons were slightly higher than one-tenth of the maximum at the highest spatial frequency tested (Fig. 4B); the spatial resolution for these cells was therefore > 0.4 c/°.

More than half of the investigated CN neurons (55/89, 62%) displayed spatial low-pass tuning characteristics under the present stimulating conditions, with no attenuation of the response for the lowest spatial frequencies (Fig. 5A). Fifteen units (17%) exhibited band-pass spatial frequency tuning (Fig. 5B). The spatial bandwidths measured at half-height of the spatial frequency-tuning curve of the 15 band-pass CN units were analysed (Fig. 4C). The CN units were narrowly tuned to spatial frequencies, and accordingly can serve as good spatial filters. The mean spatial bandwidth of the band-pass-tuned CN neurons was 1.31 octaves ($n = 15$, SD ± 0.76 octaves, range 0.37–3.0 octaves).

Temporal frequency tuning of the CN cells

Sinusoidal gratings at the optimal spatial frequency moving in the optimal direction of each unit were applied to evaluate the temporal frequency tuning of the CN neurons. Similar to the neuron whose responses are demonstrated in Fig. 3B, all of the investigated CN units responded optimally to high temporal frequencies. The mean optimal

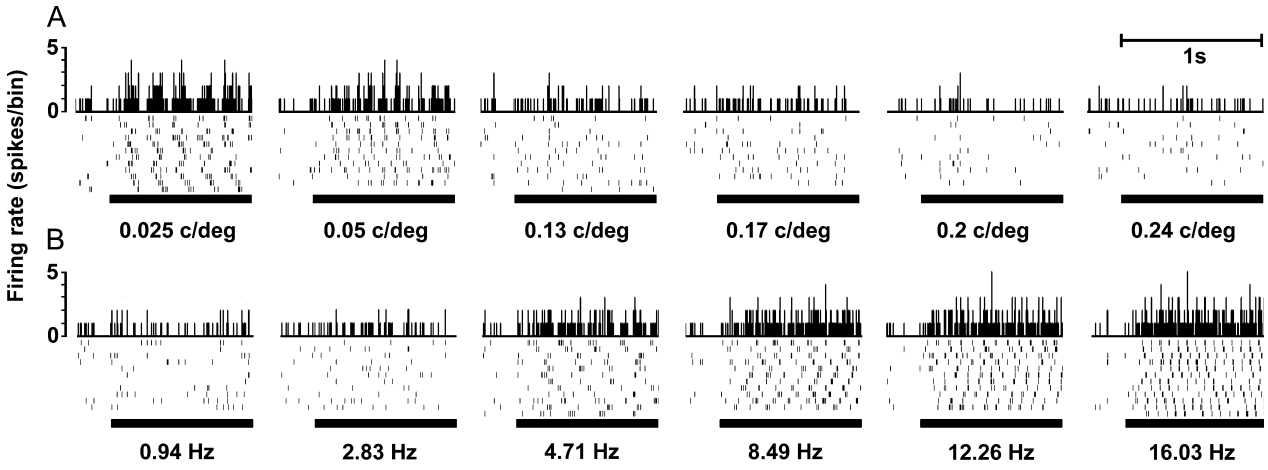

FIG. 3. PSTHs (bin width 10 ms) and raster plots of a temporal frequency-modulated CN cell responding to drifting gratings with different spatial and temporal frequencies. The ordinate denotes the discharge rate (spikes per bin). The thick black lines under the PSTHs indicate the duration of the stimulus movement for 1000 ms (peristimulus time). Corresponding spatial or temporal frequencies of the sinusoidally modulated drifting gratings are shown under the PSTHs. (A) Responses of a CN neuron to six different spatial frequencies (temporal frequency was constant at 5.66 Hz). (B) Responses of the same CN neuron to six different temporal frequencies (spatial frequency was constant at 0.025 c/°).

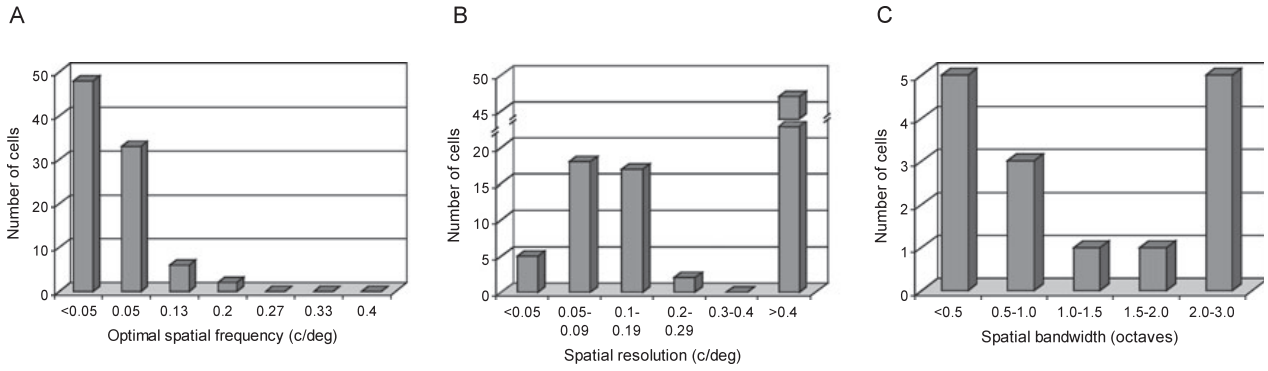

FIG. 4. Visual spatial frequency properties of the CN neurons. (A) Distribution of the optimal spatial frequencies, estimated from the spatial frequency tuning functions. All cells responded optimally to extremely low spatial frequencies. (B) Distribution of the spatial resolutions. (C) Distribution of the spatial bandwidths (full-width at half-height).

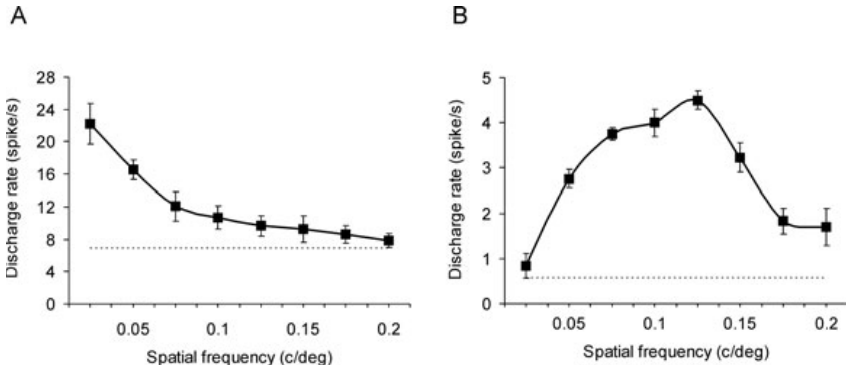

FIG. 5. Examples of spatial frequency tuning functions of the CN neurons. (A) Spatial frequency tuning curve of a spatial low-pass unit. (B) Spatial frequency tuning curve of a band-pass CN neuron. The tuning curves were fitted by using the cubic-spline technique. Each point (square symbol) corresponds to the mean firing rate (f_0 values are presented) during a 1-s grating movement (averaged over 12 stimulus repetitions) for a particular spatial frequency. Each error bar corresponds to the standard error of the mean. The dashed lines indicate the level of spontaneous activity.

temporal frequency of the CN neurons was high: 10.6 Hz ($n = 89$, SD ±4.8 Hz, range 4.6–27.6 Hz; Fig. 6A). The temporal high-frequency cut-off of the CN units was also very high. The mean temporal resolution could be calculated for 31 CN neurons: it was 20.6 Hz ($n = 31$, SD ± 5.6 Hz, range 6.3–34.0 Hz; Fig. 6B). The remaining 58 CN units still showed at least a slight response (higher than one-tenth of the maximal response) for the highest temporal frequency tested.

Fifty-five of the 89 neurons (62%) were classified as temporal band-pass cells (Fig. 7A). The band-pass CN neurons were narrowly tuned to temporal frequencies with a mean temporal bandwidth of 1.38 octaves ($n = 55$, SD ± 1.0 octave, range 0.09–5.36 octaves; Fig. 6C). Fourteen CN neurons (16%) exhibited double temporal frequency tuning with two clear optimal frequencies in the higher temporal frequency domain (Fig. 7B). Six CN units (7%) elicited temporal high-pass tuning (Fig. 7C) and another three (3%) were temporal broad-band neurons. None of the CN units exhibited low-pass temporal frequency tuning.

Discussion

Earlier electrophysiological studies described the responsivity of the CN visual neurons merely to simple geometric forms, i.e. moving spots and bars (Hikosaka *et al*., 1989; Nagy *et al*., 2003b), and were therefore essentially inappropriate to define their responsivity to extended visual stimuli. The present study is the first spectral, spatiotemporal analysis of visual cells in the CN that employs a wide range of spatial and temporal frequencies and describes the particular spectral spatiotemporal filter properties of the CN visual neurons.

Our approach allows a direct comparison of the dynamic properties of the CN with those in other areas of the brain. Table 1 lists the quantitative spatial and temporal visual properties of the subcortical and cortical visual regions investigated to date in the feline brain. The CN cells clearly preferred drifting gratings with extremely low spatial frequencies: the mean optimal spatial frequency of the CN cells was 0.05 c/°. This is a much lower value than those of the X and Y cells of the lateral geniculate nucleus (LGN; Saul & Humphrey, 1990; Humphrey & Murthy, 1999), the lateral posterior–pulvinar complex (LP-Pul) of the thalamus (Casanova *et al*., 1989), and almost all striate and extrastriate visual cortical areas (Movshon *et al*., 1978b; Zumbroich & Blakemore, 1987; Tardif *et al*., 1996, 1997; Morley & Vickery, 1997; Bergeron *et al*., 1998; Nagy *et al*., 2003a), but comparable with those of the SC, the W cells of the LGN and the LM-Sg (Pinter & Harris, 1981; Saul & Humphrey, 1990; Paróczy *et al*., 2006; Waleszczyk *et al*., 2007; Humphrey & Murthy, 1999 Mimeault *et al*., 2004).

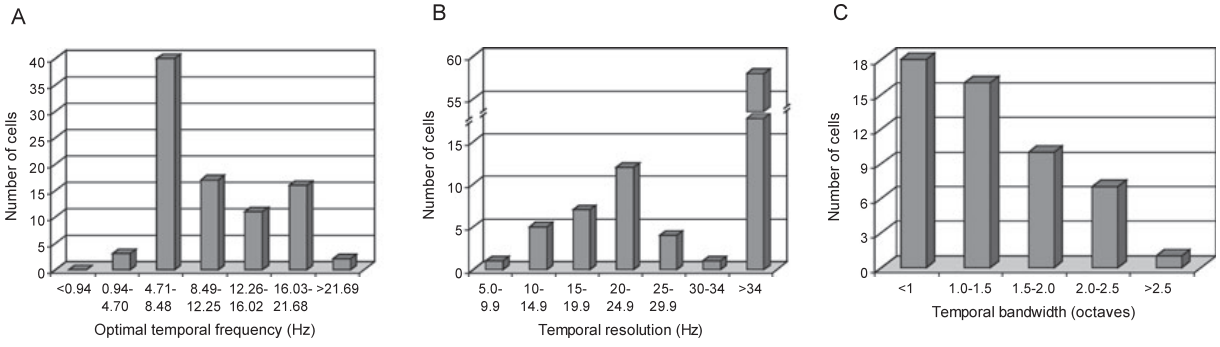

FIG. 6. Visual temporal frequency properties of the CN neurons. (A) Distribution of the optimal temporal frequencies of the cells, estimated from the temporal frequency tuning functions. The CN cells responded optimally to high temporal frequencies. (B) Distribution of the temporal resolution. The CN units consistently had a very high temporal high-frequency cut-off. (C) Distribution of the temporal bandwidths (full-width at half-height). A majority of the cells displayed a relatively narrow temporal tuning.

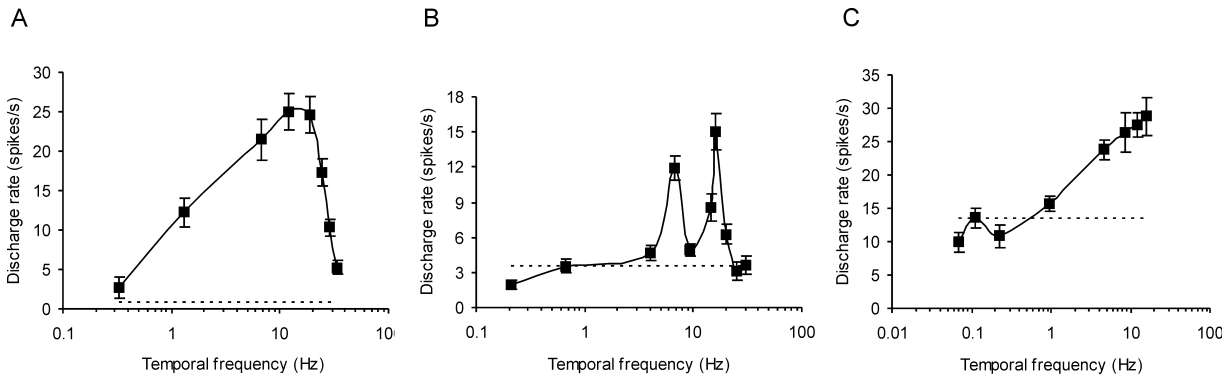

FIG. 7. Examples of temporal frequency tuning functions in the CN. (A) Temporal tuning curve of a band-pass neuron. (B) Tuning curve of a neuron tuned to two temporal frequencies. (C) Tuning curve of a temporal high-pass CN neuron. The tuning curves were fitted by using the cubic-spline technique. The conventions are the same as in Fig. 5.

TABLE 1. Quantitative spatial and temporal visual properties of cortical and subcortical structures in the feline brain

	Optimal spatial frequency (c/°)	Spatial bandwidth (octaves)	Optimal temporal frequency (Hz)	Temporal bandwidth (octaves)
CN	0.05	1.31	10.6	1.38
LM-Sg	0.05	1.07	8.53	1.66
SC	0.10	1.84	6.84	2.38
Lp-Pul	~0.20	2.20	~5.00	2.32
LGN X cells	0.85	–	2.50	–
LGN Y cells	0.14	–	5.20	–
LGN W cells	0.07	–	2.70	–
A17	0.90	1.50	2.90	1.70
A18	0.22	1.49	3.20	1.50
A19	0.17	1.90	3.00	2.90
A21a	0.27†, 0.36*	1.60*, 1.79†	3.25†, 7.00*	1.92†, 2.90*
A21b	0.08	2.20	3.20	3.30
PMLS	0.16	2.20	5.00	2.00
AES cortex	0.20	1.40	6.30	1.10

References: *Tardif *et al*. (1996), †Morley & Vickery (1997).

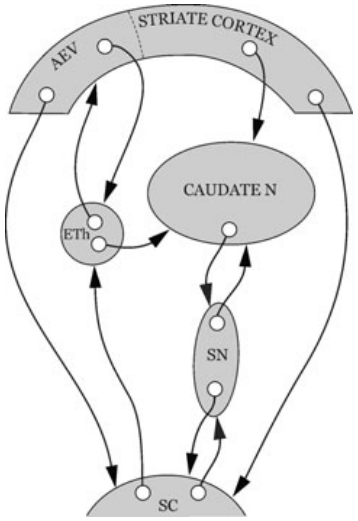

FIG. 8. Visual afferentation of the CN. Black arrows demonstrate the potential interactions between the tectal extrageniculate visual pathway and the CN, and the connection between the striate cortex and the CN. Abbreviations: AEV, anterior ectosylvian visual area; Eth, extrageniculate visual thalamus; SC, superior colliculus; SN, substantia nigra.

A majority of the CN units exhibited low-pass spatial tuning characteristics, although spatial band-pass and broad-band cells were also recorded. Low-pass cells are similarly common in the SC (Pinter & Harris, 1981; Mimeault *et al*., 2004; Waleszczyk *et al*., 2007), the posteromedial lateral suprasylvian area (PMLS; Zumbroich & Blakemore, 1987), the anteromedial lateral suprasylvian area (AMLS; Ouellette *et al*., 2004), the AES cortex (Nagy *et al*., 2003a) and the LM-Sg of the posterior thalamus (Paróczy *et al*., 2006). Nevertheless, some low-pass tuned cells have also been observed in cortical areas 17 (Ikeda & Wright, 1975), 18 (Movshon *et al*., 1978b), 19 (Bergeron *et al*., 1998), 21a (Morley & Vickery, 1997; Tardif *et al*., 2000) and 21b (Tardif *et al*., 2000), the LP-Pul and the LGN of the thalamus (see Saul & Humphrey, 1990 – for X and Y cells; Humphrey & Murthy, 1999 – for W cells) and the W cells of the retina (Rowe & Cox, 1993).

The band-pass CN neurons are narrowly tuned to spatial frequencies with a mean spatial tuning width of 1.31 octaves. This might indicate that the CN cells could act as spatial filters. The spatial tuning width of the band-pass CN neurons is comparable not only with those of the LM-Sg (Paróczy *et al*., 2006) and the AES cortex (Nagy *et al*., 2003a), but also with that of the striate visual cortex (Movshon *et al*., 1978b), but smaller than those of the other visual regions of the feline brain (Tanaka *et al*., 1987; Zumbroich & Blakemore, 1987; Bergeron *et al*., 1998; Tardif *et al*., 2000; Ouellette *et al*., 2004; Waleszczyk *et al*., 2007).

All of the investigated CN neurons responded optimally to temporal frequencies >4 Hz. The mean optimal temporal frequency found for the CN cells in this study was 10.6 Hz. This is the highest mean optimal temporal frequency reported for any part of the feline visual cortical or subcortical regions to date. It is slightly higher than those of the SC (Waleszczyk *et al*., 2007) and the brain regions that receive a tectal source of visual information, and participate in motion analysis, i.e. the LM-Sg (Paróczy *et al*., 2006), the LP-Pul (Casanova *et al*., 1989; Merabet *et al*., 1998), the AES cortex (Nagy *et al*., 2003a) and the lateral suprasylvian areas (LS; Morrone *et al*. 1986; Zumbroich & Blakemore, 1987; Ouellette *et al*., 2004), but much higher than those of areas 17 (Saul & Humphrey, 1992; Casanova, 1993), 18 (Saul &

Humphrey, 1992), 19 (Bergeron *et al*., 1998), 21a (Morley & Vickery, 1997) and 21b (Tardif *et al*., 2000), and the X and W cells of the LGN.

The temporal frequency tuning functions of the cells in the CN, similarly to those in the AES cortex (Nagy *et al*., 2003a) and the LM-Sg (Paróczy *et al*., 2006), are mainly band-pass and rarely high-pass. The band-pass CN units displayed narrow temporal frequency tuning at a mean temporal bandwidth of 1.38 octaves. This is comparable with the temporal tuning widths for the LS areas (Morrone *et al*., 1986), the AES cortex (Nagy *et al*., 2003a), areas 17 and 18 (Movshon *et al*., 1978b), and the LM-Sg (Paróczy *et al*., 2006), but much lower than those of the LP-Pul (Casanova *et al*., 1989), and areas 19 (Bergeron *et al*., 1998), 21a (Tardif *et al*., 1996) and 21b (Tardif *et al*., 2000).

There is some degree of uncertainty concerning the pathways conveying sensory information to the basal ganglia. Earlier morphological findings in cats and rabbits stressed the predominant role of the geniculostriate pathway that conveys visual information toward the CN (Webster, 1965; Hollander *et al*., 1979). However, recent morphological and physiological studies support the suggestion that the extrageniculate ascending tectofugal pathways project to the CN in reptiles, birds and mammals (Fig. 8). The dorsolateral, visual part of the CN in the cat can receive its visual afferentation from the LM-Sg of the posterior thalamus, which is connected to the AES cortex with thalamo-cortico-thalamic loops (Harting *et al*., 2001a,b; McHaffie *et al*., 2001; Nagy *et al*., 2003b, 2005; Eördegh *et al*., 2005; Guirado *et al*., 2005). The spatiotemporal visual properties of the CN neurons are extremely similar to those of the subset SC, LM-Sg and the AES cortex (Nagy *et al*., 2003a; Paróczy *et al*., 2006; Waleszczyk *et al*., 2007), with their preference for very low spatial and very high temporal frequencies and narrow spatial and temporal tuning characteristics. It must be mentioned here that areas 17 and 18 have spatial and temporal tuning widths slightly larger, although still comparable (Movshon *et al*., 1978b) with those of the CN. However, this is as far as the similarity goes between the spectral spatiotemporal properties of the CN and areas 17 and 18. Spatial low-pass units are rare in areas 17 and 18, but, similarly to the CN, most common in the extrageniculate subcortical and extrastriate cortical regions (Pinter & Harris, 1981; Casanova *et al*., 1989; Nagy *et al*., 2003a; Paróczy *et al*., 2006; Waleszczyk *et al*., 2007). Further, the optimal spatial and temporal frequency preferences of the CN units are considerably different from those in areas 17 and 18 (Movshon *et al*., 1978b). This suggests that the CN neurons receive strong Y or W signals, probably from the SC, via the LM-Sg of the thalamus and also from the AES cortex (Benedek *et al*., 1996; Nagy *et al*., 2003a, 2005; Eördegh *et al*., 2005; Paróczy *et al*., 2006), and tends to discount high spatial and low temporal frequency X input from area 17 (Movshon *et al*., 1978b).

It is an interesting phenomenon that the drifting gratings strongly modulated the responses of a majority of the CN neurons. While the SC and LM-Sg neurons responded to drifting gratings with a weakly modulated or unmodulated increase in activity (Paróczy *et al*., 2006; Waleszczyk *et al*., 2007), the AES cortex, which possesses strong temporal frequency-modulated discharges (Hicks *et al*., 1988), may be the origin of the modulation in the CN.

The CN neurons are good candidates for tasks involved in the perception of motion and probably in the perception of changes in the visual environment during self-motion (Morrone *et al*., 1986; Brosseau-Lachaine *et al*., 2001), with their extremely large receptive fields (Nagy *et al*., 2003b), their preferences for low spatial frequencies, and their fine spatial and temporal tuning. It has been reported in human psycho-physics investigations that all motion detectors are apparently finely tuned to temporal and spatial frequencies (Anderson & Burr, 1985; Burr & Ross, 1986; Burr *et al*., 1986). The narrow tuning of the CN neurons may contribute to velocity detection and the analysis of the object in motion. These properties enable the CN to play important roles in the recording of movements of the visual environment relative to the body, and in helping its participation in the adjustment of motor behavior to environmental challenges. The fact that the visual properties of the CN neurons closely resemble those described in the extrageniculate tecto-thalamo-cortical visual system supports the notion that the CN may receive its main visual input from interactions among these structures.

Acknowledgements

We thank Ágnes Farkas, Péter Gombkötõ and Andrea Petõ for their help with data collection, Gabriella Dósai, Kálmán Hermann and Joanna Smyda for their valuable technical assistance, and Péter Liszli for computer programming. The work was supported by grants OTKA/Hungary F048396, OTKA/Hungary T42610 and Polish State Committee for Scientific Research 3P04C08222. A.N. is a János Bolyai Research Fellow of the Hungarian Academy.

Abbreviations

AES, anterior ectosylvian sulcus; AMLS, anteromedial lateral suprasylvian area; CN, caudate nucleus; *DI*, direction selectivity index; LGN, lateral geniculate nucleus; LM-Sg, lateral–medial suprageniculate nucleus; LP-Pul, lateral posterior-pulvinar complex; LS, lateral suprasylvian; *MI*, modulation index; PMLS, posteromedial lateral suprasylvian area; PSTH, peristimulus time histogram; SC, superior colliculus.

References

Anderson, S.J. & Burr, D.C. (1985) Spatial and temporal selectivity of the human motion detection system. *Vision Res.*, **25**, 1147–1154.

Barneoud, P., Descombris, E., Aubin, N. & Abrous, D.N. (2000) Evaluation of simple and complex sensorimotor behaviours in rats with a partial lesion of the dopaminergic nigrostriatal system. *Eur. J. Neurosci.*, **12**, 322–336.

Benedek, G., Fischer-Szatmari, L., Kovacs, G., Perenyi, J. & Katoh, Y.Y. (1996) Visual, somatosensory and auditory modality properties along the feline suprageniculate-anterior ectosylvian sulcus/insular pathway. *Prog. Brain Res.*, **112**, 325–334.

Bergeron, A., Tardif, E., Lepore, F. & Guillemot, J.P. (1998) Spatial and temporal matching of receptive field properties of binocular cells in area 19 of the cat. *Neuroscience*, **86**, 121–134.

Bishop, P.O., Kozak, W. & Vakkur, G.J. (1962) Some quantitative aspects of the cats' eye: axis and plane of reference, visual field coordinates and optics. *J. Physiol. (Lond.)*, **163**, 466–502.

Brosseau-Lachaine, O., Faubert, J. & Casanova, C. (2001) Functional sub-regions for optic flow processing in the posteromedial lateral suprasylvian cortex of the cat. *Cereb. Cortex*, **11**, 989–1001.

Brown, V.J., Desimone, R. & Mishkin, M. (1995) Responses of cells in the tail of the caudate nucleus during visual discrimination learning. *J. Neurophysiol.*, **74**, 1083–1094.

Burr, D.C. & Ross, J. (1986) Visual processing of motion. *Trends Neurosci.*, **9**, 304–307.

Burr, D.C., Ross, J. & Morrone, M. (1986) Seeing objects in motion. *Proc. Roy. Soc. Lond. B.*, **227**, 249–265.

Casanova, C. (1993) Response properties of neurons in area 17 projecting to the striate-recipient zone of the cat's lateralis posterior-pulvinar complex: comparison with cortico-tectal cells. *Exp. Brain Res.*, **96**, 247–259.

Casanova, C., Freeman, R.D. & Nordmann, J.P. (1989) Monocular and binocular response properties of cells in the striate-recipient zone of the cat's lateral posterior-pulvinar complex. *J. Neurophysiol.*, **62**, 544–557.

De Valois, K.K., De Valois, R.L. & Yund, E.W. (1979) Responses of striate cortex cells to grating and checkerboard patterns. *J. Physiol.*, **291**, 483–505.

Dreher, B., Michalski, A., Ho, R.H., Lee, C.W. & Burke, W. (1993) Processing of form and motion in area 21a of cat visual cortex. *Vis. Neurosci.*, **10**, 93–115.

Enroth-Cugell, C. & Robson, J.G. (1966) The contrast sensitivity of retinal ganglion cells of the cat. *J. Physiol.*, **187**, 517–552.

Eördegh, G., Nagy, A., Berényi, A. & Benedek, G. (2005) Processing of spatial visual information along the pathway between the suprageniculate nucleus and the anterior ectosylvian cortex. *Brain Res. Bull.*, **67**, 281–289.

Guirado, S., Real, M.A. & Davila, J.C. (2005) The ascending tectofugal visual system in amniotes: new insights. *Brain Res. Bull.*, **66**, 290–296.

Harting, J.K., Updyke, B.V. & Van Lieshout, D.P. (2001a) Striatal projections from the cat visual thalamus. *Eur. J. Neurosci.*, **14**, 893–896.

Harting, J.K., Updyke, B.V. & Van Lieshout, D.P. (2001b) The visual-oculomotor striatum of the cat: functional relationship to the superior colliculus. *Exp. Brain Res.*, **136**, 138–142.

Hicks, T.P., Benedek, G. & Thurlow, G.A. (1988) Organization and properties of neurons in a visual area within the insular cortex of the cat. *J. Neurophysiol.*, **60**, 397–421.

Hikosaka, O., Sakamoto, M. & Usui, S. (1989) Functional properties of monkey caudate neurons. II. Visual and auditory responses. *J. Neurophysiol.*, **61**, 799–813.

Hikosaka, O., Takikawa, Y. & Kawagoe, R. (2000) Role of the basal ganglia in the control of purposive saccadic eye movements. *Physiol. Rev.*, **80**, 953–978.

Hollander, H., Tietze, J. & Distel, H. (1979) An autoradiographic study of the subcortical projections of the rabbit striate cortex in the adult and during postnatal development. *J. Comp. Neurol.*, **184**, 783–794.

Humphrey, A.L. & Murthy, A. (1999) Cell types and response timings in the medial interlaminar nucleus and C-layers of the cat lateral geniculate nucleus. *Vis. Neurosci.*, **16**, 513–525.

Ikeda, H. & Wright, M.J. (1975) Spatial and temporal properties of 'sustained' and 'transient' neurones in area 17 of the cat's visual cortex. *J. Physiol. (Lond.)*, **22**, 363–383.

Kolomiets, B. (1993) A possible visual pathway to the cat caudate nucleus involving the pulvinar. *Exp. Brain Res.*, **97**, 317–324.

Lynd-Balta, E. & Haber, S.N. (1994) The organization of midbrain projections to the striatum in the primate: sensorimotor-related striatum versus ventral striatum. *Neuroscience*, **59**, 625–640.

McHaffie, J.G., Thomson, C.M. & Stein, B.E. (2001) Corticotectal and corticostriatal projections from the frontal eye fields of the cat: an anatomical examination using WGA-HRP. *Somatosens. Mot. Res.*, **18**, 117–130.

Merabet, L., Desautels, A., Minville, K. & Casanova, C. (1998) Motion integration in a thalamic visual nucleus. *Nature*, **396**, 265–268.

Mimeault, D., Paquet, V., Molotchnikoff, S., Lepore, F. & Guillemot, J.P. (2004) Disparity sensitivity in the superior colliculus of the cat. *Brain Res.*, **1010**, 87–94.

Morley, J.W. & Vickery, R.M. (1997) Spatial and temporal frequency selectivity of cells in area 21a of the cat. *J. Physiol. (Lond.)*, **501**, 405–413.

Morrone, M.C., Di Stefano, M. & Burr, D.C. (1986) Spatial and temporal properties of neurons of the lateral suprasylvian cortex of the cat. *J. Neurophysiol.*, **56**, 969–986.

Movshon, J.A., Thompson, I.D. & Tolhurst, D.J. (1978a) Spatial summation in the receptive fields of simple cells in the cat's striate cortex. *J. Physiol. (Lond.)*, **283**, 53–77.

Movshon, J.A., Thompson, I.D. & Tolhurst, D.J. (1978b) Spatial and temporal contrast sensitivity of neurones in areas 17 and 18 of the cat's visual cortex. *J. Physiol. (Lond.)*, **283**, 101–120.

Nagy, A., Eördegh, G. & Benedek, G. (2003a) Spatial and temporal visual properties of single neurons in the feline anterior ectosylvian visual area. *Exp. Brain Res.*, **151**, 108–114.

Nagy, A., Eördegh, G., Norita, M. & Benedek, G. (2003b) Visual receptive field properties of neurons in the feline caudate nucleus. *Eur. J. Neurosci.*, **18**, 449–452.

Nagy, A., Paróczy, Z., Norita, M. & Benedek, G. (2005) Multisensory responses and receptive field properties of neurons in the substantia nigra and in the caudate nucleus. *Eur. J. Neurosci.*, **22**, 419–424.

Ouellette, B.G., Minville, K., Faubert, J. & Casanova, C. (2004) Simple and complex visual motion response properties in the anterior medial bank of the lateral suprasylvian cortex. *Neuroscience*, **123**, 231–345.

Paróczy, Z., Nagy, A., Márkus, Z., Waleszczyk, W.J., Wypych, M. & Benedek, G. (2006) Spatial and temporal visual properties of single neurons in the suprageniculate nucleus of the thalamus. *Neuroscience*, **137**, 1397–1404.

Pettigrew, J.D., Cooper, M.L. & Blasdel, G.G. (1979) Improved use of tapetal reflection for eye-position monitoring. *Invest. Ophthalmol. Vis. Sci.*, **18**, 490–495.

Pinter, R.B. & Harris, L.R. (1981) Temporal and spatial response characteristics of the cat superior colliculus. *Brain Res.*, **207**, 73–94.

Pouderoux, C. & Freton, E. (1979) Patterns of unit responses to visual stimuli in the cat caudate nucleus under chloralose anesthesia. *Neurosci. Lett.*, **11**, 53–58.

Rolls, E.T., Thorpe, S.J. & Maddison, S.P. (1983) Responses of striatal neurons in the behaving monkey. 1. Head of the caudate nucleus. *Behav. Brain Res.*, **7**, 179–210.

Rowe, M.H. & Cox, J.F. (1993) Spatial receptive-field structure of cat retinal W cells. *Vis. Neurosci.*, **10**, 765–779.

Saul, A.B. & Humphrey, A.L. (1990) Spatial and temporal response properties of lagged and nonlagged cells in cat lateral geniculate nucleus. *J. Neurophysiol.*, **64**, 206–224.

Saul, A.B. & Humphrey, A.L. (1992) Temporal-frequency tuning of direction selectivity in cat visual cortex. *Vis. Neurosci.*, **8**, 365–372.

Strecker, E.R., Steinfels, G., Abercrombie, E.D. & Jacobs, B.L. (1985) Caudate unit activity in freely moving cats: effects of phasic auditory and visual stimuli. *Brain Res.*, **329**, 350–353.

Tanaka, K., Ohzawa, I., Ramoa, A.S. & Freeman, R.D. (1987) Receptive field properties of cells in area 19 of the cat. *Exp. Brain Res.*, **65**, 549–558.

Tardif, E., Bergeron, A., Lepore, F. & Guillemot, J.P. (1996) Spatial and temporal frequency tuning and contrast sensitivity of single neurons in area 21a of the cat. *Brain Res.*, **716**, 219–223.

Tardif, E., Lepore, F. & Guillemot, J.P. (2000) Spatial properties and direction selectivity of single neurons in area 21b of the cat. *Neuroscience*, **97**, 625–634.

Tardif, E., Richer, L., Bergeron, A., Lepore, F. & Guillemot, J.P. (1997) Spatial resolution and contrast sensitivity of single neurons in area 19 of split-chiasm cats: a comparison with primary visual cortex. *Eur. J. Neurosci.*, **9**, 1929–1939.

Villeneuve, M.Y. & Casanova, C. (2003) On the use of isoflurane versus halothane in the study of visual response properties of single cells in the primary visual cortex. *J. Neurosci. Methods*, **129**, 19–31.

Waleszczyk, W.J., Nagy, A., Wypych, M., Berényi, A., Paróczy, Z., Eördegh, G., Ghazaryan, A. & Benedek, G. (2007) Spectral receptive field properties of neurons in the feline superior colliculus. *Exp. Brain Res.*, **181**, 87–98.

Webster, K.E. (1965) The cortico-striatal projections in the cat. *J. Anat.*, **99**, 329–337.

Zumbroich, T.J. & Blakemore, C. (1987) Spatial and temporal selectivity in the suprasylvian visual cortex of the cat. *J. Neurosci.*, **7**, 482–500.

Zumbroich, T., Price, D.J. & Blakemore, C. (1988) Development of spatial and temporal selectivity in the suprasylvian visual cortex of the cat. *J. Neurosci.*, **8**, 2713–2728.